Dissertation
submitted to the
Combined Faculties for the Natural Sciences and for Mathematics
of the Ruperto-Carola University of Heidelberg, Germany
for the degree of
Doctor of Natural Sciences

presented by
Master of Science Konrad Beyer
Born in: Erfurt, Germany
Oral-examination: 21.09.2017

Collective motion and adhesin dynamics of *Plasmodium* sporozoites

First examiner: Prof. Dr. Ulrich Schwarz

Second examiner: Prof. Dr. Friedrich Frischknecht

I hereby declare, that the experiments for this thesis were conducted between May 2013 and December 2016 in the laboratory of Prof. Dr. Friedrich Frischknecht at the parasitology unit of the centre of infectious diseases at the Ruperto-Carola University in Heidelberg.

I further declare that I wrote this thesis independently and that I used no other sources than those indicated throughout the thesis.

_____ _____

Date Signature

Acknowledgements

I hereby want to thank quite a great bunch of people I was lucky enough to get to know. Thank you all for your direct and indirect contribution to this thesis. Without you guys this thesis would never exist.

Freddy, for giving me the opportunity to conduct this thesis at your lab, for everything I learned from you throughout these years, for challenging and motivating me from time to time, your patience towards the end of my thesis, kicking my ass when needed, your always open office door and quick responses and not to forget all the lab outings and BBQs in your garden.

Ulrich, for being my first examiner, TAC member and for the great collaboration throughout this thesis. Thank you for all your advice.

Prof. Dr. Michael Lanzer, for giving me the opportunity to write this thesis at the parasitology department.

Mirko and Dennis, for teaching me almost everything I needed to know to get this thesis done, for answering all my little and not so little questions, for all your advice and motivation, for the weekly runs especially during the writing phase (only Mirko…Dennis not so much;). It was a pleasure to work with both of you.

Ross, for showing me a whole new level of puns (I admit I had no idea), always being that cheerful, optimistic and calm person you are, for all your advice and patience.

Ben, for being my brother from another mother, for all the lunch and coffee breaks in the botanical garden, for being my personal SnapGene expert, for all the laughs and "Lachs - Nudel sessions" and most of all for being a great colleague and even better friend throughout all these years.

Marek, for being one of my TAC members, for all the "quick" climbing – lunch breaks (sorry again for the foot thing), for your advice and for being that inspiring and cheerful friend.

Paul, for being a curious, ambitious and hard-working bachelor student. You have been a great support for this thesis.

Frea, for being that joyful, energetic and silly student, for making me laugh every single day we spent together, for showing me “odds” and teaching me some fancy English expressions, for travelling with me to all these hauntingly beautiful places and for bearing with me for a whole year of your life.

Miriam, for assisting me in some of these experiment, for being this overly genial, obliging person and for all these hours you spent to fill up the mosquito cages I needed.

Noa, for all the advice and motivation you gave me, all the joyful moments, for hosting me during my travels in Israel and for becoming a good friend.

All the people in my office, for creating a wonderful, relaxing and supportive atmosphere.

My family and friends, for all the support you gave me throughout this thesis.

Freddy, Dennis, Julia, Katharina, Saskia and Ross for proofreading this thesis and all the helpful comments.

My collaboration partners Anna Battista and Sabrina Rossberger, for all the discussions and hard work which will hopefully result in a stunning publication.

The complete AG Frischknecht: Freddy Frischknecht, Marek Cyrklaff, Julia Sattler, Saskia Egarter, Mendi Muthinja, Julia Aktories, Léanne Strauß, Benjamin Spreng, Jessica Kehrer, Catherine Moreau, Katharina Quadt, Gunnar Mair, Hirdesh Kumar, Kartik Bane, Hannah Fleckenstein, Rebekka Weber, Markus Ganter, Dennis Klug, Mirko Singer, Ross Douglas, Miriam Reinig, Johanna Ripp, Henriette Prinz and Christian Sommerauer for the enjoyable time, coffee breaks and so much tasty cake. I wish you all the best for your future!

Table of contents

Abstract

To fulfill its complex life cycle *Plasmodium* needs to cross various tissue barriers and invade specific cell types. Its journey inside the mosquito involves active invasion of sporozoites into salivary glands from where these motile forms can be transmitted to the host. To perform active movement inside the mosquito as well as the skin and liver of the host, sporozoites possess an uncommon form of locomotion termed "gliding motility". Force required for motility is generated by an actin - myosin motor complex and currently thought to be transduced to the sporozoite environment via surface adhesins belonging to the TRAP family. Sporozoites are curved and highly polarized cells capable of active circular movement *in vitro*. For the first time, our group has observed collective motion of sporozoites within infected salivary glands of *Anopheles stephensi* mosquitoes following preparation. Most interestingly we observed them to form circling formations, which we termed "vortices" containing up to a hundred sporozoites as well as "swarms" of two to seven sporozoites gliding closely associated to each other.

The first part of my thesis was to reach a deeper understanding of these collective migration phenomenons. Here, I show that vortices and swarms emerge from "resting" stacks of sporozoites that redistribute from the central gland cavity to the gland periphery during the preparation process and actively start to migrate individually at the basal membrane surrounding the gland. I further observed vortices to form over several minutes and be stable for hours whereas swarms form in the range of seconds and are stable for up to several minutes. Analysis of basic physical parameters of vortices (e.g. size, speed, angular speed and curvature) helped to broaden our understanding of their characteristics. Most interestingly, we observed vortices to consist of one up to several layers. Investigation of two mutant parasite lines revealed that sporozoites lacking the actin bundling protein *coronin* are still able to form vortices as well as swarms besides showing aberrant gliding on glass. In contrast, sporozoites lacking the chaperone HSP20 completely fail to form vortices and swarms.

In the second part of my thesis I focused on the interplay of the three known sporozoite adhesins (TRAP, S6 and TLP), which have already been characterized

independently throughout various studies and are known to play a major role in invasion and gliding motility of sporozoites. As a first step, I used double homologous recombination to create the double knockouts (ΔTRAP/ΔS6, ΔTLP/ΔTRAP and ΔTLP/ΔS6), two independent triple knockout lines (ΔTRAP/ΔTLP/ΔS6) as well as the TRAP complemented ΔTLP/ΔS6 line. Characterization of the generated lines confirmed the dominating TRAP and S6 phenotype blocking and strongly reducing sporozoite salivary gland invasion, respectively. I further demonstrate that once inside the salivary gland, TLP/S6 knockout sporozoites are still capable to undergo natural transmission via mosquito bites. Astonishingly, triple knockout sporozoites in the mosquito hemolymph can still attach and show the so-called patch gliding behavior, a limited form of gliding, indicating the existence of at least one further surface adhesin involved in gliding motility.

Taken together, this study provides fundamental insights into the previously undescribed collective motion of *Plasmodium* sporozoites which might serve as model system for future studies and broadened our understanding of the interplay of sporozoite surface adhesins.

Zusammenfassung

Um seinen komplexen Lebenszyklus zu durchlaufen, muss *Plasmodium* verschiedene Zellbarrieren überwinden und in spezifische Zellarten eindringen. Seine Reise innerhalb des Moskitos beinhaltet unter anderem die aktive Invasion von Sporozoiten in die Speicheldrüse, von wo aus diese bewegliche Form des Parasiten in den Wirt übertragen werden kann. Um sich innerhalb des Moskitos, der Haut, sowie Leber des Wirtes aktiv zu bewegen, besitzt der Sporozoit eine ungewöhnliche Art der Fortbewegung, die als „gliding motility“ bezeichnet wird. Die Kraft, die für diese Art der Bewegung benötigt wird, wird von einem Aktin-Myosin Motorkomplex erzeugt und wird nach derzeitigem Verständnis über Oberflächenproteine – den Adhäsinen der TRAP Familie – an die Umgebung des Parasiten übertragen. Sporozoiten sind gekrümmte, stark polarisierte Zellen und dazu fähig sich *in vitro* aktiv und kreisförmig zu bewegen. Erstmalig hat unsere Arbeitsgruppe die kollektive Bewegung von Sporozoiten innerhalb von infizierten Speicheldrüsenpräparaten von *Anopheles stephensi* Moskitos beobachtet. Interessanterweise haben wir gesehen wie sie kreisende Formationen aus bis zu hundert Sporozoiten bildeten, die wir „Wirbel“ genannt haben. Weiterhin konnten wir bewegliche „Schwärme“ bestehend aus zwei bis sieben dicht assoziierten Sporozoiten beobachten.

Der erste Teil meiner Arbeit beschäftigt sich damit, ein tieferes Verständnis dieser Phänomene der kollektiven Bewegung zu erlangen. Hierbei zeige ich, dass Wirbel und Schwärme aus „ruhenden“ Sporozoitenstapeln hervorgehen, die sich während des Präparationsvorgangs von der zentralen Speicheldrüsenhöhle in die Peripherie der Speicheldrüse verteilen und sich zunächst als einzelne Sporozoiten an der umgebenden Basalmembran entlang bewegen. Weiterhin konnte ich beobachten, wie sich „Wirbel“ innerhalb von Minuten formieren und über mehrere Stunden stabil bleiben, wohingegen sich Schwärme innerhalb von Sekunden bilden und sich nur mehrere Minuten stabil bewegen. Eine Analyse der grundlegenden physikalischen Parameter (z.B. Größe, Geschwindigkeit, Winkelgeschwindigkeit und Krümmung) half uns, unser Verständnis über deren Eigenschaften zu erweitern. Interessanterweise konnten wir beobachten, dass Sporozoiten-Wirbel aus einer oder mehreren Schichten

bestehen. Die Untersuchung zweier mutierter Parasitenlinien offenbarte, dass Sporozoiten, denen das Aktin-bündelnde Protein „Coronin“ fehlt, weiterhin Wirbel und Schwärme ausbilden, auch wenn sie sich auf Glas nur sehr eingeschränkt fortbewegen. Im Gegensatz hierzu bilden Sporozoiten, denen das Chaperon „HSP20“ fehlt, keine Wirbel und Schwärme aus.

Im zweiten Teil meiner Arbeit fokussiere ich mich auf das Zusammenspiel der drei bekannten Sporozoiten-Adhäsine (TRAP, S6 und TLP), welche bereits unabhängig voneinander in verschiedenen Studien untersucht worden sind und eine zentrale Rolle bei der Invasion und Fortbewegung der Sporozoiten spielen. Als ersten Schritt habe ich die doppelt homologe Rekombination genutzt, um die jeweiligen Doppel-Knockoutlinien (ΔTRAP/ΔS6, ΔTLP/ΔTRAP und ΔTLP/ΔS6), zwei unabhängige Tripel-Knockoutlinien (ΔTRAP/ΔTLP/ΔS6), sowie hieraus eine mit TRAP komplementierte zweite ΔTLP/ΔS6 Linie zu generieren. Die Charakterisierung der generierten Parasitenlinien bestätigte den dominanten TRAP und S6 Knockout Phänotyp, der jeweilig entweder zu einer vollständigen Blockade oder stark verringerten Speicheldrüseninvasion führt. Weiterhin zeige ich, dass ΔTLP/ΔS6 Sporozoiten weiterhin auf natürlichem Weg durch einen Moskitostich übertragen werden können. Erstaunlicherweise waren Tripel Knockout Sporozoiten aus der Hämolymphe des Moskitos weiterhin im Stande sich an einer Glasoberfläche anzuheften und ein sogenanntes „patch gliding“ - Bewegungsmuster zu zeigen, eine Art der eingeschränkten Bewegung. Dies deutet darauf hin, dass zumindest ein weiteres Oberflächenprotein existiert, welches an der Bewegung der Sporozoiten beteiligt ist.

Zusammenfassend liefert diese Arbeit grundlegende Einsichten in die bislang unbeschriebene kollektive Bewegung von *Plasmodium* Sporozoiten, welches als zukünftiges Modelsystem dienen könnte und erweitert unser Verständnis über die Zusammenwirkung der Oberflächenadhäsine der Sporozoiten.

Abbreviations

°C	degree Celsius
5-FC	5-fluorocytosine
5-FCTP	5-fluorocytosine triphosphate
aa	amino acid
Amp	ampicillin
bp	base pair
BSA	bovine serum albumine
CO_2	carbon dioxide
CTP	cytidine triphosphate
DAPI	4',6-Diamidino-2-phenylindol
ddH_2O	double-distilled water
DDT	dichlorodiphenyltrichloroethane
DHFR	dihydrofolate reductase
DHFS	dihydrofolate synthase
DIC	differential interference contrast
DMEM	Dulbecco´s Modified Eagle Medium
DNA	deoxyribonucleic acid
dNTP	deoxyribonucleotide triphosphate
E. coli	Escherichia coli
FBS	fetal bovine serum
g	gram
GFP	green fluorescent protein
h	hour
HCl	hydrogen chloride
HEPES	4-(2-hydroxyethyl)-1-piperazineethanesulfonic acid
HSP20	heat shock protein 20
i.p.	intraperitoneal
i.v.	intravenous

IMC	inner membrane complex
kb	kilobases
KCl	potassium chloride
kg	kilogram
KO	knockout
KOH	potassium hydroxide
M	molar mass (kg/mol)
MG	midgut
mg	milligram
$MgCl_2$	magnesium chloride
min	minute
ml	milliliter
mmol	millimole
NMRI	Naval Medical Research Institute
P/S	penicilline-streptomycine
Pb	Plasmodium berghei
PBS	phosphate buffered saline
PCR	polymerase chain reaction
RPMI	Roswell Park Memorial Institute medium
RT	room temperature
s	second
SG	salivary gland
Spz	sporozoites
TAE	Tris-Acetate-EDTA
taq	thermus aquaticus
TLP	TRAP-like protein
TRAP	thrombospondin-related anonymous protein
TREP (S6)	TRAP-related protein
TrisHCl	tris(hydroxymethyl)aminomethane hydrogen chloride
TSR	thrombospondin type 1 repeat

UPRT	uridyl phosphoribosyl transferase
UTR	untranslated region
v/v	volume/ volume, volume percent
w/v	weight/ volume
WGA	wheat germ agglutinin
WHO	World Health Organisation
WT	wild type
yFCU	yeast fusion gene
µl	microliter
µM	micromolar

List of figures

List of tables

List of formulas

1 Introduction

1.1 *Plasmodium* life cycle

Plasmodium spp. parasites undergo a complex life cycle alternating between the female *Anopheles* mosquito vector and the vertebrate host (Fig 1.1). They belong to the phylum of *Apicomplexa* – a unicellular and spore forming group of obligate endoparasites. Human infections are caused by five different species: *P.falciparum, P.vivax, P.ovale, P.malariae* and *P.knowlesi* with *P.falciparum* and *P.vivax* being the most prevalent *Plasmodium* species (White 2011). During its life cycle, the various extra - and intracellular environments require the parasite to constantly adapt by not only changing its shape but also its motility and metabolism (Rénia and Goh 2016). *Plasmodium* sporozoites, the infectious forms of the parasite, are transmitted to the mammalian host during the bite of an infected, female mosquito. The parasite gets inoculated into the dermis of the host alongside with saliva which prevents the blood from clotting (Sidjanski et al. 1997; Frischknecht et al. 2004; Amino et al. 2006). After injection, the parasites migrate through the skin tissue by an active form of substrate dependent migration termed “gliding motility” (Vanderberg and Frevert 2004; Amino et al. 2006; Hopp et al. 2015). While migrating, sporozoites reach remarkable speeds of 1-3 µm/s in comparison to lymphocytes migrating with about 0.1 µm/s (Miller et al. 2003; Amino et al. 2006; Hellmann et al. 2011; Hopp et al. 2015). When finally reaching a blood vessel they invade the circulatory system and get passively carried away to the liver (Vanderberg and Frevert 2004; Douglas et al. 2015). After sequestration in the liver sinusoids, sporozoites traverse the sinusoidal layer via endothelial or Kupffer cells (Tavares et al. 2013). Subsequently, sporozoites migrate through several hepatocytes and establish a parasitophorus vacuole inside a final hepatocyte (Mota et al. 2002). Breaching the sinusoidal barrier and invading hepatocytes requires the parasite to actively migrate and interact with the host cells (Kappe et al. 2003; Baum et al. 2008). After formation of the parasitophorus vacuole, the parasite develops and replicates into thousands of new parasites (merozoites) within the hepatocyte (Prudêncio et al. 2006). Merozoite filled vesicles (so called merosomes) bud of from the infected hepatocytes, re-enter the liver sinusoids and finally release the merozoites into the

blood circulatory system during the passage through lung capillaries (Sturm et al. 2006; Baer et al. 2007). *P. vivax* and *P. ovale* are further known to form dormant stages in the liver (hypnozoites) which can reactivate and continue to form merozoites after several weeks or even years (Terzakis et al. 1967). Free merozoites rapidly attach to and actively invade erythrocytes in a dynamic and multistep process (Weiss et al. 2015). Once inside the erythrocyte the parasite undergoes asexual replication and cell division and develops into a mature schizont stage. In this stage 10 up to 30 new merozoites are formed which are released after lysis of the parasitophorus vacuole membrane (PVM) and the erythrocyte membrane. These merozoites invade new erythrocytes and continue the asexual replication cycle causing the clinical symptoms of the disease like fever, chills, headache and flu-like symptoms (Crawley et al. 2010). During each cycle, a small proportion of parasites develops into the sexual form known as male and female gametocytes (Josling and Llinás 2015). These sexual forms are taken up during the bite of a female mosquito and differentiate into mature gametes inside the mosquito midgut (Sinden and Croll 1975). Fertilization of male and female gametes result in a diploid zygote which in turn develops into a motile cell called ookinete. Ookinetes penetrate the peritrophic matrix, a semi-permeable structure surrounding the blood meal and the underlying epithelial cells of the mosquito midgut to form extracellular oocysts (Angrisano et al. 2012). Approximately a thousand sporozoites are formed inside each oocyst and are released into the hemolymph of the mosquito (Vanderberg and Rhodin 1967). Within the hemolymph, they get passively carried throughout the open circulatory system until they attach and actively invade the salivary glands of the mosquito from where they get injected into the host (Kappe et al. 2004).

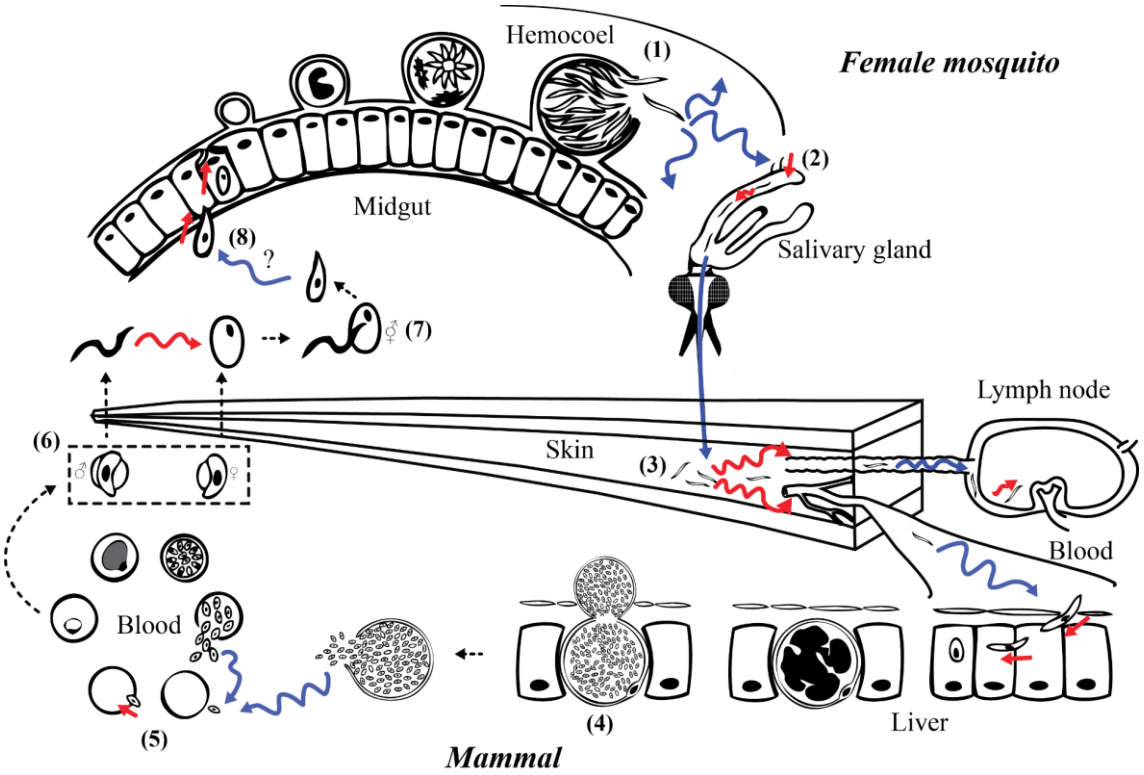

Fig. 1.1 The *Plasmodium* life cycle. (Douglas et al. 2015) Sporozoites are injected into the skin (3) of the mammalian host during the blood meal of a female Anopheles mosquito. They target the liver where they invade hepatocytes and develop into more than ten thousand of hepatic merozoites (4). These merozoites re-enter the blood circulatory system and invade erythrocytes (5). Here, they reproduce asexually forming ~10-30 new merozoites during each cycle. Some parasites transform into sexual stages, male and female gametocytes, which are taken up by the mosquito during a blood meal (6). Inside the mosquito midgut, the gametocytes develop into mature gametes and fertilize into diploid zygotes (7). The motile zygote called ookinete penetrates the gut epithelium (8) and transforms into an oocyst in which about a thousand sporozoites develop. Sporozoites are released into the hemolymph of the mosquito (1) where they reach and invade the salivary glands (2). Inside the gland cavity the sporozoites partly enter the salivary duct and are again transmitted into a mammalian host during the next bite (3). Blue arrows indicate passive transport of the parasite while red arrows indicate active migration or invasion.

1.2 Sporozoite development within the mosquito

Sporozoites are formed within the oocysts at the midgut wall of infected *Anopheles* mosquitoes. The oocyst is described as a distinct structure surrounded by a capsule and an underlying plasma membrane (Vanderberg and Rhodin 1967). Oocysts maturate within about 1-2 weeks depending on the *Plasmodium* species (Smith and Barillas-Mury 2016). During this time, the oocyst substantially grows and undergoes a process called sporogony in which multiple nuclear divisions take place and thousands of sporozoites are released into the hemolymph of the mosquito (Vanderberg and Rhodin 1967). Sporozoites bud of from a vesicular structure called the sporoblast located in the center of the cyst (Nagasawa et al. 1988; Aikawa et al. 1990). During early sporogony, the sporoblast deeply invaginates creating an enlarged membrane surface. Sporozoite buds emerge at the membrane surface of the sporoblast marked by the occurrence of the inner membrane complex (IMC) and sub-pellicular microtubles close to the sporoblast plasma membrane (Kappe et al. 2003; Frischknecht and Matuschewski 2017). The sporozoites bud grows further into the cisternal space of the oocyst by simultaneous extension of IMC, plasma membrane as well as the microtubles (Kappe et al. 2004). During this process, the plasma membrane of the sporoblast becomes the plasma membrane of the sporozoites whereas the IMC is presumably generated *de novo* from Golgi-derived cytoplasmic vesicles (Sinden and Strong 1978; Beier 1998). Finally, the complete sporozoites bud of from the sporoblast into the cisternal oocyst space. Only little is known regarding the molecular details leading to sporogony. However, the circumsporozoite protein (CSP) has been identified to be essential for sporozoite formation. CSP is the most abundant surface protein of sporozoites and linked to their plasma membrane via a glycosylphosphatidylinositol (GPI) anchor. CSP is already strongly expressed during early sporogeny at the plasma membrane of the sporoblast and accumulates at budding sites (Nagasawa et al. 1988; Posthuma et al. 1988; Aikawa et al. 1990). Parasites lacking CSP (CSP-KO) showed a complete block of sporozoite generation despite normal formation of oocysts (Ménard et al. 1997). In these mutants, the IMC was not restricted to the budding sites but was distributed at the complete oocyst plasma membrane. Further, down regulation of CSP resulted in only small numbers of normal formed sporozoites whereas the majority were shortened, malformed and unable to infect salivary glands (Thathy et al. 2002).

However, the detailed mechanism of CSP during sporogony remains to be resolved. After complete maturation of the oocyst sporozoites are released into the hemolymph of the mosquito. Several proteins, such as the TRAP related Protein 1 (TRP1) and the protease Sera5 have been identified to be crucial during oocyst egress (Aly and Matuschewski 2005; Klug and Frischknecht 2017). Inside the hemolymph sporozoites get passively carried through the body cavity of the mosquito until they reach the salivary glands. Sporozoites initially attach to the filamentous basal lamina, which is surrounding the gland (Ghosh and Jacobs-Lorena 2009). The parasite actively traverses the basal lamina as well as the underlying acinar cells to accumulate inside the gland cavity (Sterling et al. 1973; Douglas et al. 2015; Pimenta et al. 1997). Mainly the median and distal lateral lobes were invaded suggesting the existents of specific receptors (Sterling et al. 1973). Several proteins have been identified to play a role in specific recognition and attachment to the glands. Region I of CSP has been shown to specifically bind to salivary glands when compared to other organs in the mosquito indicating a role in initial sporozoite attachment (Sidjanski et al. 1997; Myung et al. 2004). Despite CSP, at least three other sporozoites surface proteins seem to be involved in salivary gland invasion. The thrombospondin-anonymous related protein (TRAP) is specifically expressed in sporozoites and has been shown to be essential in salivary gland invasion and gliding motility of sporozoites. Sporozoites lacking TRAP are unable to glide continuously and completely fail to invade salivary glands (Sultan et al. 1997; Münter et al. 2009). The surface protein S6 also has been shown to be involved in salivary gland invasion as its depletion leads to strongly reduced sporozoite numbers inside the gland (Combe et al. 2009; Steinbuechel and Matuschewski 2009). Furthermore, disruption of the membrane antigen erythrocyte binding-like protein (MAEBL) was leading to strong reduction of sporozoite attachment to the glands (Kariu et al. 2002). Inside the glands, the parasites undergo further maturation and prepare for their upcoming tasks inside the vertebrate host. This maturation process of sporozoites was already indicated by a study showing that isolated salivary gland sporozoites lose the ability to reinfect salivary glands when injected into mosquitoes (Touray et al. 1992). Gene expression profiling further revealed that sporozoite maturation correlates with the developmental upregulation of several genes prior to sporozoites release into the skin (e.g. MCP-1, UIS1, UIS10) (Matuschewski, Ross, et al.

2002). Unlike midgut sporozoites, salivary gland sporozoites are highly infectious *in vivo*. Even sporozoites collected from the midgut and hemolymph of the mosquito can cause an infection when injected artificially into the host (Shute 1943; Vanderberg 1975; Sato et al. 2014). For natural transmission, a small proportion of the salivary gland sporozoites actively invades the salivary duct of the mosquito and is deposited into the host skin during the bite of the mosquito (Frischknecht et al. 2004; Hopp et al. 2015). The difference of infectivity of the three sporozoite stages is due to the ongoing maturation from midgut to salivary gland sporozoites. Consequently, salivary gland sporozoites demonstrate a higher rate of gliding motility (Vanderberg 1974; Matuschewski 2006), an essential feature of the sporozoite not only to enter the salivary glands and pre-invade the salivary duct but also to migrate through the skin after injection. *Plasmodium* sporozoites evolved a complex gliding machinery to complete its challenging journey.

1.3 Gliding motility *of Plasmodium*

P*lasmodium* undergoes active and fast migration through host cells and tissues in several stages of its life cycle as well as active penetration of host cells along its journey (Douglas et al. 2015). It is a crucial feature for sporozoites to migrate through the skin to find a blood vessel as well as for ookinetes to traverse the midgut epithelium. Despite the lack of motor organelles (e.g. cilia, flagella) *Plasmodium* can reach average speeds of 1 – 3 µm/s in a special form of substrate dependent locomotion called “gliding motility” unique to *Apicomplexa* including the related parasite *Toxoplasma gondii* (Heintzelman 2015). The macromolecular motor complex generating these incredible speeds is termed “the glideosome” and is localized in between the inner membrane complex (IMC) and the plasma membrane of the parasite – the supra-alveolar space (fig. 1.2) (Heintzelman 2015). Myosins are indirectly anchored in the IMC and drive the rearward locomotion of actin associated cell surface molecules (adhesins) which in turn leads to the forward migration of the parasite when adhesins are bound to the substrate or host cell (Meissner et al. 2002; Bullen et al. 2009; Heintzelman 2015).

Force is generated by rearward directed power strokes of a single-headed myosin only found in *Apicomplexa* (myoA, class XIV) (Heintzelman and Schwartzman 1999; Herm-Götz et al. 2002; Opitz and Soldati 2002; Keeley and Soldati 2004). This type of myosin lacks a canonical tail domain normally required to direct the myosin to its intracellular location (Heintzelman and Schwartzman 1997). Instead, this function is fulfilled by the myosin A tail interacting protein (MTIP) which mediates the interaction of myosin to GAP45 - one of the gliding associated proteins (GAPs). GAP45 links the myoA/MTIP complex to the IMC and spans the space between IMC and plasma membrane of the parasite which is suggested to ensure structural integrity of the supra-alveolar space (Bergman et al. 2003; Frénal et al. 2010). GAP50 – an integral membrane glycoprotein - has been shown to anchor the GAP45/MyoA/MTIP complex in the IMC (Gaskins et al. 2004). Anchored in the IMC myosins bind to actin filaments (F-actin) and drive them rearwards within the parasite. In contrast to most eukaryotic cells, the vast majority of *Plasmodium* actin exists in the globular form (G-actin) and polymerizing filaments are rather short and instable (Schmitz et al. 2005; Skillman et al. 2011). Interestingly, these characteristics of parasite actin are important for normal migration as drug (e.g. via cyto D and jasplakinolide) induced alteration of F-actin stability caused impaired gliding motility and invasion of the parasite (Wetzel et al. 2003; Münter et al. 2009; Skillman et al. 2011). Actin dynamics are carefully regulated by so called actin-binding proteins (ABPs) (Sattler et al. 2011). To get traction and consequently propel itself forward, the parasite needs to transiently adhere to the substrate or host cell surface. A set of adhesins are secreted from vesicular organelles called micronemes into the plasma membrane at the apical end of the parasite and are translocated to the posterior end linking the motor complex to the adhesion site (Heintzelman 2015). These include the apical membrane antigen-1 (AMA1) protein and members of the thrombospondin-related anonymous protein (TRAP) family (Boucher and Bosch 2015). Adhesins are thought to be indirectly connected to the actin filaments. When reaching the posterior end of the parasite, adhesins are thought to be cleaved by rhomboid proteases in their transmembrane region and left behind as extracellular trails (Morahan et al. 2009; Ejigiri et al. 2012). Despite being extensively studied throughout the last decades the complex gliding machinery of *Plasmodium* is still not fully understood and remains subject of further studies.

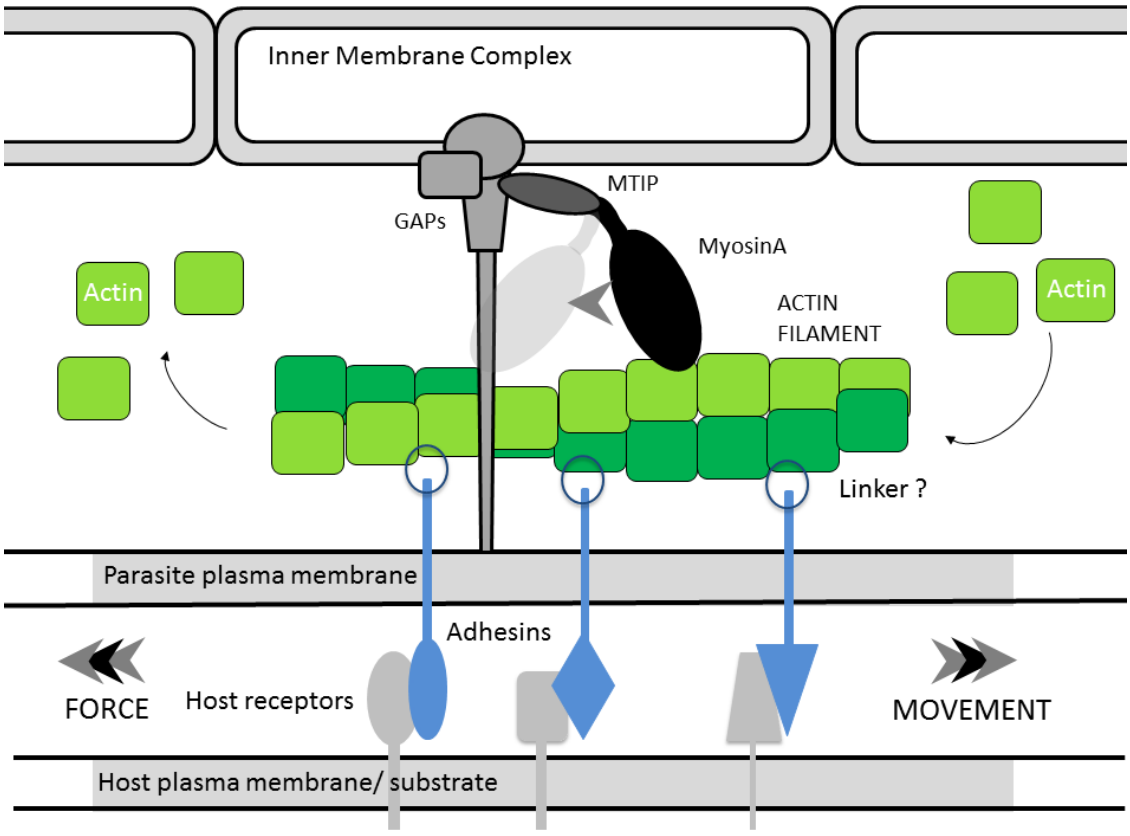

Fig 1.2 Linear gliding motility model of Plasmodium. (modified scheme from Ross Douglas and Julia Aktories). The actin-myosin motor is situated in between the inner membrane complex (IMC) and the plasma membrane of the parasite. Adhesins are secreted into the plasma membrane at the apical end of the parasite and are translocated to the posterior end linking the motor complex to the adhesion site. Myosin A (Myo A) is anchored into the IMC via the myosin-A tail interacting protein (MTIP) as well as gliding associated proteins (GAPs) and binds to short actin filaments (F-actin) underneath the plasma membrane. A power stroke of Myo A generates a rearward directed force which leads to retrograde flow of F-actin. Adhesins bind to the substrate or host cell receptors and are connected to actin filaments via an unknown linker resulting in a forward propulsion of the parasite.

1.4 Sporozoite adhesins

Adhesive surface proteins play a crucial role during gliding motility of the parasite as it needs to recognize, migrate through and invade various host cells along its complex journey. The set of expressed adhesins varies depending on the life cycle stage and suggests specific roles of adhesins in different environments. In this section, I will concentrate on the sporozoite stage of *Plasmodium*. As mentioned before, members of the thrombospondin-related anonymous protein (TRAP) family have been identified to be important adhesins to ensure efficient gliding of *Plasmodium* sporozoites

(Moreira et al. 2008). At least three members are known to be involved in gliding motility of sporozoites – TRAP, TLP (TRAP like protein) and S6. Despite varying in length, they all are transmembrane proteins secreted to the surface of the sporozoites and share an overall similar structure (fig 1.3). TRAP and TLP are suggested to be stored in vesicles called micronemes at the apical tip of the parasite, from where they are released to the plasma membrane and transported to the rear of the parasite (Montagna 2012). TRAP, TLP as well as S6 display variable numbers of two adhesive domains in their extracellular part – the von Willebrand factor type A (VWA) domain and the thrombospondin type I repeat (TSR) domain (Kappe et al. 2004). Mutation studies of both adhesive domains in TRAP revealed an important role during salivary gland and liver cell invasion (Matuschewski, Nunes, et al. 2002). Further, all three adhesins contain at least one transmembrane domain (TMD) and a short, acidic cytoplasmic tail domain (CTD) including a conserved, penultimate tryptophan (W) (Kappe et al. 1999). Point mutations in conserved regions of the cytoplasmic tail of TRAP were leading to aberrant gliding motility of sporozoites demonstrating its linking function to the actin myosin motor (Kappe et al. 1999). Interestingly, mutants with a replaced cytoplasmic tail of TRAP against that of TLP were still able to glide proving them to be at least partially functional interchangeable (Heiss et al. 2008).

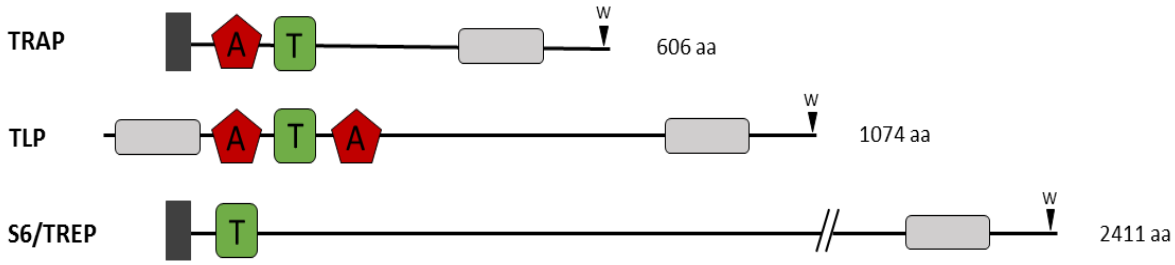

Fig. 1.3. TRAP family protein members expressed in Plasmodium sporozoites. Scheme representing the domain structure of TRAP family adhesins. Von Willebrand A domains are shown as red pentagons (labeled with A) and thrombospondin repeat domains as green boxes (labeled with T). Signal peptides are represented as dark grey and transmembrane domains as light grey boxes. Note that TLP is predicted to contain two transmembrane domains. The conserved tryptophans are indicated as W. Protein lengths are not drawn to scale and amino acid (aa) numbers refer to *P. berghei* proteins. (modified from Lacroix and Menard 2008)

Various deletion studies of TRAP, TLP and S6 were leading to the observation of different phenotypes during the sporozoite stage. Parasites lacking TRAP show the most prominent phenotype including a life cycle arrest as they completely fail to invade mosquito salivary glands, adhere less and are unable to undergo directed, circular gliding (Sultan et al. 1997; Wengelnik et al. 1999; Münter et al. 2009; Hegge et al. 2010). However, TRAP depleted sporozoites isolated from the mosquito hemolymph are still capable to attach to substrates and move in a non-directed, back-and-forth manner using a single adhesion site. This movement pattern is termed patch gliding (Münter et al. 2009). The majority of TRAP is stored within the micronemes of the sporozoite but only a small proportion is released to the parasite surface during gliding and invasion (Morahan et al. 2009; Kehrer et al. 2016). TRAP is known to be involved in invasion of hepatocytes as its extracellular part binds to heparin sulphate proteoglycans at the surface of hepatocytes (Coppi et al. 2011). Further, *in vitro* experiments revealed that TRAP binds to Saglin, a surface receptor of salivary glands essential for sporozoite invasion (Ghosh et al. 2009). In contrast to TRAP, TLP depleted parasites are still capable to complete the life cycle and show only a subtle defect (Moreira et al. 2008). Besides a partial blood stage delay TLP depleted parasites have a decreased capacity to traverse cells *in vitro* and show reduced infectivity *in vivo* when injected into the host skin (Heiss et al. 2008; Lacroix and Menard 2008; Moreira et al. 2008; Hellmann et al. 2011). Sporozoites lacking TLP are still capable of continuous gliding *in vitro* but were shown to detach more frequently during gliding (Hegge et al. 2010). Based on these studies, TLP is believed to play a role during skin migration and might have a regulatory function in adhesion formation and detachment of the sporozoite (Hegge et al. 2010). Further, a recent study suggests TLP to act in coupling retrograde flow to force production as TLP depleted parasites show increased retrograde flow despite reduced adhesion forces (Quadt et al. 2016). In contrast to TLP being mainly expressed in the salivary gland stage of the parasite, the majority of S6 is expressed in midgut and hemolymph sporozoites (Combe et al. 2009). S6 depleted parasites have been found to enter salivary glands in strongly reduced numbers, accumulate inside the mosquito hemolymph and show severely impaired gliding motility *in vitro* when isolated from the hemolymph (Combe et al. 2009; Steinbuechel and Matuschewski 2009; Hegge et al. 2010; Hegge et al. 2012). All three adhesins are

suggested to act in concert with actin filaments to ensure optimal gliding motility but it is likely that further known and unknown proteins are involved in this process (Hegge et al. 2012). Potential candidates are cysteine repeat modular proteins (PCRMP 1 and 2) which are known to be located at the surface of hemolymph and salivary gland sporozoites (Thompson et al. 2007; Douradinha et al. 2011) as well as TRSP (Kaiser et al. 2004; Labaied et al. 2007), RON4 (Giovannini et al. 2011) and the circumsporozoite protein (CSP) (Myung et al. 2004). A further candidate is LIMP, a recently described surface protein, which turned out to be crucial for gliding motility and infectivity of *Plasmodium* sporozoites in the mosquito as well as the rodent host (Santos et al. 2017). Sporozoites lacking LIMP show a ten fold reduced salivary gland invasion and fail to attach to liver cells causing an absence of liver cell invasion. Therefore, LIMP was suggested to be a key regulator for adhesion in gliding motility as well as salivary gland and hepatocyte invasion (Santos et al. 2017). Recent proteomic studies reveal further candidates to extend our current understanding (Lindner et al. 2013, El-Manzalawy et al. 2016, see section 5.3).

1.5 Collective motion

Collective motion, a form of collective behavior, is a rapidly developing and highly interdisciplinary field aiming to study the “spontaneous emergence of ordered movement in a system compound of a large number of self-propelled agents” (Vicsek and Zafeiris 2012). Most common examples of collective motion are flocks of birds (e.g. starlings) or school of fish (e.g. sardines and tuna). In fact, however, collective motion is a ubiquitous phenomenon found throughout nature, spanning various scales and occurs when groups of similar interacting units move with about the same speed (Vicsek and Zafeiris 2012). Examples are observed in a diverse range of biological systems from bacteria, amoeba and cells to larger organism like insects, fish, birds and a high variety of mammals (Vicsek and Zafeiris 2012). Collective motion even extends to the non-living world e.g. shaken metallic rods or discs and macromolecules (Blair et al. 2002; Kudrolli et al. 2008; Schaller et al. 2010). A key feature of such collection behavior is that the motion of a single unit is influenced by other units causing it to behave different from the way it would behave individually (Czirók et al. 2001). Collective phenomena can be the result of simple interaction rules between individuals

such as attraction and repulsion (e.g. collision avoidance) or interactions of individuals with their environment (e.g. attraction towards a food source) (Couzin and Krause 2003; Tunstrøm et al. 2013; Delcourt et al. 2016). Further, they can turn out to be rather complex as a combined result of several simple interactions (Vicsek and Zafeiris 2012). In general, collective motion can be classified into three major groups: "Swarms" show only a weak synchronization of movement and are observed to be rather stationary. "Polarized schools" are highly synchronized groups that undergo directed movement and "vortices" (rotating circular formations) which are groups of individuals that turn around a common center (Delcourt et al. 2016). As Vortex behavior is the most relevant form of collective motion regarding this thesis it will be described in greater detail in the following section.

1.6 Vortex behavior

Like other forms of collective motion vortex behavior is a ubiquitous phenomenon widespread in nature. Early described examples include circular columns of caterpillars and vortices formed by army ants and cat fish (Fabre 1879; Wheeler 1910; Parr 1927). Similar formations have been observed in protists, bacteria, insects, amphibians, birds, fish and mammals (Delcourt et al. 2016). Up to now, there is no general definition of vortex behavior throughout the literature. Vortices have been suggested to be "systems (groups of animals) in which there is a correlated radial motion of components of this system (individuals) around a common center" (Ben-Jacob et al. 1997; Delcourt et al. 2016). Further, they have been suggested to be a subcase of polarized groups as individuals inside a vortex usually exhibit a high degree of alignment to other nearby individuals resulting in a synchronization of movements (Delcourt and Poncin 2012). The size and number of individuals inside a vortex shows a high variability reaching from only two individuals like northern shoveler ducks (Bode et al. 2013) to millions of coordinated circling cells observed in bacterial cultures (Ben-Jacob 2003). Depending on the species, vortex formation is only observed when sufficient individuals get in close contact. Vortex formation of spadefoot toad tadpoles requires several hundred individuals (Bazazi et al. 2012). The biggest so far reported example of vortex formation had a diameter of 365 m and consisted of army ants migrating in a loop with up to six lanes (Beebe and Beebe 1921). In contrast, vortices

were observed in confined bacterial suspensions of 30 – 100 µm (Lushi et al. 2014). In addition to that broad range of scales, vortices exhibit varying lifespans. Vortices of fish (e.g. “golden shiners”) were shown to persist for only several seconds or minutes (Tunstrøm et al. 2013) whereas some vortices consisting of caterpillars or ants were observed to least for several days (Fabre 1879; Schneirla 1944). So far, clockwise and anticlockwise movement directions have been observed in all reported vortex examples. However, the majority of individuals inside a vortex follows only one direction (Delcourt et al. 2016).

Potential causes for vortex formation are based on social and non-social forces and might be beneficial in terms of protection against predators, accessibility to resources and collective locomotion (Delcourt et al. 2016). A non-social force can be a local stimulus in a small area which attracts individuals that need to avoid collisions e.g. water fleas rotating around a light beam (Vollmer et al. 2006). Also, peripheral repulsive stimuli (e.g. predators) and constraints (e.g. obstacles and walls) can lead to vortex formation (Delcourt et al. 2016). Further, vortices can be formed by individuals that modify their environment in a way that affects the behavior of other individuals causing self-organization without direct interaction – a mechanism referred to as “stigmergy” (Grassé 1959). Locally favorable conditions can be created by the movement of individuals or the secretion of chemical trails (e.g. pheromone tracks of ants) leading to a positive feed-back mechanism (Delcourt et al. 2016). A further example for stigmergy are filter-feeding ducks which have been suggested to cause nutrients to rise to the water surface and create a local attractive area by moving in vortex formations consisting of several tens of individuals (Todd 1979; Gooders and Boyer 1986; Bode et al. 2013). In contrast to non-social forces, social forces act via direct interaction between individuals usually mediated via visual and sound stimuli (Delcourt et al. 2016). Models for social interactions include simple behavioral rules like movement towards other individuals, collision avoidance and alignment of movement direction and have been demonstrated to explain the formation of several collective phenomena such as vortex behavior (Couzin and Krause 2003; Sumpter 2010). In case of social interactions, the formation of swarms, polarized schools and vortices depend on a mix of short range and long-range interactions. In this context, vortices can be explained by collision avoidance and movement alignment restricted to

nearby individuals and simultaneous attraction of individuals further apart ensuring movement towards the group center (Couzin et al. 2002). Observation of schools of fish (e.g. golden shiners) in an experimental setup lacking external stimuli revealed that the frequency of transitions between collective states and their stability depends on the group size. Further, these transitions are suggested to be influenced by interactions between individuals as well as individuals with spatial boundaries (e.g. tank walls) (Tunstrøm et al. 2013). Interestingly, state transitions were observed in cases when individual behavior rules changed but were also happening when these rules were unchanged (Calovi et al. 2014). The formation of vortex patterns can be of potential advantage to individuals like energy and survival benefits which might have evolutionary origins (Delcourt et al. 2016) e.g. mexican spadefood toads which release and suspend additional nutrients by moving in a vortex pattern (Bazazi et al. 2012). Another recent study revealed that a species of marine flat worms form vortices which is suggested to be beneficial in generating biofilms in order to form a “superorganismic seaweed” in a habitat where individual worms could not anchor themselves individually (Franks et al. 2016). Another advantage for vortex formations is the movement of bacteria on hard, nutrient poor surfaces. Here, vortex formation is supposed to ensure a high density of bacteria which combined with the collective generation of a common fluid enables them to translocate as one unit which would otherwise not be possible (Ben-Jacob 2003). Further, schools of fish are supposed to form vortices to be better protected against predator attacks as predators are earlier detected by many individuals (Lima 1995; Rieucau and Martin 2008) and individuals can hide themselves inside the group reducing the risk of being predated (Wood and Ackland 2007).

Despite their ubiquity throughout nature and an increasing number of studies, the overall function and dynamics of vortex formation is yet fragmented and poorly understood. More detailed studies on vortex behaviors including multi-tracking and computer simulations are required to reach a better understanding of these phenomena (Delcourt et al. 2016).

1.7 Aims and objectives of the study

For the first time our group has observed collective motion of sporozoites within infected salivary glands of *Anopheles stephensi* mosquitoes following preparation. Most interestingly they have been observed to form rotating formations of five up to hundred sporozoites we termed “vortices” as well as groups of two to seven sporozoites gliding closely associated to each other we call “swarms”. The first part of my thesis is an attempt to reach a deeper understanding of these fascinating, yet complex phenomenons. In particular, I was aiming to understand where these collective phenomena are located inside the mosquito salivary gland and how they form and behave over time. I therefore analysed basic physical parameters of vortices (e.g. size, speed, angular speed and curvature) to broaden our understanding of their overall dynamics. To address these questions, I was using mainly epifluorescence and spinning disc confocal microscopy combined with quantitative image analysis. Finally, I analysed the collective behavior of two genetically modified parasite lines (*hsp20(-)* and *coronin(-)*) which show altered motility *in vitro* as well as *in vivo* (Montagna et al. 2012; Bane et al. 2016).

In the second part of my thesis I was targeting the three TRAP family adhesins expressed in the sporozoite stage of *Plasmodium* (TRAP, S6 and TLP), which have already been characterized independently throughout various studies and are known to play a major role in invasion and gliding motility of sporozoites. To reveal a potential interplay of these adhesins, I generated the respective double knockout (ΔTRAP/ΔS6, ΔTLP/ΔTRAP and ΔTLP/ΔS6) and triple knockout lines (ΔTRAP/ΔTLP/ΔS6) in *Plasmodium berghei*. Subsequently, I analysed the generated knockout lines *in vitro* and *in vivo* to detect potential synergistic or antagonistic effects.

2 Materials

2.1 Technical equipment

Device	Manufacturer
Amaxa Nucleofector II	Lonza, Germany
Analytic balance TE124S-OCE	Sartorius, Germany
Axiostar plus transmitted-light microscope	Zeiss, Germany
Axiovert 200M inverted microscope	Zeiss, Germany
Balance EW600-2M	Kern, Germany
Binocular SMZ 1500	Nikon, Japan
Centrifuge 5417 C	Eppendorf, Germany
Centrifuge Galaxy Mini	VWR, Germany
Centrifuge Labofuge 400e	Heraeus, Germany
Centrifuge Multifuge 1 S-R	Heraeus, Germany
Centrifuge Pico 17	Heraeus, Germany
CO_2 incubator MCO-17AI	Sanyo, Japan
Electrophoresis power supply E831	Consort, Belgium
Electrophoresis power supply EV231	Consort, Belgium
Heat block neoBlock 1	neoLab, Germany
Hotplate stirrer CB162	Bibby Scientific, UK
Incubator MIR-253	Sanyo, Japan
Microcentrifuge Capsule HF-120	Tomy Seiko, USA
Microwave oven	Medion, Germany
Mobile drive 500 GB	LaCie, USA
Mosquito cages	BioQuip Products, USA
Neubauer improved chamber	Brand, Germany
Nikon coolpix 5400	Nikon, Japan

Pipetus	Sigma-Aldrich, Germany
Safety cabinet Herasafe KS 15	ThermoScientific, Germany
Shaking incubator Multitron 2	Infors, Switzerland
Thermal cycler 3Prime	Bibby Scientific, UK
Thermal cycler Mastercycler 5341	Eppendorf, Germany
UV-table UVT-28 L	Herolab, Germany
Vacuum pump N86KN.18	Neuberger, Germany
Vibrating Shaker REAX top	Heidolph, Germany
Waterbath Isotemp 210	Fischer Scientific, Germany

2.2 Computer Software

Program	Manufacturer
Adobe Illustrator CS5.1	Adobe Systems, USA
Adobe Photoshop CS5.1	Adobe Systems, USA
AxioVision	Zeiss
E.A.S.Y Win 32	Herolab
EndNote X6	Thomson Reuters
FIJI	https://fiji.sc/
GraphPad Prism	GraphPad Software, USA
Mendeley Desktop	Mendeley Ltd., USA
Microsoft Office 2010	Microsoft Corporation
SnapGene	GSL Biotech, USA
Volocity	PerkinElmer, USA

2.3 Consumables and reagents

Consumable	Manufacturer
24 well cell culture plate	Greiner Bio-One, Germany
96 well optical plates	Thermo Scientific, USA
Cell culture dishes	Greiner Bio-One, Germany
Cell culture flasks	Greiner Bio-One, Germany
Chamber slides	Thermo Scientific, Denmark
Cover slips	Roth, Germany
Cryo tubes	Greiner Bio-One, Germany
Insulin syringes	Becton Dickinson, France
Latex gloves	Semperit, Austria
Mattek glass bottom dishes	MatTEK corporation, USA
Microscope slides	Marienfeld
Needles	Becton Dickinson, Ireland
Nitrile gloves	Ansell, Belgium
Parafilm	Bemis, Belgium
Pasteur pipettes	Corning, USA
PCR tubes	Thermo Scientific
Pestles	Bel-Art Products, USA
Pipette tips	Steinbrenner Laborsysteme, Germany
Plastic pipettes 5 ml, 10 ml, 25 ml	Greiner Bio-One, Germany
Reaction tubes 0.5 ml, 1.5 ml, 15 ml, 50 ml	Sarstedt, Germany
Reaction tubes 2 ml	Greiner Bio-One, Germany
Sterile filter	Merck Millipore, Ireland
Syringes	Becton Dickinson, Spain

2.4 Chemicals

Chemical, reagent	Manufacturer
1 kb DNA ladder	New England Biolabs, Germany
2-Propanol	Sigma-Aldrich, Germany
Accudenz	Accurate Chemical & Scientific Corporation, USA
Acetic acid	Sigma-Aldrich, Germany
Agarose NEEO ultra-quality	Carl Roth, Germany
Albumin Fraktion V (BSA)	Carl Roth, Germany
Alsever's solution	Sigma-Aldrich, Germany
DMEM	Invitrogen, Germany
Ethanol > 99.8%	Sigma-Aldrich, Germany
Ethylenediaminetetraacetic acid (EDTA)	Sigma-Aldrich, Germany
Fetal bovine serum (FBS)	Invitrogen, Germany
Gel loading dye purple (6x)	New England Biolabs, Germany
Giemsa's azur eosin methylene blue solution	Merck, Germany
Glycerol 99%, water-free	Sigma-Aldrich, Germany
Glycine	AppliChem, Germany
HEPES	Carl Roth, Germany
Hydrochloric acid (HCl)	Merck, Germany
Immersion oil	ZEISS, Germany
L-Glutamine	Sigma-Aldrich, Germany
Mercury dibromo fluorescein disodium salt (Mercurochrome)	Sigma-Aldrich, Germany
Methanol	Sigma-Aldrich, Germany
$MgCl_2$ 25 mM & 50 mM	Thermo Scientific, Germany
Midori Green	NIPPON Genetics EUROPE, Germany

Nonidet P40 (NP-40)	AppliChem, Germany
Nycodenz	Axis-Shield PoC, Norway
Paraffin 50-52 °C reinst	Carl Roth, Germany
Paraformaldehyde (PFA)	Riedel-de Haen, Germany
Phosphate-buffered saline (PBS) tablets	Thermo Fisher Scientific, Germany
Potassium chloride (KCl)	AppliChem, Germany
Potassium hydroxide (KOH)	Riedel-de Haen, Germany
RPMI-1640	PAA, Austria
Saponin	Sigma-Aldrich, Germany
Sodium hydroxide (NaOH)	Merck, Germany
Trisbase	Carl Roth, Germany
Tris-hydrochloride (HCl)	AppliChem, Germany
Triton X-100	Merck, Germany
Trypan blue	Sigma-Aldrich, Germany
Trypsine	c.c.pro, Germany
Tryptone	Sigma-Aldrich, Germany
Yeast extract	Sigma-Aldrich, Germany

2.5 Buffers, media and solutions

Buffers, media and solutions	Composition
Accudenz	17% (w/v) Accudenz in ddH_2O
Blocking solution	2% (w/v) BSA in PBS
DMEM complete	500 ml DMEM
	10% FBS
	2mM glutamine
Freezing solution	10% (v/v) glycerol in Alsever's solution
Giemsa staining solution	14% (v/v) Giemsa in Sörensen staining buffer

LB agar	LB medium
	1.5% (w/v) agarose
LB medium	1% (w/v) tryptone
	0.5 % (w/v) yeast extract
	1% (w/v) NaCl
	adjusted to pH 7
Mercurochrome	0.1% (v/v) Mercurochrome in PBS
NP-40	1% (v/v) NP-40 in PBS
Nycodenz	276 g/l Nycodenz
	10 mmol/l TrisHCl
	6 mmol/l KCl
	0.6 mmol Na_2EDTA
	adjusted to pH 7.5 with 5 M KOH or HCl
Permeabilisation solution	0.2 % (v/v) Triton X-100 in blocking solution
PFA	4% (w/v) PFA in PBS
RPMI-1640 + Pen/Strep	500 ml RPMI-1640
	5 ml Pen/Strep (100x)
Saponin stock solution	2.8%
	(w/v) saponin in PBS
Sörensen staining buffer	0.508 g/l KH_2PO_4
	0.11 g/l Na_2HPO_4
	adjusted to pH 7.2 with NaOH
Sporozoite activating buffer	3% (w/v) BSA in RPMI-1640
Transfection medium (T-medium)	15 ml FBS (USA) heat inactivated
	60 ml RPMI (with 25 mM HEPES)
	22,5 µl Gentamycin
Tris-acetate-EDTA buffer (TAE) 50 x	242 g trisbase,
	57,1 ml acetic acid,
	50 ml 0.5 M EDTA
	ddH_2O to 1 l

2.6 Enzymes and buffers

Enzyme, buffer	Manufacturer
10x Taq Buffer with $(NH_4)_2SO_4$	Thermo Scientific, Germany
5x Phusion GC & HF buffer	Thermo Scientific, Germany
CutSmart	New England BioLabs, Germany
Ligase	New England BioLabs, Germany
Ligase Buffer	New England BioLabs, Germany
Phusion taq	Thermo Scientific, Germany
Restriction Endonucleases	New England BioLabs, Germany
Taq DNA Polymerase (recombinant)	Thermo Scientific, Germany

2.7 Kits

Kit	Manufacturer
AccuPrep Plasmid Mini Extraction Kit	BioNeer, Korea
Amaxa Human T Cell Nucleofector Kit	Lonza, Germany
DNeasy Blood & Tissue Kit	Qiagen, Germany
High Pure PCR Product Purification Kit	Roche, Germany
QIAprep Spin Miniprep Kit	Qiagen, Germany

2.8 Drugs

Drug	Final concentration
Ampicillin	100 µg/ml
Kanamycin	50 µg/ml
5-fluorocytosine	1 mg/ml
Ketamin/ Xylazin	100 mg/ml Ketamin, 20 mg/ml Xylazin in PBS

2.9 Primers

Number	Target	Sequence (5’ - 3’)
P99	hDHFR reverse	CTAGCTAGCTTAATCATTCTTCTCATATACTTC
P104	S6 5’UTR forward	GGCTTTTAGCATTTTATTAACAATCG
P105	S6 3`UTR reverse	GGATAATCATTTTTTTCACCTGAAGC
P112	PbTLP forward	TTTTGAGAAGGTATAACCCATATTCC
P113	PbTLP reverse	TCCCCGCGGAACATCCATATTAAATAACATCG
P134	PbChr12_5’UTR forward	GAGCATACAAAAATACATGCACAC
P137	PbChr12_3’UTR reverse	TGATTTACTTCCATCATTTTGCCC
P169	PbTLP_3’UTR forward	GGAAAGAAAAACACACCCTC
P170	PbTLP_5’UTR reverse	TCCATTTTTATCATTTCCTGTGTCG
P171	TRAP 5'UTR forward	GAATACATGTAAAAAAGAGAAATTCCTTCG
P174	TRAP 3'UTR reverse	GTAAAATAAGCGATATAGAAGGGAGC
P221	S6 5`UTR reverse	CGATATCATATTTGTAATGATGCCCGCGCCG GCCCTTTACAAAAATCAAAAATAAACGG
P222	S6 3`UTR forward	CAGCTTTGCATGGGGAAAGAGTGGCTTATA GACATGGAACACAAAGAGGATAGC
P233	ef1a forward	CCCAGGGCCCAATTCTTTTCGAGCTCTTTATGC
P234	ef1a reverse	CTTGCACCGGTTTTTATAAAATTTTTATTTATTT ATAAGC
P244	CSpromotor reverse	ACGCAACCTTATATTCCTCAATTAC
P332	S6tag S6 reverse	CCGGATATCCCATCTTTATGGGCTTCGC
P512	PbDHFS_3’UTR forward	CTGTTTAAACCATCAACATTGATAGCGATATAGCG
P513	PbDHFR_3’UTR reverse	GAGTTTAAACCTGTAAAAATGTGTATGTTGTGTGC
P549	PbTRAP forward	AAGAGCAACTTTTTCTACTTCCTGACAAACTTTAG
P586	PbDHFR_3’UTR forward	CATACTAGCCATTTTATGTG
P595	QCR1_ TRAP forward	GCCATCGGGGGTGCAGAACC
P599	QCR2_TRAP reverse	TCGCTGCATTAATGATTTGCCT
P600	hDHFRyFCUbox reverse	CCCAAGCTTCAAAAAAGCAGGCTTGCCGC
P601	hDHFRyFCUbox forward	GCCGATATCCAAGAAAGCTGGGTGGTACCC

P692	DK042	GGCCCCGTTTTTCTTACTTATATATTTATACCAATTG
P759	CSpromotor forward	ACAATTGTATATATGTAAGC
P760	PbDHFS reverse	GATGTTATCTTTAATTGGCC
P850	eEF1α promotor reverse	TTCGAGAATTCGTTTACAATTTAATATTCATACTTTAAG
P960	yFCU_seq_reverse	TAATTCAAAGGGACGAGG
P961	yFCU_seq_forward	ATCCTCTGGTAATTTTTCG
P1336	cmTRAP forward	GCAAACGCATAGACATGTTTATATATGGCC
P1337	cmTRAP reverse	CATCTAGATATATATGTTAATTAATTAGTTCCAGTCG
GT	upstreamTRAP reverse	TGGGTAGGGGAAATTGTCTTACCCA
GW1	PbDHFR_3'UTR forward	CATACTAGCCATTTTATGTG
GW2	yFCU reverse	CTTTGGTGACAGATACTAC
QCR1	PbTRAP reverse	CCAAGACGTGGGGGACTACCG
QCR2	PbTRAP forward	TGCTGCAGCGCTACTTCCTGC

2.10 Organisms and mutants

Organism	Supplier
Anopheles stephensi (SDA500)	Nijmegen, Netherlands
Plasmodium berghei ANKA	isolated in Antwerp/Kasapa (ANKA) by Vincke and Lips 1948
NK65 (for CSGFP line)	isolated by Vincke et al. in New York/ Katanga 1964
XL1 blue competent cells	New England BioLabs
NMRI mice	Janvier
C57BL/6 mice	Charles River

Mutants	Origin
Coronin - KO	from Kartik Bane/ Simone Lepper
CSGFP	from R. Natarajan et al. 2001
HSP20 – KO	from Georgina Montagna
Ef1alphaGFPCSmCh (RG line)	from Dennis Klug
TLP- KO mCh	generated during this thesis
TLP/S6 - KO mCh	generated during this thesis
TLP/TRAP - KO mCh	generated during this thesis
TRAP/S6 - KO mCh	generated during this thesis
TLP/TRAP/S6 - KO mCh	generated during this thesis
TLP/S6/TRAP - KO mCh	generated during this thesis
TLP/S6 - KO mCh (TRAPcomp)	generated during this thesis

2.11 Plasmids

Plasmid	Function	Origin
Pb301 TLP-KO	TLP- KO (vector)	generated by Mirko Singer
Pb262CSmChef1ahDHFRyFCU	TLP/S6-KO (insert)	generated by Dennis Klug
PbCSmchYFCU_TLPKO	TLP-KO construct	generated during this thesis
Pb238S6KOef1aGFPhDHFR	S6-KO (vector)	generated by Mirko Singer
Pb238CSmCherryef1aGFPhDHFR_S6KO	S6-KO construct	generated during this thesis
Pb238ef1aGFPhDHFR_S6KO	S6-KO construct	generated during this thesis
TRAP KO vector_107890	TRAP-KO construct	PlasmoGEM
TRAP complementation vector	TRAP -complementation	generated by Dennis Klug

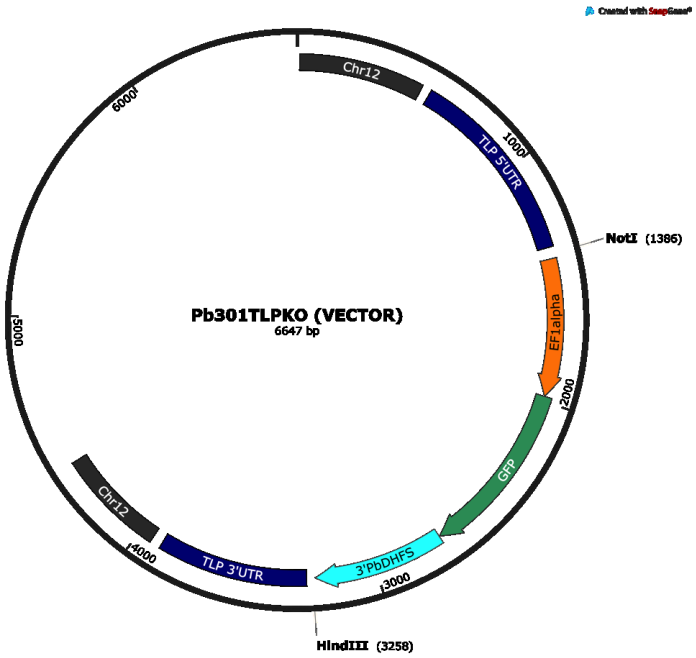

Fig. 2.1 Pb301 TLP-KO vector – This construct (provided by Mirko Singer) was used to generate the final TLP-KO construct. Indicated features: TLP 5' and 3' untranslated region (UTR), ef1α-promoter, GFP reporter gene, 3'PbDHFS, chromosome 12 integration sites and NotI/HindIII restriction sites used for cloning.

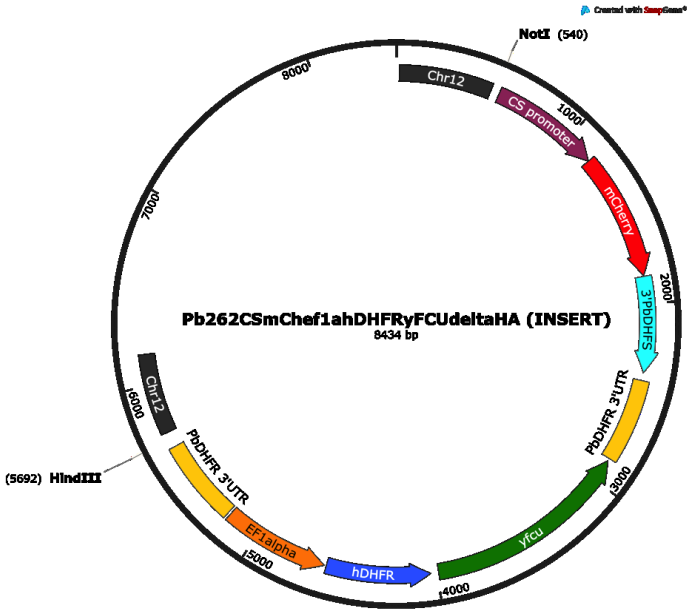

Fig 2.2 Pb262CSmChef1ahDHFRyFCUdeltaHA – This construct (provided by Dennis Klug) was used to generate the final TLP - and S6KO construct. Indicated features: chromosome 12 integration sites, CS- promoter, mCherry reporter gene, Pb DHFS, 3' untranslated region of PDHFR, ef1α-promoter, selection marker cassette (hDHFR, yFCU), NotI/HindIII restriction sites used for cloning.

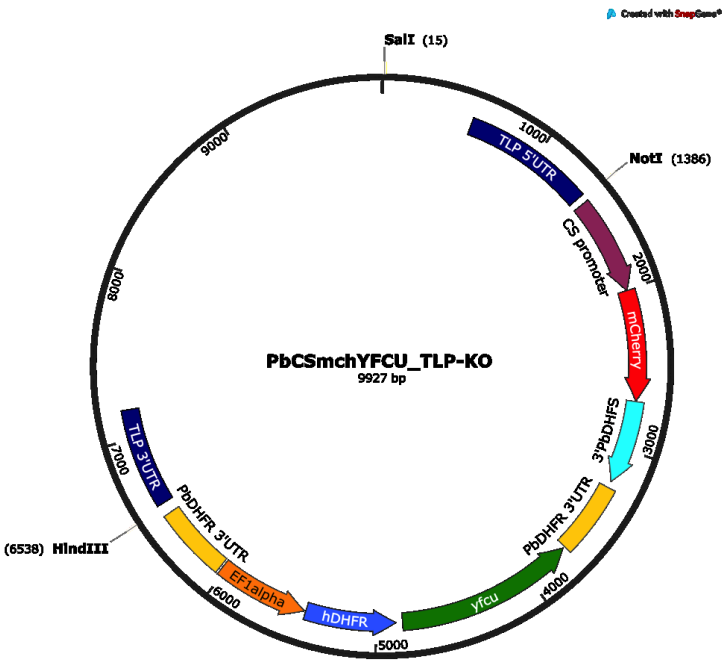

Fig 2.3 PbCSmchYFCU_TLPKO This construct (generated during this thesis) was used for generation of the TLP single, double and triple KO lines. Indicated features: TLP 5' and 3' untranslated region, CS- promoter, mCherry reporter gene, 3' PbDHFS, 3' untranslated region of PbDHFR, ef1α-promoter, selection marker cassette (hDHFR, yFCU) and NotI and HindIII restriction sites used for cloning.

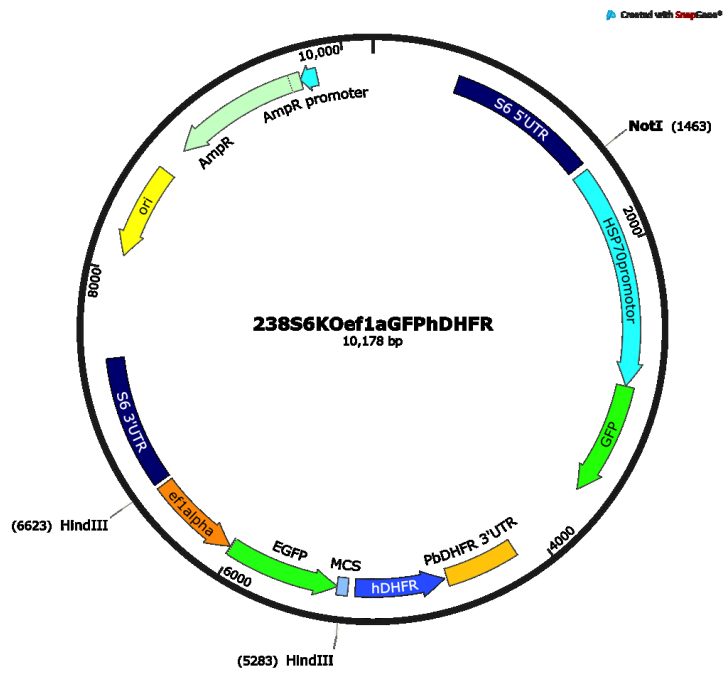

Fig 2.4 Pb238S6KOef1aGFPhDHFR This construct (provided by Dennis Klug) was used to generate the final S6-KO construct. Indicated features: Ampicillin resistance gene (AmpR) and promoter, origin, 5' and 3' UTR of S6, ef1α and HSP70 promoter, eGFP and GFP reporter genes, multiple cloning site (MCS), hDHFR selection marker, PbDHFR 3'UTR and NotI/HindIII restriction sites used for cloning.

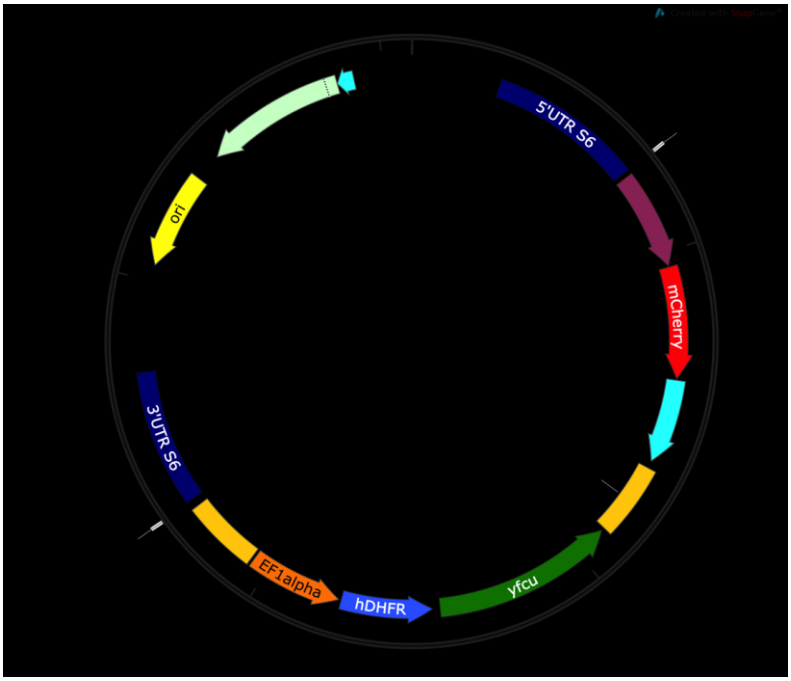

Fig 2.5 Pb238CSmCherryef1aGFPhDHFR_S6KO This construct (generated during this thesis) was used to generate the S6-KO double and triple KO lines. Indicated features: Ampicillin resistance gene (AmpR) and promoter, origin, 3' and 5' UTR of S6, CS- promoter, mCherry reporter gene, 3' PbDHFS, 3' UTR of PbDHFR, ef1α-promoter, selection marker cassette (hDHFR, yFCU) and NotI/HindIII restriction sites used for cloning.

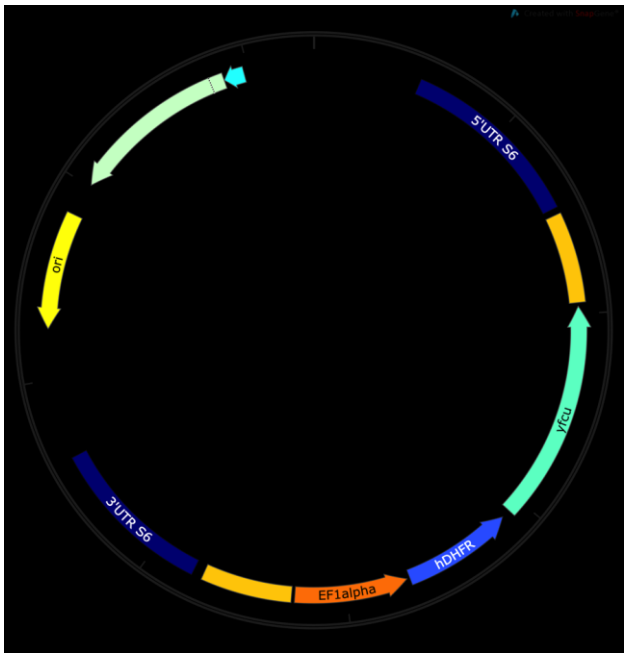

Fig 2.6 Pb238ef1aGFPhDHFR_S6KO This construct (generated during this thesis) was used to generate the S6-KO double and triple KO lines. Indicated features: Ampicillin resistance gene (AmpR) and promoter, origin, 3' and 5' UTR of S6, CS- promoter, mCherry reporter gene, 3' PbDHFS, 3' UTR of PbDHFR, ef1α-promoter, selection marker cassette (hDHFR, yFCU) and NotI/HindIII restriction sites used for cloning.

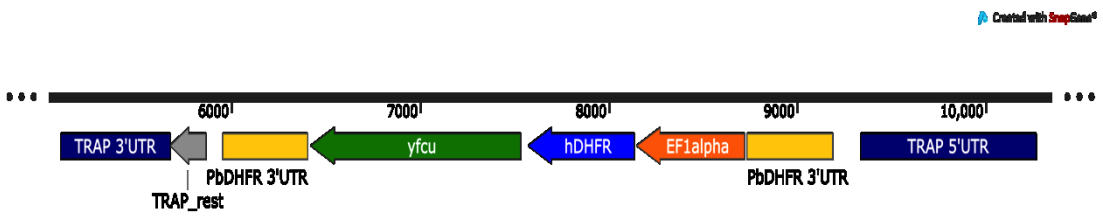

Fig 2.7 TRAP-KO vector – (134980-KO) This construct (provided by PlasmoGEM) was used to generate the TRAP double and Triple KO lines. Indicated features: 3' and 5' UTR of TRAP, ef1α-promoter and selection cassette (hDHFR, yFCU).

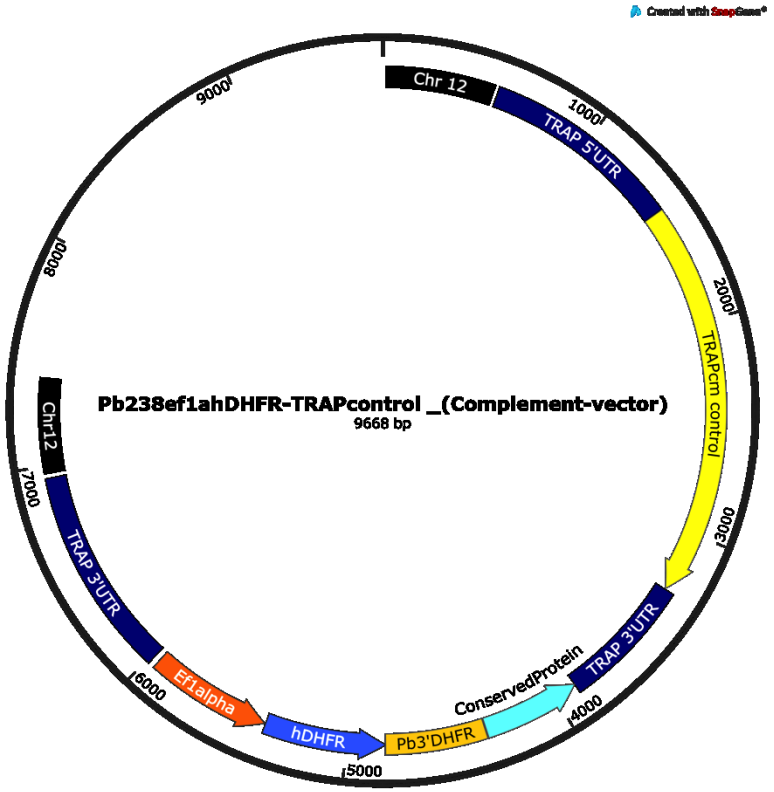

Fig 2.8 TRAP complementation vector This construct (provided by Dennis Klug) was used for generation of the 2nd TLP/S6 double KO line by complementation of the Triple KO with a codon modified TRAP gene. Indicated features: Chromosome 12 integration sites (not relevant for transfection), 3' and 5' TRAP UTR, 3'DHFR, codon modified TRAP (cmTRAP), ef1α-promoter and hDHFR selection marker.

3 Methods

3.1 Molecular biological methods

3.1.1 Polymerase chain reaction (PCR)

During this thesis, PCR was mainly used to control for correct insertion of the knockout constructs in the proposed gen loci and for preparative purposes during cloning. Further, PCR was used to amplify certain gene segments for sequencing. Phusion HF polymerase (Thermo Scientific) was used to amplify sequences during cloning as it has a reduced error rate. Taq DNA polymerase (Thermo Scientific) was used after each integration and selection step. The pipetting schemes and thermocycler conditions are listed in Table 1 - 4 below. PCR primer are listed in 2.9 of the materials part.

Component	**Volume (µl)**
5x Phusion HF buffer	10
dNTPs (2 mM)	5
Primer forward (100 µM)	0,25
Primer reverse (100 µM)	0,25
Template DNA	1
Polymerase	0,5
ddH2O	33

Table 1 Phusion polymerase PCR pipetting scheme for total volume of 50 µl.

Step	**Temperature [°C]**	**Time**	**Cycles**
Initial denaturation	98	30 s	1
Denaturation	98	30 s	30-35
Annealing	Tm*	30 s	
Extension	72	30 s/kb	
Final extension	72	5 min	1

Table 2 Thermal cycler conditions for Phusion polymerase PCR. * The annealing temperature was chosen according to the primer with the lowest melting temperature (Tm).

Component	Volume (µl)
10x Taq buffer	2,5
MgCl2	1,5
dNTPs	2,5
forward Primer (20 nM)	0,25
reverse Primer (20 nM)	0,25
Taq DNA polymerase	0,25
gDNA or plasmid	1
ddH_2O	16,75

Table 3 Taq polymerase PCR pipetting scheme for total volume of 25 µl**.**

Step	Temperature [°C]	Time	Cycles
Initial denaturation	94	90 s	1
Denaturation	94	90 s	30-35
Annealing	Tm	30 s	
Extension	60	1 min/ kb + 30 s	
Final extension	60	10 min	1

Table 4 Thermal cycler conditions for Taq polymerase PCR**.** * The annealing temperature was chosen according to the primer with the lowest melting temperature (Tm).

3.1.2 PCR product purification

PCR products and DNA fragments extracted from preparative gels were purified according to the instructions of the High Pure PCR product purification protocol Kit by Roche. The purified DNA was either diluted in 35 µl ddH_2O or dilution buffer provided in the kit.

3.1.3 Agarose gel electrophoresis

Agarose gel electrophoresis was used to determine either the length of amplified PCR products and restriction digest samples. UltraPureTM Agarose (Invitrogen) was boiled in 1x TAE buffer at a concentration of 0.8% and used to prepare the gels. DNA samples

were prepared in a mix with Gel Loading Dye Blue 6x (New England Biolabs) and Midori Green Advanced DNAStain (Nippon Genetics Europe GmbH; 1:500). After polymerization, the gel was placed into the gel chamber, the chamber was filled with 1x TAE buffer and a voltage of 90 to 150 V was applied until DNA fragments were sufficiently separated. Afterwards, the gel was documented using an UV illuminator UVT-28 L (Herolab).

3.1.4 Sequencing

Sequencing was used to verify the quality of all transfection vectors generated in this thesis. All sequencing was done by GATC Biotech (Konstanz, Sanger sequencing). Sequences were evaluated via alignment with sequences from PlasmoDB using SnapGene.

3.1.5 Transformation

Amplification of plasmids was proceeded via transformation of competent *E. coli* XL-1 Blue. *E. coli* (35 µl) were thawed on ice and mixed with 0.68 µl β-mercaptoethanol to permeabilize the cells. After ten minutes of incubation, five to ten µl of the plasmid ligation mix were added and incubated for another 30 minutes on ice. Transformation was induced using a heat shock at 42°C for 50 seconds. Afterwards, the bacterial solution was placed on ice and incubated for another two minutes and spread on LB agar plates containing ampicillin (0.1 mg/ml). The agar plates were at 37°C for about 16 hours until colonies were formed.

3.1.6 Plasmid purification

Plasmid DNA was purified using the Fast-N-Easy Plasmid Purification Kit (Jena Bioscience). Bacterial colonies were picked from overnight cultures and DNA was prepared according to the provided manufacturer protocol. After purification, DNA was eluted in either 40 µl ddH2O or the provided elution buffer. The DNA samples were either stored at -20°C or used for transfection.

3.1.7 Restriction digest

Restriction digests were used during generation of the knockout constructs and linearization of constructs prior to transfection. All enzymes used in this thesis were ordered at New England Biolabs. Digests were performed according to the manufacturer protocol (Table 5). Incubation times varied from 1.5 to 3 hours at 37°C or were kept at room temperature overnight.

Component	**Volume (µl)**
Mini Prep (purified plasmid DNA)	35 (35)
10x CutSmart buffer	5 (10)
restriction enzyme	0,2 (1)
ddH_2O	10 (54)

Table 5 Restriction digest for complete volume of 50 or 100 µl.

3.1.8 Ligation

Ligations of about 1 µg DNA was conducted by mixing vector and insert at a molar ratio of 1:1, 1:3 and 1:10. T4 DNA Ligase Buffer, T4 DNA Ligase and ddH_2O were added according to the manufacturer protocol (New England Biolabs, table 6). The reaction was incubated at room temperature for about 2 hours or at 4°C overnight.

Component	**Volume (µl)**
T4 DNA Ligase Buffer (10X)	2
Vector DNA	50 ng (0.020 pmol)
Insert DNA	37.5 ng (0.060 pmol)
T4 DNA Ligase	1
ddH_2O	to 20 µl

Table 6 Ligation for complete volume of 20 µl.

3.2 Parasitological methods

3.2.1 Schizont culture

For transfection of constructs into *P. berghei* parasites a blood stabilate of either WT PbANKA or the respective receiver line was injected i.p. into a NMRI mouse about four to five days before transfection. When parasitemia reached between 2-3%, the mouse was bled by cardiac puncture, 10 ml T-medium as well as 250 µl heparin were added and the sample was centrifuged at 1000 rpm for 8 minutes. After centrifugation, the supernatant was discarded and the blood pellet was resuspended in 10 ml T-medium. As a next step, the suspension was transferred to a cell culture flask (T175) containing 28 ml T-medium. The blood culture was placed in an incubator at 37 °C for a period of 18-20 h (90% N_2, 5% O_2 and 5% CO_2). After incubation, a blood smear was prepared and stained to control for successful schizont formation. The blood culture was transferred to a falcon tube (50 ml) and underlaid with prewarmed 55% Nycodenz® solution (37 °C). After centrifugation for 25 min at 10.000 rpm (without break), the brownish interphase layer between Nycodenz® solution and T-medium (containing the schizonts) was transferred into a falcon tube (15 ml). 10 ml of T-medium was added and the sample was centrifuged for 10 min at 1000 rpm (Heraeus Multifuge 1S-R). The supernatant was discarded and the schizont pellet was resuspended in the respective amount of T-medium (1 ml per transfection).

3.2.2 Transfection and isolation of blood stage parasites

For integration of the generated knockout constructs into the *P. berghei* genome, prepared schizonts were transfected using the Amaxa electroporator. For each transfection, 100 µl nucleofector (Amaxa Nucleofector Kit by Lonza) was added to 45 µl purified and linearized construct DNA followed by centrifugation at 13000 rpm for 15 s (Heraeus Biofuge pico). After centrifugation, the pellet was resuspended with DNA and transferred to a cuvette (provided in the kit). Electroporation was carried out by placing the cuvette in the Amaxa electroporator using program U33. Afterwards, 50 µl T-medium was added to the sample and the total volume was injected i.v. into a NMRI mouse. On the next day, drinking water of the mouse was replaced with water

containing pyrimethamine (0.07 mg/ml) for positive selection for about 7-10 days. Pyrimethamine inhibits the dihydrofolate reductase (DHFR) of protozoans – an enzyme important in the folic acid metabolism - and causes the death of untransfected parasites. However, parasites that integrated the provided construct DNA also likely integrated the *human* dhfr gene contained in the marker cassette in turn leading to resistance of the parasite to pyrimethamine (Orr et al. 2012). After mouse blood parasitemia was detected to be above 2%, the mouse was bled and blood stabilates were stored in liquid nitrogen. The rest of the blood (0,5 – 1 ml) was mixed with 13 ml PBS containing about 0.03% saponin for erythrocyte lysation. After centrifugation at 2800 rpm at 4°C, the pellet containing the parasites was resuspended in 1 ml PBS and centrifuged once more at 7000 rpm at 4°C. The resulting pellet was resuspended in 200 µl PBS and gDNA was extracted by using the DNeasy blood and tissue kit (Qiagen) according to the manufacturer's instructions.

3.2.3 Negative selection

Negative selection was performed to kill parasites that contain the selection cassette to allow for introduction of multiple genetic manipulations (Braks et al. 2006; Orr et al. 2012). The selection cassette used in this thesis contains the yFCU gene which encodes the bifunctional *yeast* derived enzyme consisting of cytosine deaminase and uridyl phosphoribosyl transferase (UPRT). This enzyme metabolizes 5 fluorocytosine (5-FC) into 5-fluorouracil which is toxic to the parasite unless the selection marker cassette is randomly "looped out" via homolog recombination. To start a negative selection, a blood stabilate of a "parental parasite line" containing a selection cassette within its genome was injected i.p. into two naïve NMRI mice. 5-FC (1 mg/ ml) was applied via the drinking water from day 3 after injection. As 5-FC is light sensitive, fresh drinking water containing 5-FC was prepared every three days in opaque drinking bottles. When parasitemia reached about 1%, the positive mice were bled via cardiac puncture. Blood stabilates were prepared and stored in liquid nitrogen. The rest of the blood was used for gDNA preparation.

3.2.4 Limiting dilution

Limiting dilution was performed to generate a clonal parasite line from a mixed parental line via injection of statistically less than one parasite into a single mouse. Limiting dilution was done after each positive and negative selection. A blood stabilate of the respective parental line was injected into a “donor” NMRI mouse. On the next day, selective pressure was applied via administration of pyrimethamine or 5-FC via the drinking water. When blood parasitemia reached between 0.3 – 1%, the mouse was bled via cardiac puncture and diluted in PBS to a final concentration of 0.7 parasites per 100 µl. Afterwards, eight naive NMRI mice were injected i.v. with 100 µl (0.7 parasites) each. Blood parasitemia was controlled via blood smears from day 7 onwards after the injection. Once parasitemia reached between 1 and 3%, mice were bled via cardiac puncture and blood stabilates were stored in liquid nitrogen.

3.2.5 Parasitemia determination

Blood parasitemia was determined by using a small drop of blood taken after puncture of the mouse tail with a needle. The blood drop was transferred to a glass slide and smeared by use of the edge of another glass slide. The blood smear was allowed to dry on air and was fixed in methanol for about 10 s. Subsequently, the blood smear was incubated in Giemsa solution for a period of 20 min. The slide was quickly rinsed with tap water and observed using a light microscope (Axiostar plus transmitted-light microscope, Zeiss) and the 100x oil immersion objective. Parasites of a minimum of 10 fields were counted and parasitemia was calculated using the formula below.

$$P = \frac{infected\ erythrocytes\ x100}{\frac{total\ erythrocytes}{counted\ fields}}$$

Formula 1 Calculation of the parasitemia. P = parasitemia [in %]

3.2.6 Cardiac puncture and generation of stabilates

Blood was directly taken from the heart by cardiac puncture. Therefore, the mouse was anesthetized by i.p. injection of Ketamine (100 mg/ml)/Xylazine (20 mg/ml) (100 µl per 25 g body weight) and the toe withdrawal reflex was used to test if the animal was anesthetized. The dead volume of a 1 ml syringe was filled with heparin to prevent blood from clotting. Next, blood was taken from the heart using the syringe and the mouse was killed via cervical dislocation. For blood stabilates, 100 µl of blood was mixed with 200 µl precooled freezing solution in a cryotube on ice and stored in liquid nitrogen.

3.2.7 Injection of mice

Injection of mice was either carried out intraperitoneal (i.p.) or intravenously (i.v.) into one of the tail veins. For i.v. injection a maximum volume of 100 µl was injected whereas during i.p. injection the maximal injected volume did not exceed 200 µl. During blood stabilate injection (i.p) a distinct number of parasites was injected using the formula below.

$$V = \frac{20\ x\ 10^6\ infected\ erythrocytes}{P\ x\ 7\ x\ 10^6\ erythrocytes\ per\ \mu l}$$

Formula 2 Example formula used to inject 20 mio. infected erythrocytes. P = parasitemia [in %], V = injection volume [in µl]

3.2.8 Infection of mosquitoes

To prepare infection of *A. stephensi* mosquitoes with *P. berghei* parasites, a blood stabilate was injected i.p. into two NMRI mice. When blood parasitemia reached about 2-3% (usually day five after injection), a drop of blood was taken via needle puncture of each mouse tail, transferred to a glass slides and covered with coverslips. After incubation at room temperature or on top of the ice machine for about 10 minutes, the blood samples were checked for exflagellation events (Zeiss Axiostar plus, 40x objective, air). When at least 2 – 3 exflagellation events per field of view were

observable, infected mice were anaesthetized via i.p. injection of 100 µl ketamine (100 mg/ml) /xylazine (20 mg/ml) solution per 25 g body weight and placed on top of an uninfected mosquito cage containing about 200 – 300 mosquitoes for about 20 minutes. During this time, mice were turned from dorsal to ventral and back after 5 minutes. For optimal results, this procedure was repeated on the following day. Afterwards, mice were killed via cervical dislocation and the mosquito cage was placed in an incubator at 21°C. To ensure high biting frequencies of the mosquitoes sugar pads were removed about 16 - 24h before the cage feed.

3.2.9 Mosquito dissection

Mosquitoes were dissected between day 12 and 25 after the blood meal. For dissection, mosquitoes were transferred into a 15 ml falcon tube and incubated on ice for about 5 minutes. Next, the mosquitoes were rinsed with 70% ethanol, transferred to a glass slide with a drop of PBS and observed under the SMZ 1500 binocular microscope (Nikon). Female mosquitoes were identified and dissected with two syringe cannulae. In case of a fluorescent parasite line, infected mosquitoes were preselected by use of the respective fluorescent light. One cannula was used to fixate the mosquito thorax while the last two to three segments of the abdomen were cut off and the midgut was exposed. Subsequently, the midgut was transferred to an Eppendorf tube containing 50 µl RPMI with 3% BSA. Next, the mosquito head was pulled from the thorax and the salivary glands were isolated and transferred to a separate Eppendorf tube again containing RPMI with 3% BSA. Hemolymph of the mosquitos was collected on two days between day 14 and 16 after the blood meal. As described above mosquitoes were quickly rinsed in ethanol and transferred to a glass slide. To collect hemolymph parasites, the tip of a pasteur pipette was stretched using a bunsen burner flame resulting in a thin pipette tip. The tip was injected into the mosquito thorax after removing the last two segments of the abdomen and RPMI with 3% BSA was injected via the pipette until a drop formed at the cut mosquito abdomen. This drop (about 30 to 50 µl per mosquito) contained the mosquito hemolymph was collected on a piece of parafilm and transferred to an Eppendorf tube.

3.2.10 Counting of oocysts and sporozoites

Midgut oocysts were counted on day 12 after the bloodmeal. Oocysts numbers of fluorescent lines were counted manually using epifluorescence and the SMZ 1500 binocular microscope (Nikon). Sporozoite numbers of midgut, salivary gland and hemolymph were counted using a hemocytometer (Neubauer improved). The collected midgut and salivary glands of at least ten infected mosquitoes were smashed with a pestle in a volume of 50 µl RPMI/ 3% BSA each. Next, midgut and salivary gland solutions were diluted 1:2 and 1:5 respectively and 10 µl each were transferred to the hemocytometer. Sporozoites were allowed to settle for 5 minutes, counted and the total number of sporozoites per midgut and salivary gland was calculated. For counting of hemolymph sporozoites, hemolymph of at least ten infected mosquitoes was centrifuged at 13.000 rpm (Centrifuge Pico 17, Heraeus) for one minute and supernatant was discarded until 100 µl was left in the Eppendorf tube. Sporozoites were resuspended, transferred to the hemocytometer and counted as described before.

3.2.11 Mercurochrome staining

Mercurochrome staining was performed to stain WT PbANKA infected midguts to be able to count oocysts. Midguts were dissected into a 24 well plate filled with 1.5 ml PBS on day 12 after the blood meal. For permeabilization, PBS was replaced with 1 ml NP-40 (1%) and midguts were incubated for 20 minutes at room temperature. Afterwards, NP-40 was replaced by 1 ml 0,1% mercurochrome (0,1%) in PBS and incubated for 30 minutes to stain the oocysts (Sinden et al. 2002). After the staining, midguts were washed four times with PBS, transferred to a glass slide. A cover slip was applied, sealed with wax and midguts were observed using the 10x air objective of the Zeiss microscope (Axiovert 200M). Oocysts numbers were counted manually applying a green filter in the DIC channel.

3.2.12 Sporozoite motility assays

To examine movement patterns of sporozoites, gliding assays of hemolymph and salivary gland sporozoites were performed at various days (in between day 14 to 19) after the bloodmeal. Hemolymph and salivary glands of at least ten infected mosquitoes were collected as described before (3.2.9). Salivary glands were smashed with a pestle in an Eppendorf tube containing 50 µl PBS. The released sporozoites were pelleted at 10.000 rpm for 3 minutes (Centrifuge Pico 17, Heraeus) and resuspended in 100 µl RPMI with 3% BSA. Hemolymph sporozoites were also pelleted at 10.000 rpm and taken up in 100 µl RPMI containing 3% BSA. The sporozoite solutions were transferred to a 96 – well microtiter plate and centrifuged for 3 minutes at 1.000 rpm (Centrifuge Multifuge 1 S-R, Heraeus). Next, sporozoite motility was imaged in the DIC and mCherry channel using the 10x objective (NA 0.5, air) and 25x objective (NA 0.8, water) of the Axiovert 200M (Carl Zeiss GmbH, Jena, Germany) epifluorescence microscope. Time-lapse videos were taken at one frame per three seconds for a total of five minutes per video and analysed with Fiji (ImageJ, SciJava). Sporozoites were classified into several categories. “Drifting” sporozoites did not attach during the observed time und were floating in the solution close to the glass surface. “Attached” sporozoites were either attached with one or both ends or with the complete body, but did not migrate on the surface. “Gliding” sporozoites were migrating rather continuously at the surface in a circular manner and did not stop for more than 30 seconds (Hegge et al. 2009). “Patch gliding” sporozoites were moving back and forth in a star-like pattern over the same adhesion spot (Münter et al. 2009). Gliding sporozoites were observed to migrate in circles in both directions – clockwise and counterclockwise – although the majority (> 90%) of sporozoites were moving counterclockwise. Gliding speed was analysed using the Manual Tracking plugin of Fiji. Gliding sporozoites were tracked for at least 60 frames (3 minutes) to calculate the average speed.

3.2.13 *In vivo* sporozoite infectivity

To examine if the generated parasite mutants can infect naive C57BL/6 mice, either infected mosquitoes were allowed to bite the mice or isolated hemolymph or salivary

gland sporozoites were injected i.v. into the tail vein of the mice. Experiments were performed on day 16 – 19 after the blood meal. For natural transmission experiments, at least 40 infected mosquitoes were preselected on ice using the abdominal mCherry signal of the oocysts, transferred to a cup with a net cover and starved overnight. For each experiment, four mice were anesthetized via i.p. injection of K/X solution (100 µl/ 25 g body weight). Ten infected mosquitoes per mouse were allowed to bite for 15 minutes. Afterwards, the blood-filled mosquitoes were dissected and the average number of salivary gland sporozoites per mosquito was calculated (3.2.10). For i.v. injections either 10.000 hemolymph or 100 salivary gland sporozoites per mouse were diluted in 100 µl RPMI with 3% BSA and injected into the tail vein. Prepatency was checked from day 3 onwards via thorough observation of Giemsa stained blood smears. Mice were sacrificed on day 4 after the first blood stage parasites were detected.

3.2.14 Preparation and imaging of salivary glands

For imaging, infected salivary glands were isolated as described in 3.2.9. Salivary glands were carefully cleaned in PBS to remove the attached tissue and transferred to a MatTek glass bottom dish (MatTek corporation) in a small drop of about 10 µl RPMI containing 3% BSA. The RPMI/ BSA medium was always freshly prepared and contained 10 µg/ml Hoechst as well as 1 µg/ml wheat germ agglutinin-594 (WGA-594, Thermo Fisher). Hoechst was used to stain the DNA of the acinar cells of the salivary gland and sporozoites. Wheat germ agglutinin is a lectin which binds to sialic acid and N-Acetylglucosamine and was used to stain the basal membrane of the mosquito salivary glands as well as plasma membranes of the acinar cells. Up to five salivary glands were transferred to a single MatTek dish and a cover slip was carefully applied. Samples were observed using a Nikon TE 2000-E microscope equipped with an Ultra View ERS spinning disc confocal unit (Perkin-Elmer) with the 20x (NA=0.85, oil), 60x (NA 1.49, oil) and 100x (NA 1.4, oil) objectives. Images and time lapse videos were taken using the RFP channel (561 nm laser) to detect the WGA-594 or mCherry signal, the DAPI channel (405 nm laser) to detect the Hoechst signal, the GFP channel (488 nm laser) to detect GFP expressing sporozoites and the DIC channel. All images were acquired using the Volocity 5.0 software (Improvision/ Perkin Elmer).

3.3 Cloning and transfection strategy

3.3.1 Generation of transfection constructs

To generate the double and triple knockout parasites of TLP, S6 and TRAP the following three transfection vectors were created. All generated vectors were based on either the Pb238 or Pb301 transfection vector (provided by Mirko Singer) containing the 5' and 3' UTRs of TLP and S6 as well as a GFP reporter gene (Fig. 2.1 and 2.4). The final TLP-KO transfection vector (PbCSmCherryYFCU_TLP-KO) was planned to contain the 5' and 3' UTRs of TLP, the hDHFR-yFCU selection marker cassette (Braks et al. 2006), which would allow for positive-negative selection and the mCherry reporter gene. To create this construct, we made use of the Pb262 vector (provided by Dennis Klug) containing the selection cassette and the reporter gene mCherry under control of the *CSP* promoter (Fig. 2.2). Using the respective *HindIII* and *NotI* restriction sites of both plasmids the GFP reporter gene of Pb301 was replaced by the selection cassette and the mCherry reporter gene of the Pb262 plasmid to create the final TLP-KO transfection plasmid (Fig. 2.3). The S6-KO transfection vector (PbCSmChYFCU_S6-KO) was generated in a similar way to the TLP-KO vector. Therefore, the Pb238-S6 KO construct (provided by Mirko Singer) was used containing the S6 5' and 3'UTR and an insert encoding for eGFP and hDHFR under control of the *ef1α* promoter (Fig. 2.4). As before, this insert was replaced by the *hDHFR-yFCU* selection cassette and the mCherry reporter gene of the Pb262 vector using the *HindIII* and *NotI* restriction sites (Fig. 2.5). Furthermore, a second S6-KO transfection vector (PbYFCU_S6-KO) was created lacking the mCherry reporter gene as for two of the planned knockout lines (ΔTLP/ΔS6 and ΔTLP/ΔTRAP/ΔS6) the mCherry gene would be already present in the TLP locus. In order to remove the mCherry reporter gene and the *CSP* promoter, PbCSmChYFCU_S6-KO was digested with *NotI* and *EcoRV*, blunted to get rid of any overhangs and finally re-ligated (Fig. 2.6). The TRAP-KO transfection vector (TRAP KO vector_107890) used to create the following double and triple KO mutants was ordered at *plasmo*GEM (Gomes et al. 2015; Schwach et al. 2015). It contains the 5' and 3'UTR of TRAP as well as the *hDHFR-yFCU* selection cassette (Fig. 2.7). In order to generate a second independent TLP/S6 clone the 1st Triple-KO line was complemented

with a TRAP complementation construct (generated by Dennis Klug, Fig. 2.8) encoding a codon modified TRAP.

3.3.2 Generation of parasites with adhesin double and triple knockouts

The transfection constructs described previously (section 3.3.1) were used to sequentially knockout the adhesins TRAP, S6 and TLP which are exclusively expressed in the sporozoite stage of *Plasmodium*. TLP is located on chromosome 11 whereas TRAP and S6 are located on chromosome 13 of the *P. berghei* genome. Our aim was to generate the respective double and triple knockout lines ΔTRAP/ΔS6, ΔTLP/ΔTRAP, ΔTLP/ΔS6 and ΔTLP/ΔTRAP/ΔS6. All knockout lines were created using a repeated positive/negative selection strategy (Orr et al. 2012) to allow for sequential genetic modifications (Fig. 3.1 A-C). To knockout the gene of interest (GOI) the respective transfection construct was linearized to terminally expose the flanking 3' and 5' UTRs. During transfection, the gene of interest was replaced via double crossover integration with a marker gene encoding for *mCherry* under control of the CSP promoter. Furthermore, the transfection constructs contained a resistance cassette encoding for *human* dihydrofolate reductase (*hDHFR*) as well as the negative selectable marker *yFCU* (Fig. 3.1 A). The resistance cassette allowed for positive selection of the parasites that successfully integrated the transfection construct in their genome via administration of pyrimethamine (Fig. 3.1 B). After limiting dilution, one of the resulting clonal lines was further treated with 5-fluorocytosine (5-FC) to select for parasites that looped out the selection marker cassette (Orr et al. 2012). Hence, a resistance marker free knockout line was created only containing the *mCherry* gene under control of the CSP promoter (Fig. 3.1 C) that could function as a recipient line for subsequent genetic modification. The overall transfection scheme is depicted in Figure 3.1 D. As a first step TLP was knocked out in the wild type strain *Pb*ANKA (Vincke and Lips 1948). The resulting negatively selected knockout line (ΔTLP/mCh) was further used as a recipient line to generate the TLP/TRAP and TLP/S6 double knockout lines (ΔTLP/ΔTRAP/mCh and ΔTLP/ΔS6/mCh). Both lines were used to generate two independent triple knockout lines (ΔTLP/ΔTRAP/ΔS6/mCh) by knocking out S6 or TRAP respectively. The third double knockout line lacking TRAP and S6 resulted from

transfection of the TRAP-KO line with the S6-KO construct (ΔTRAP/ΔS6/mCh). Finally, a 2nd TLP/S6 knockout line was generated by complementation of the 1st triple-KO with TRAP (Fig. 3.2).

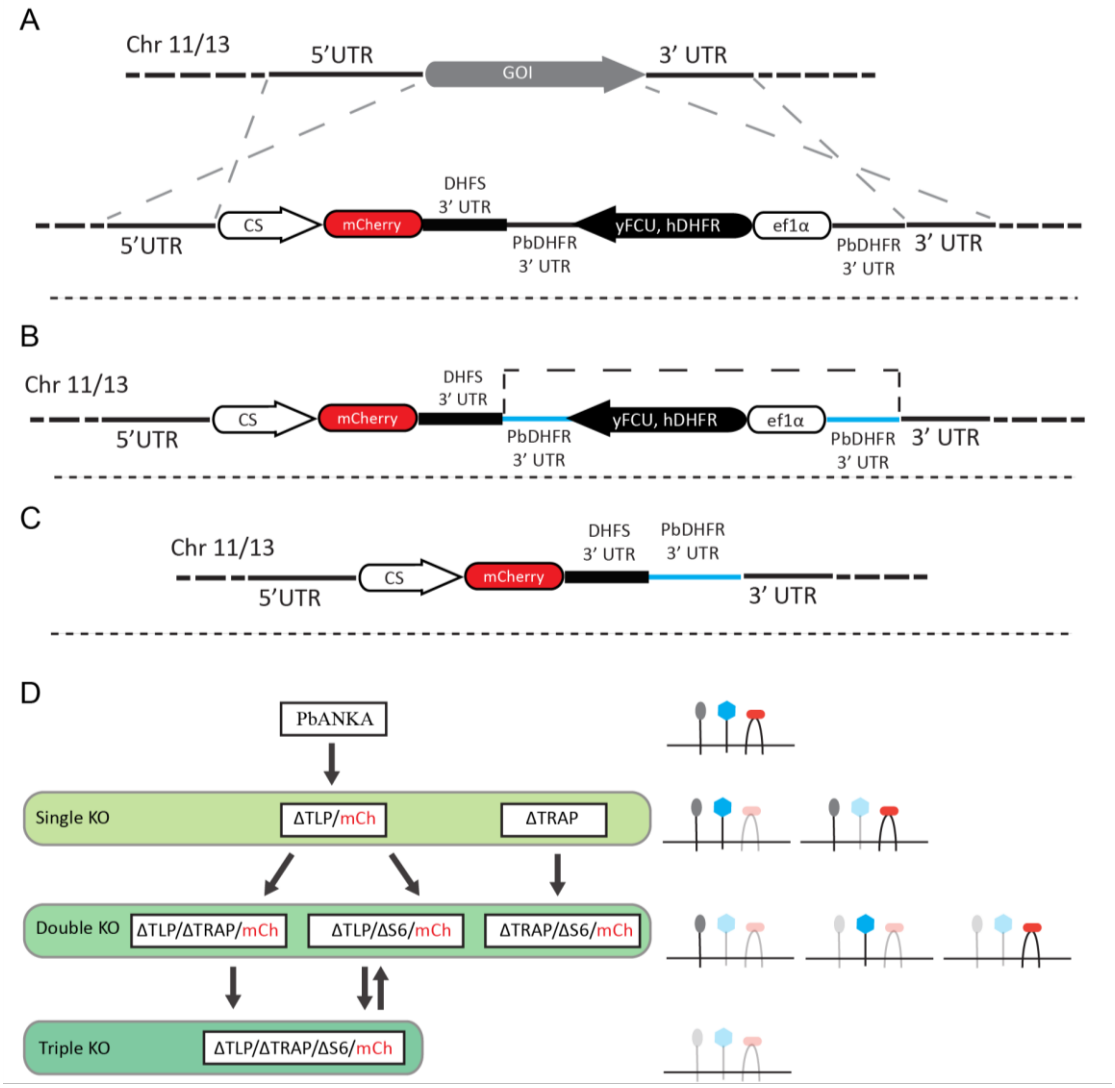

Fig. 3.1 General integration and transfection scheme of single, double and triple knockout lines lacking the proteins TRAP, TLP and S6. (A-C) Transfection strategy for gene knockout. (A) The gene of interest (GOI) is replaced via double crossover homologous recombination (grey dotted lines) with the *mCherry* marker gene under control of the CSP promoter and the resistance cassette (*yFCU/hDHFR*) allowing for positive/negative selection. The 3' and 5' untranslated regions (UTRs) of the respective gene function as recombination sites for integration. (B) Schematic representation of gene locus after successful transfection. To allow for subsequent transfections we selected for parasites that looped out the *hDHFR/yFCU* resistance cassette (grey dotted line) via negative selection with 5-fluorocytosine (5FC). (C) Locus after negative selection without selection cassette. The gene locus only contains the *mCherry* reporter under control of the *CSP* promoter, *DHFS* 3'UTR and *PbDHFR* 3'UTR. (D) Transfection scheme demonstrating subsequent generation of single, double and

triple knockout lines (left). All lines were generated in the *Pb*ANKA wild type background and contain a single *mCherry* marker gene (*mCh*). Two independent triple KO lines were generated. The cartoon next to the transfection scheme indicates the absence or presence of the respective adhesion protein. (S6 - grey, TRAP – blue, TLP – red)

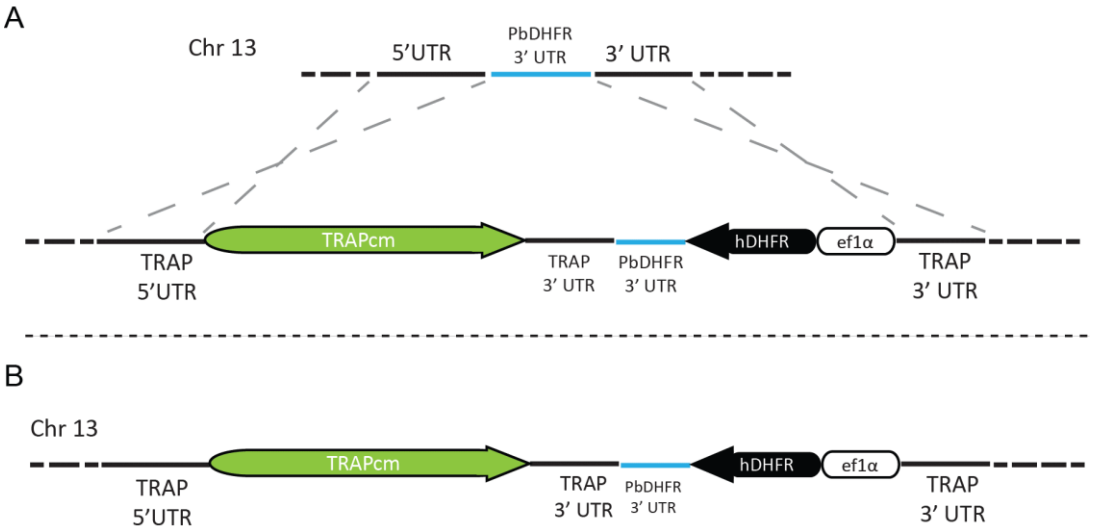

Fig. 3.2 TRAP complementation scheme for generation of an independent 2nd TLP/S6 KO. (A) A codon modified version of the TRAP open reading frame (*TRAPcm*) was integrated into the TRAP KO locus via double crossover homologous recombination (grey dotted lines). The 3' and 5' UTRs of TRAP function as recombination sites. The transfection construct contains the TRAP gene codon modified for *E. coli* K12 as well as a *hDHFR* resistance cassette under control of the *ef1α* promoter for positive selection. Codon modification was performed to differentiate wild type TRAP from the complemented TRAP via PCR. **(B)** The complemented TRAP locus after successful integration of *TRAPcm* and *hDHFR* resistance cassette.

3.3.3 Genotyping of TLP single knockout line

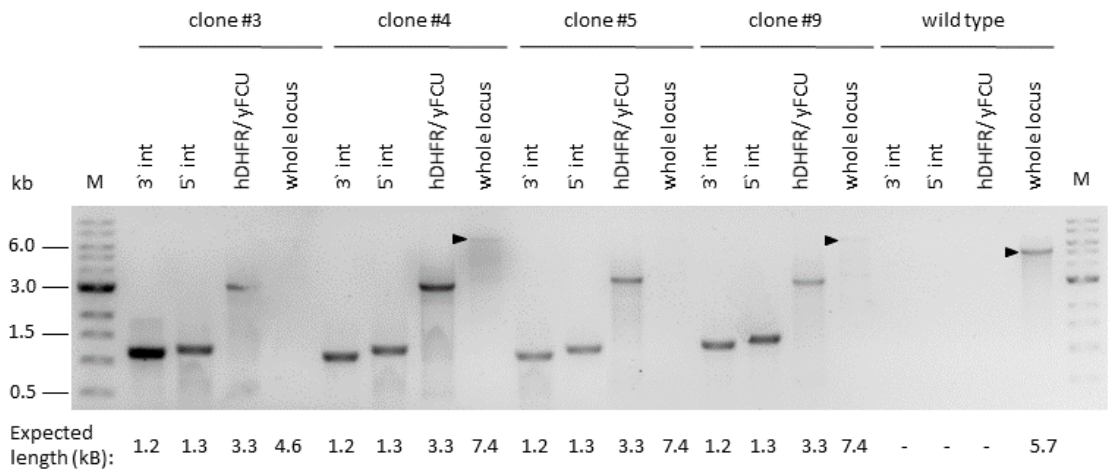

target	forward primer	reverse primer	predicted length
5’ integration	P112	P244	1.3kb
3’ integration	P586	P113	1.2kb
hDHFR/yFCU	P601	P600	3.3kb
whole locus TLP KO	P112	P113	7.4kb
whole locus WT	P112	P113	5.7kb

Fig. 3.3 Genotyping of TLP knockout clones after positive selection and limiting dilution. Expected PCR product sizes are shown below the gel image as well as in the table. Feint whole locus bands are marked with black arrowheads. Successful integration of the transfected construct is shown by amplification of the 5’ and 3’ end as well as the selection marker cassette (hDHFR/yFCU). The whole locus band was not visible for clone 3 and 5 due to difficulties in amplification of large DNA fragments. Wild type *Pb*ANKA was used as a control. M – 1 kb DNA ladder (New England Biolabs).

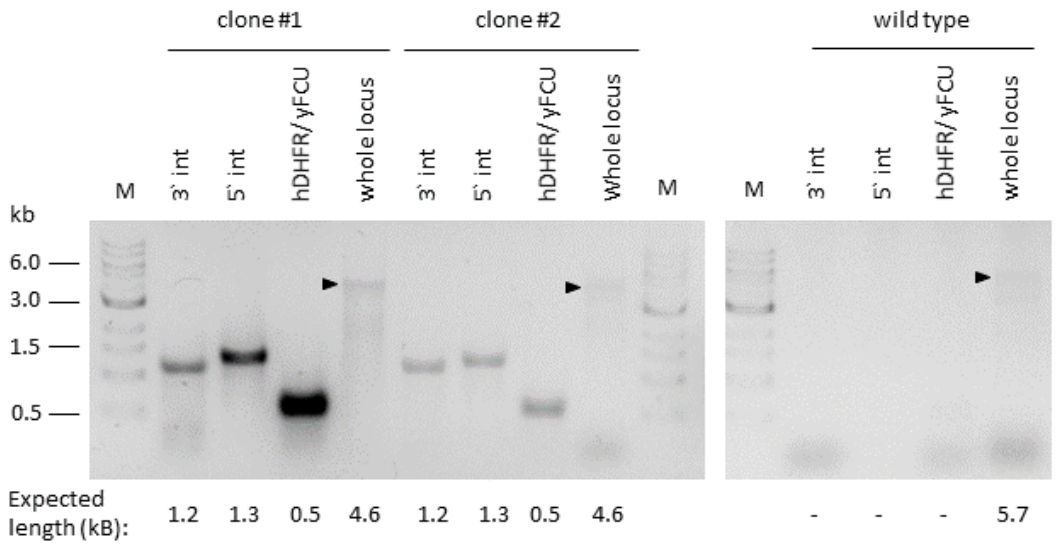

target	forward primer	reverse primer	predicted length
5’ integration	P112	P244	1.3kb
3’integration	P586	P113	1.2kb
hDHFR/yFCU	P601	P600	0.5kb
whole locus	P112	P113	4.6kb
TLP KO			
whole locus WT	P112	P113	5.7kb

Fig. 3.4 Genotyping of TLP knockout clones after negative selection and limiting dilution. Expected PCR product sizes are shown below the gel image as well as in the table. Feint whole locus bands are marked with black arrowhead

s. Successful integration of the transfected construct is shown by amplification of the 5’ and 3’ end as. The selection marker cassette (hDHFR/yFCU) of the two clones was successfully removed during negative selection as indicated by the short ampilficate (0.5 kb). Wild type *Pb*ANKA was used as a control. M – 1 kb DNA ladder (New England Biolabs).

3.3.4 Genotyping of adhesin double and triple knockout lines

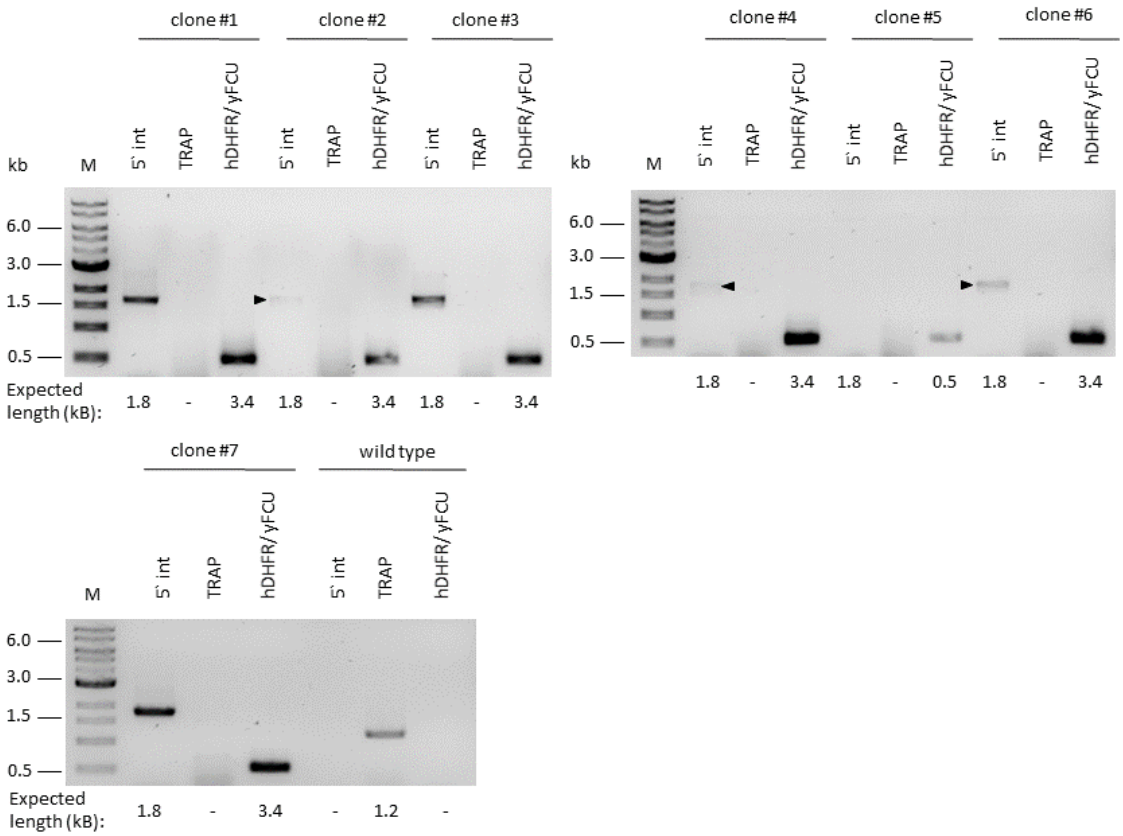

target	forward primer	reverse primer	predicted length
5’ integration	P112	P244	1.8 kb
TRAP	GW1	GT	1.2 kb
hDHFR/ yFCU	P601	P600	3.4 kb / 0.5 kb

Fig. 3.5 Genotyping of TRAP locus of TLP/TRAP knockout clones after positive selection and limiting dilution. Expected PCR product sizes are shown below the gel images as well as in the table. Feint 5’ integration bands (clone 2, 4 and 6) are marked with black arrowheads. Successful integration of the transfected construct is shown by amplification of the 5’ as well as the selection marker cassette (hDHFR/yFCU). Note that the selection marker (hDHFR/yFCU) PCR product shows a band at 0.5 kb instead of the expected 3.4 kb as the primers presumably amplified the flanking regions of the removed selection marker of the TLP locus. The 5’ integration band was not visible for clone 5. Wild type *Pb*ANKA was used as a control. M – 1 kb DNA ladder (New England Biolabs).

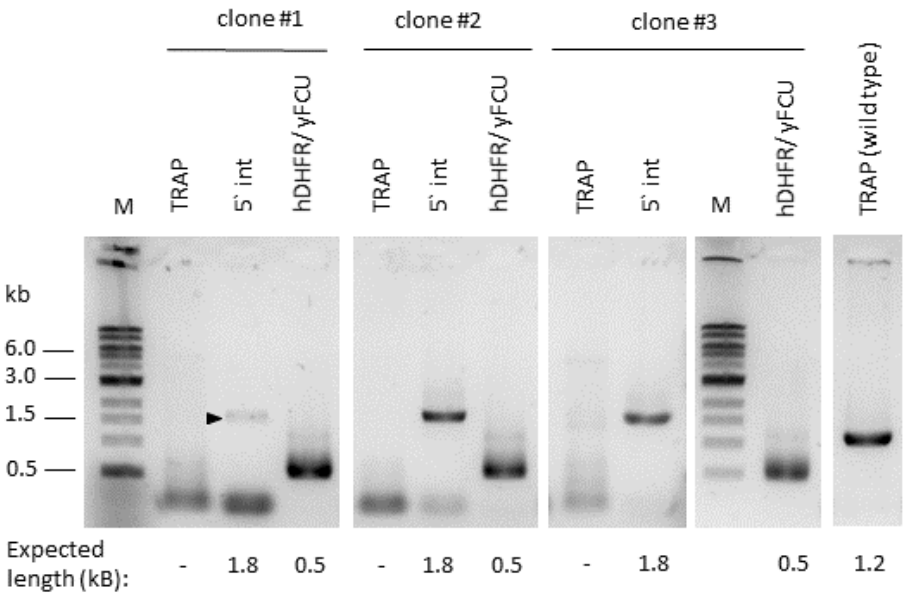

target	forward primer	reverse primer	predicted length
TRAP wild type	P599	P595	1.2 kb
5‘ integration	P586	P591	1.8 kb
hDHFR/yFCU	P601	P600	0.5 kb

Fig. 3.6 Genotyping of TRAP locus of TLP/TRAP knockout clones after negative selection and limiting dilution. Expected PCR product sizes are shown below the gel images as well as in the table. Feint 5’ integration band (clone 1) is marked with a black arrowhead. Successful integration of the transfected construct is shown by amplification of the 5’ end. The selection marker cassette (hDHFR/yFCU) of the three clones was removed during negative selection as indicated by the short ampilficate (0.5 kb). M – 1 kb DNA ladder (New England Biolabs).

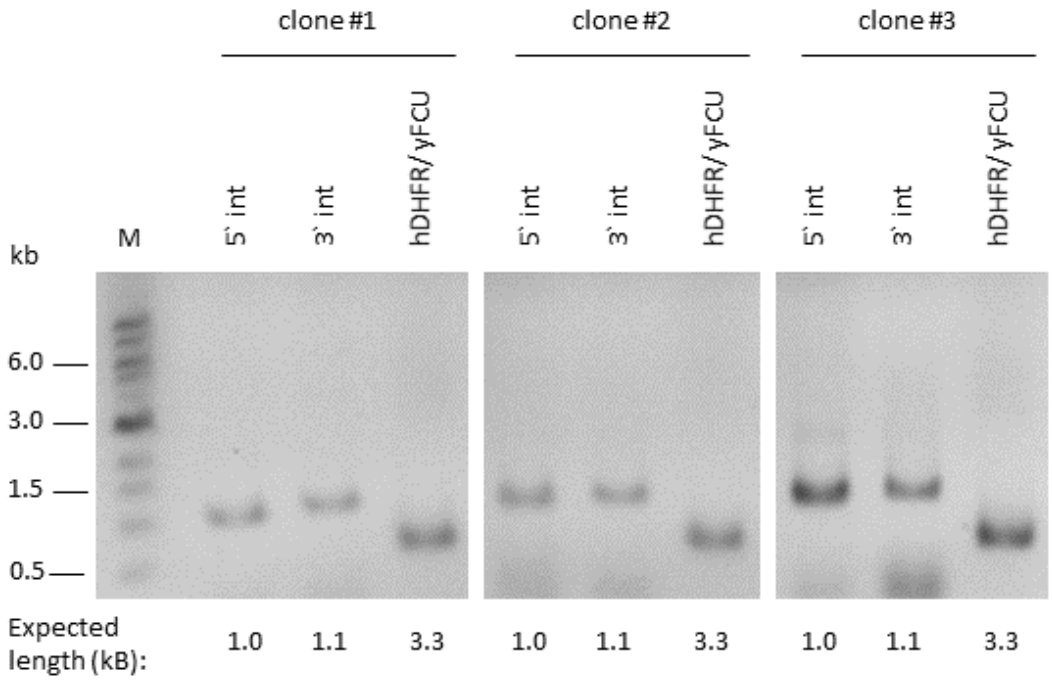

target	forward primer	reverse primer	predicted length
5’ integration	P104	P244	1.0 kb
3’ integration	P586	P105	1.1 kb
hDHFR/ yFCU	P601	P600	3.3 kb / 0.6 kb

Fig. 3.7 Genotyping of S6 locus of TRAP/S6 knockout clones after positive selection and limiting dilution. Expected PCR product sizes are shown below the gel image as well as in the table. Successful integration of the transfected construct is shown by amplification of the 5’ and 3’ ends. Note that the selection marker (hDHFR/yFCU) PCR product shows a band at 0.6 kb instead of 3.3 kb as the primers presumably amplified the flanking regions of the removed selection marker of the TRAP locus. M – 1 kb DNA ladder (New England Biolabs).

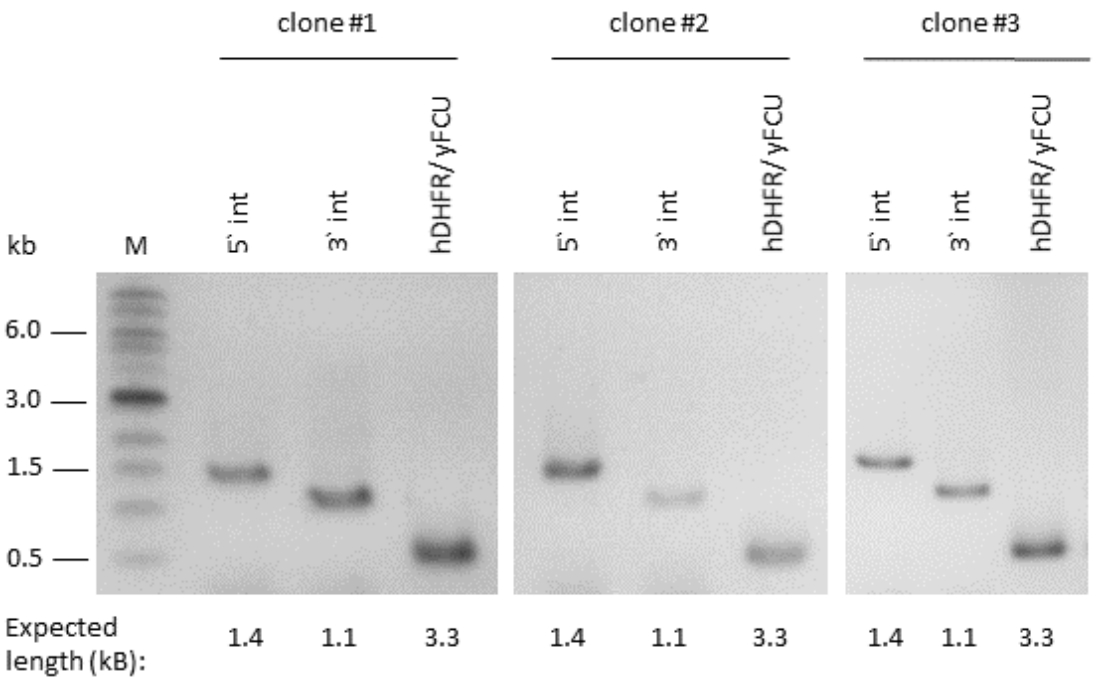

target	forward primer	reverse primer	predicted length
5’ integration	P104	P244	1.4 kb
3’ integration	P586	P105	1.1 kb
hDHFR/ yFCU	P601	P600	3.3 kb / 0.5 kb

Fig. 3.8 Genotyping of S6 locus of TLP/S6 knockout clones after positive selection and limiting dilution. Expected PCR product sizes are shown below the gel image as well as in the table. Successful integration of the transfected construct is shown by amplification of the 5’ and 3’ ends. Note that the selection marker (hDHFR/yFCU) PCR product shows a band at 0.5 kb instead of the expected 3.3 kb as the primers presumably amplified the flanking regions of the removed selection marker of the TLP locus. M – 1 kb DNA ladder (New England Biolabs).

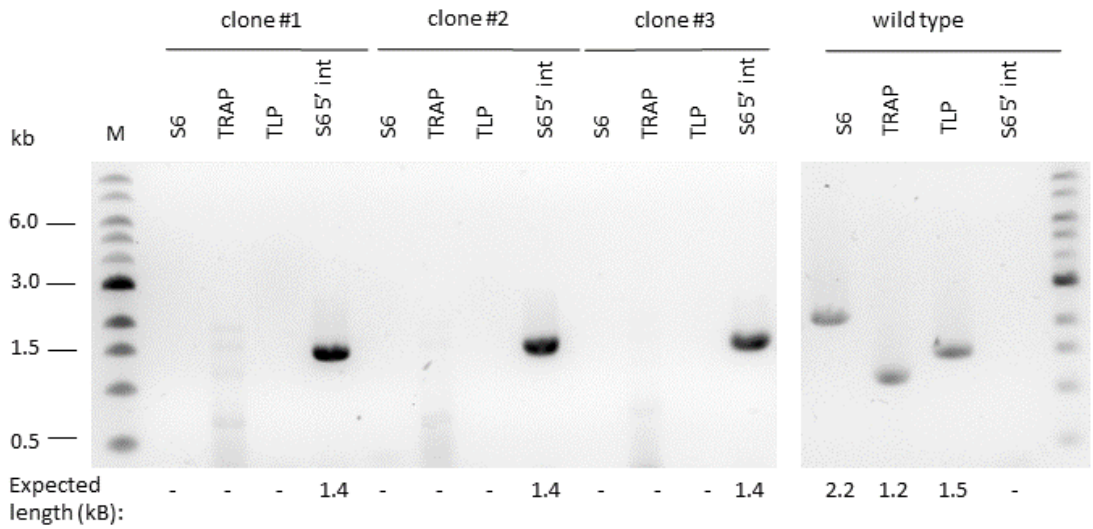

target	forward primer	reverse primer	predicted length
S6	P104	P332	2.3 kb
TRAP	P595	P599	1.2 kb
TLP	P170	P112	1.5 kb
5` integration S6	P104	P692	1.4 kb

Fig. 3.9 Genotyping of TLP/TRAP/S6 triple knockout clones after positive selection and limiting dilution. Expected PCR product sizes are shown below the gel image as well as in the table. Successful integration of the transfected S6 KO construct is shown by amplification of the 5' end as well as the lack of PCR products of S6, TRAP and TLP. Wild type *Pb*ANKA was used as a control. M – 1 kb DNA ladder (New England Biolabs).

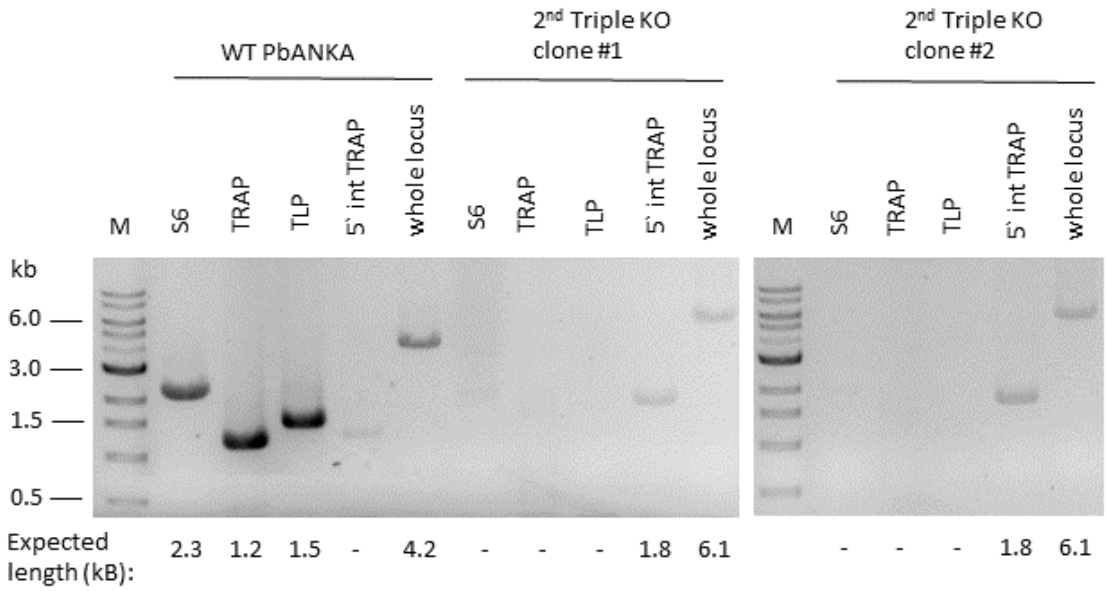

target	forward primer	reverse primer	predicted length
S6	P104	P332	2.3 kb
TRAP	P595	P599	1.2 kb
TLP	P170	P112	1.5 kb
5` integration TRAP	P586	P591	1.8 kb
Whole locus TRAP WT	P171	P174	4.2 kb
Whole locus TRAP KO	P171	P174	6.1 kb

Fig. 3.10 Genotyping of 2nd TLP/S6/TRAP triple knockout clones after negative selection and limiting dilution. Expected PCR product sizes are shown below the gel image as well as in the table. Successful integration of the transfected TRAP KO construct is shown by amplification of the 5' end as well as the lack of PCR products of S6, TRAP and TLP. Wild type *Pb*ANKA was used as a control. M – 1 kb DNA ladder (New England Biolabs).

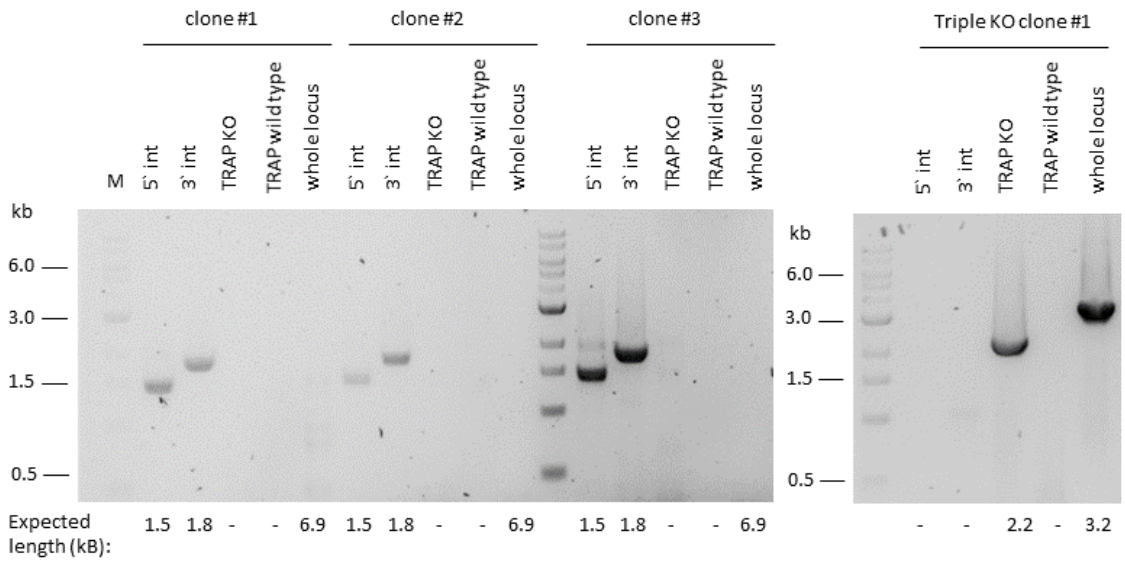

target	forward primer	reverse primer	predicted length
5’ integration	P171	P1202	1.5 kb
3’ integration	P234	P174	1.8 kb
TRAP KO	P600	P601	2.2 kb
TRAP WT	P171	P549	1.8 kb
Whole locus TRAP comp.	P171	P174	6.9 kB
Whole locus Triple KO	P171	P174	3.2 kb

Fig. 3.11 Genotyping of complemented TRAP locus of 2nd TLP/S6 knockout clones after positive selection and limiting dilution. Expected PCR product sizes are shown below the gel image as well as in the table. Successful integration of the transfected TRAP complementation construct is shown by amplification of the 5’ and 3` ends as well as the lack of PCR products of S6, TRAP and TLP. The whole locus band was not visible for the three generated clones due to difficulties in amplification of the large DNA fragments (6.9 kb). The Triple KO clone 1 used to generate the complemented TLP/S6 KO clones was used as a control. M – 1 kb DNA ladder (New England Biolabs).

4 Results

4.1 Vortex and swarm behavior

After invasion of the mosquito salivary glands, sporozoites rest in non-motile stack-like formations inside the central cavity of the lateral salivary gland lobes (Janzen and Wright 1971) (Fig. 4.1). During fresh preparation and imaging of infected salivary glands in 3% BSA/RPMI we noticed that glands can be damaged and sporozoite stacks can disintegrate. Sporozoites of these damaged glands were redistributed towards the gland periphery and started to migrate in the periphery of the gland between basal membrane and acinar cells (Fig. 4.2 and 4.3). Besides individual movement sporozoites were occasionally observed to move in small groups of two to seven closely associated parasites we term “swarms” (Fig. 4.4). Even more strikingly, sporozoites aggregated to circular structures – “vortices” containing five to a hundred sporozoites moving clockwise (observed using an inverted microscope) around a common centre (Fig. 4.5) which is the opposite direction of most individual migrating sporozoites *in vitro*. Despite being undescribed so far, sporozoites vortices and swarms are highly reminiscent to forms of collective motion observed in other organisms throughout nature (Delcourt and Poncin 2012; Vicsek and Zafeiris 2012). To broaden our understanding of these phenomena I analysed basic parameters of vortices and swarms (e.g. size, curvature and speed). Furthermore, I observed the effect of actin modulating drugs (cyto D and jasplakinolide) on vortices and investigated vortex and swarm behavior of two mutant lines lacking key proteins involved in sporozoite gliding.

4.1.1 Imaging of infected salivary glands

Our initial interest was to investigate the sporozoite when resident in the salivary gland in greater detail. For the following studies on vortices and swarms I used sporozoites expressing cytosolic GFP under the CS promoter (CSGFP) within the salivary gland (Natarajan et al. 2001). I dissected the glands of *Anopheles stephensi* mosquitoes 17-23 days after infection with the CSGFP line. The salivary glands are located pairwise inside the mosquito thorax (Fig. 4.1 A). Each gland consists of two

elongated lateral lobes and a shorter median lobe in the centre (Fig. 4.1 B). The gland itself consists of acinar cells, which secrete saliva components into the gland cavity at the core of the lobe. The acinar cells are surrounded by the “basal lamina” or “basal membrane” - extracellular matrix components secreted by the underlying acinar cells (Vanderberg 1974). For detailed imaging the gland was treated with wheat germ agglutinin - 594 conjugate (WGA594), a lectin staining the basal membrane as well as the plasma membrane of the acinar cells. Hoechst was used to stain the nuclei of the acinar cells and sporozoites. After dissection in PBS the glands were directly transferred to 3% BSA/RPMI and imaged using a spinning disc confocal microscope.

In conformity with the literature, glands appeared to be usually infected at the distal region of the lateral lobes. In case of a high infection sporozoites were also detected in the median lobe (Sterling et al. 1973). The majority of sporozoites were located in non-motile stack like formations in the central cavity of the lobe. In addition, individual non-motile sporozoites were found in the gland periphery (Fig. 4.1 C-E).

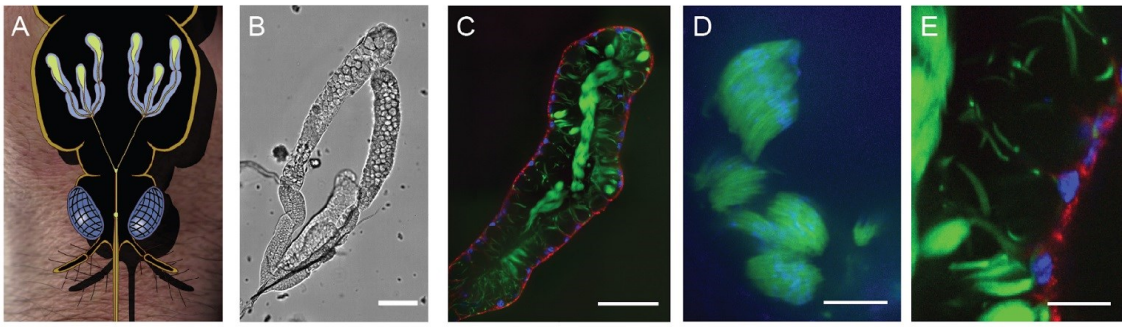

Fig. 4.1 Localization of salivary glands and images of infected gland following fresh dissection. (A) Scheme of an *Anopheles* mosquito and its two salivary glands. Glands are located in the mosquito thorax and are connected via the lateral salivary gland ducts, which join into a common duct leading to the proboscis (Frischknecht et al. 2004). **(B)** Brightfield image of salivary gland after dissection. Note that each gland consists of two elongated lateral lobes and a single, shorter lobe in the centre (medial lobe). Scale bar corresponds to 100 µm. **(C-E)** Spinning disc confocal images of lateral lobe infected with CSGFP sporozoites (green). Hoechst staining (10 µg/ml) was used to visualize the nuclei (blue). Basal membrane and plasma membrane of acinar cells was stained with wheat germ agglutinin - 594 (red) **(C)** Confocal image of a highly infected lateral lobe. CSGFP sporozoites (green) are clustered in non-motile stacks inside the central cavity of the lobe. Scale bar corresponds to 50 µm. **(D)** Magnified image of sporozoite stacks. Scale bar corresponds to 10 µm. **(E)** Magnified image of single sporozoites in the periphery of the gland. Scale bar corresponds to 10 µm.

Glands were often observed to be already damaged in the preparation process. Others disintegrated during imaging of the glands (Fig. 4.2). Swelling of the acinar cells caused

individual cells to rupture and sporozoites to be distributed towards the periphery of the gland (Fig. 4.3). Further, the basal membrane was often observed to gradually detach from the underlying acinar cells creating a space between the acinar cells and the basal membrane itself. Both observations were probably caused by osmotic influx of medium into the gland.

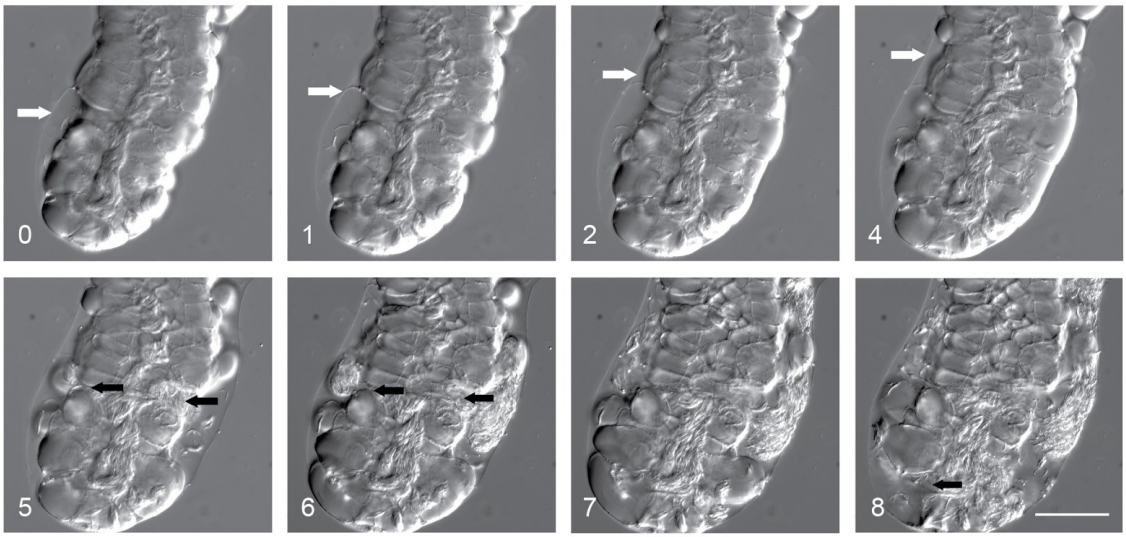

Fig. 4.2 Salivary gland swelling and release of sporozoite stacks to the gland periphery. DIC image series (0-8 min) of infected salivary gland after fresh preparation in 3% BSA/RPMI. **0-4 min:** Sporozoites rest in stack formations inside the central cavity of the gland. White arrows mark region of increasing detachment of basal membrane from acinar cells. **5-8 min:** Disintegration and burst of acinar cells causing release and distribution of sporozoites to the periphery of the gland. Black arrows mark sites of cell disruption. Scale bar corresponds to 50 µm.

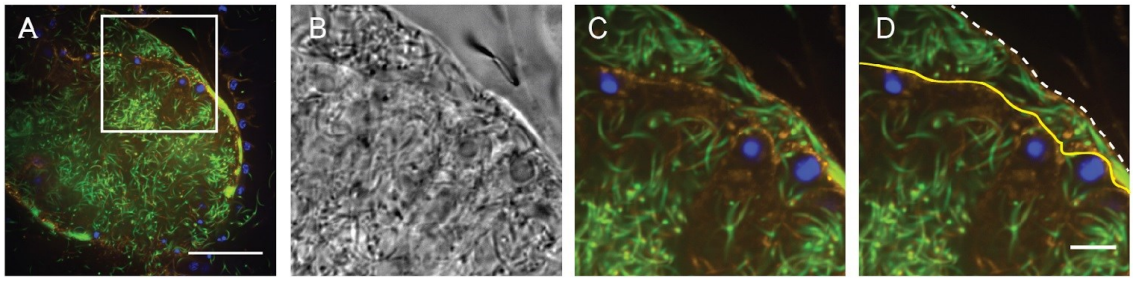

Fig. 4.3 Disintegration of sporozoite stacks and redistribution of sporozoites in damaged glands. Confocal **(A, C, D)** and brightfield **(B)** images of infected salivary gland. GFP expressing sporozoites (green) are distributed inside the gland. **(B-D)** Magnified image (indicated with white box in A) shows high density of sporozoites between narrow space of basal membrane (white dotted line) and plasma membrane of acinar cells (yellow line). Wheat germ agglutinin-594 (WGA-594) was used to visualize membranes (yellow). Hoechst (10 µg/ml) was used to visualize the nuclei (blue). Scale bar corresponds to 50 µm (A) and 10 µm (D).

Taking a closer look at the basal membrane, we noticed that sporozoites were in a highly active gliding state (Fig. 4.4 A). Almost all (> 90%) the sporozoites were observed to be motile, whereas *in vitro* up to 60% of sporozoites actively migrate. Sporozoites in the centre of the gland as well as sporozoites that leaked out of the gland were barely moving. The gliding speed of individual gliding sporozoites at the basal membrane was reduced (~1.5 µm/s) in comparison to sporozoites gliding individually on glass (~2.2 µm/s). However, 1.5 µm/s is still within the normal range of sporozoite gliding speeds and this reduced speed might be caused by obstacles (e.g. cell debris) encountered by the sporozoites in the gland periphery. Interestingly, we noticed that BSA was not required to induce sporozoite gliding at the basal membrane. *In vitro*, BSA is essential to induce sporozoite motility. Surprisingly, even the gliding speeds of sporozoites at the basal membrane were not affected whether BSA was present or not (Fig. 4.4 B).

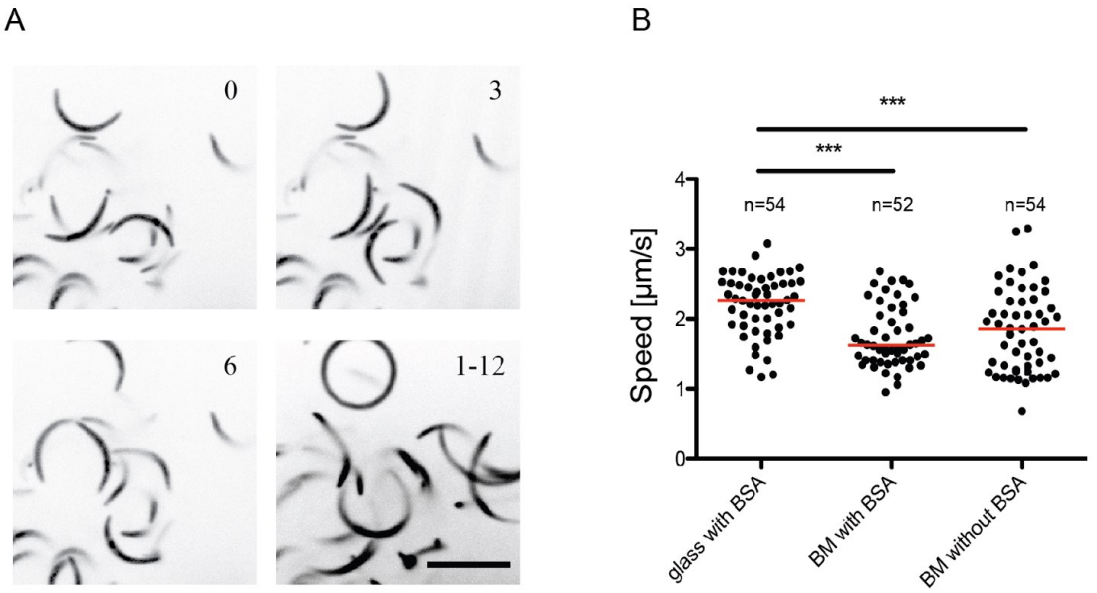

Fig. 4.4 Individual gliding sporozoites at the basal membrane of an infected gland. (A) Time series (0, 3 and 6 s) and maximum projection (1-12 s) of gliding sporozoites at basal membrane. Scale bar corresponds to 10 µm. **(B)** Gliding speed of single sporozoites on glass and basal membrane (BM) in RPMI medium with and without 3% BSA. Speed was measured for 30 s following imaging of sporozoites at the basal membrane of freshly dissected salivary glands and compared to sporozoites moving on glass. Median is indicated with red line. Images were taken at the spinning disc confocal microscope (60x). Data was analysed using the one-way ANOVA and Kruskal-Wallis test (a p-value of $p \leq 0.05$ was considered to be significant, *** refers to a p-value ≤ 0.001).

Besides individual moving sporozoites, we occasionally observed small groups of two to seven sporozoites moving as a single unit at the basal membrane (Fig. 4.5 and 4.7). The sporozoites within a “swarm” appeared to be laterally attached to each other for up to several minutes while moving with about the same speed. Even more fascinating, we imaged sporozoites to form circular ensembles - “vortices” - at the basal membrane containing a broad range of five up to about 100 sporozoites (Fig. 4.6 and 4.7). The majority of sporozoites inside a vortex were gliding in a clockwise manner enclosing a common centre. Vortices are highly dynamic and stable formations which are observable for up to two to three hours. Their “lifetime” was only limited by the complete disintegration of the glands due to rupture of the basal membrane and desiccation of the sample. The experimental setup did not allow for longer observations. The diameter of vortices varied in a range of 10-30 µm depending on the sporozoite number. Both phenomena have so far not been reported in the literature and raised several questions addressed in the following sections.

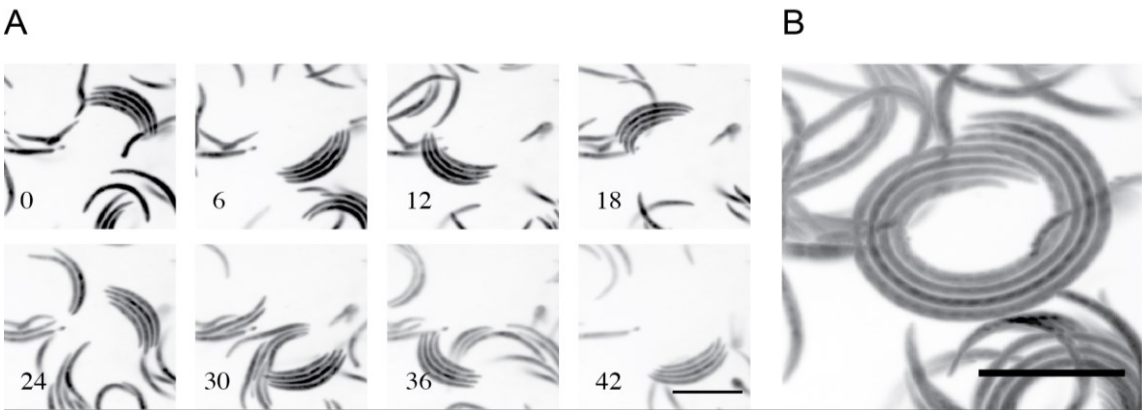

Fig. 4.5 Sporozoites were occasionally observed to move in swarms. (A) Time series of swarm containing four sporozoites gliding in circles at the basal membrane of a lateral salivary gland lobe (42 s). Note that sporozoites remain lateral attached to each other during the observed time. **(B)** Maximum projection of the same swarm gliding in a circle (20 s). Scale bars correspond to 10 µm.

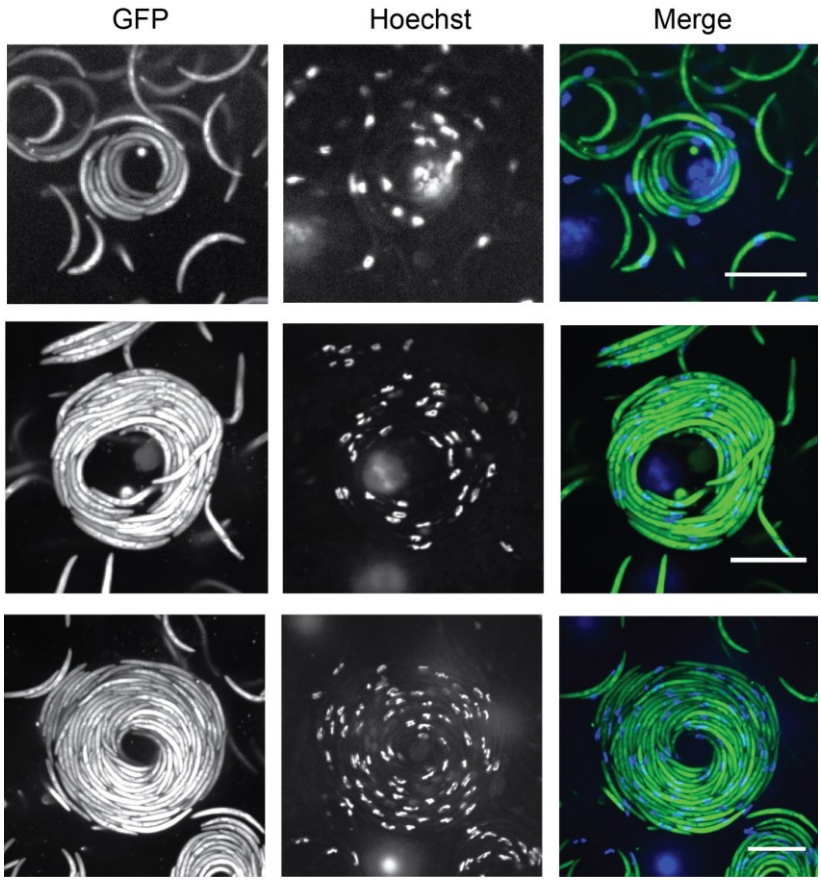

Fig. 4.6 Vortex formations of GFP expressing sporozoites (CSGFP) after fresh preparation of Anopheles stephensi salivary glands (SG). Shown are three vortices of different size (upper row: small vortex containing 11 spz, middle row: medium vortex containing 38 spz, lower row: large vortex containing >70 spz). SG were dissected in RPMI medium containing 3% BSA. In addition, Hoechst (10 µg/ml) was used to visualize the nucleus. Vortices vary in diameter (10-30 µm), as well as sporozoite number (5 - 100). Scale bars correspond to 10 µm.

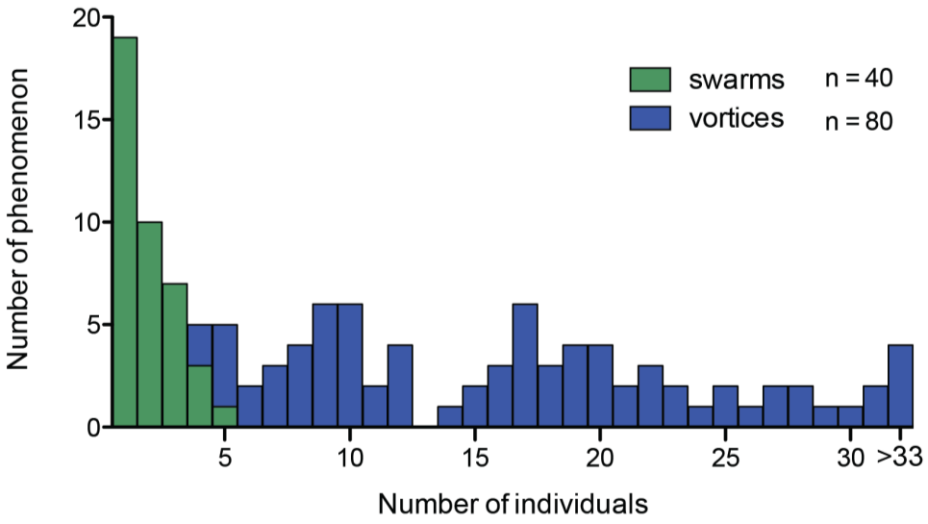

Fig. 4.7 Number of individuals per swarm and vortex. Shown are the individual numbers of sporozoites in 40 swarms and 80 vortices. n - refers to number of swarms/vortices.

4.1.2 Formation of vortices and swarms

To further analyse vortices as well as swarm formations we were interested in how they are initially forming. Vortices were quickly emerging after sample preparation as the glands were often already disintegrated even before we started to image. As an approximation, vortices were emerging in 30-50% of the observed glands on a regular basis. In general, the likelihood of vortex formation was higher when the glands were appearing to be well infected containing a large number (approx. > 10.000) of sporozoites. In rare occasions, we imaged vortex formation during imaging. Individual sporozoites were observed to gradually cluster up during a range of several minutes. The forming vortices then grew to a certain size (Fig. 4.8). The observed size range of 10-30 µm leads to the assumption that the vortex size is not only limited by the number of sporozoites but might also be constrained by other conditions (e.g. limitations of the surrounding space or curvature of sporozoites).

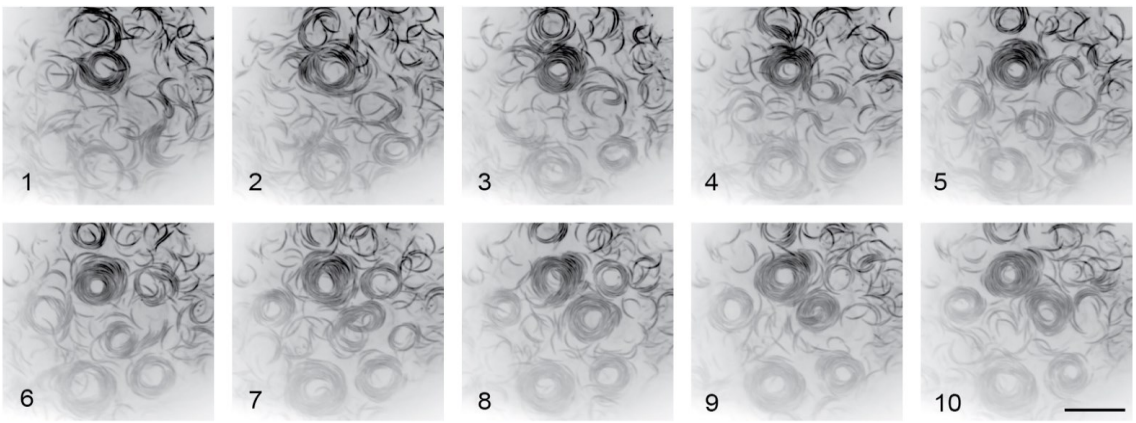

Fig. 4.8 Vortex formation at basal membrane of salivary gland. Time series of vortices gradually forming at basal membrane over period of 10 min. Salivary gland of CSGFP infected mosquito was freshly dissected, transferred to 3% BSA/RPMI medium and imaged using the Zeiss microscope (63x). Scale bar corresponds to 20 µm.

In contrast to vortices, swarms were observed to form rather quickly over the course of seconds (Fig. 4.9). Again, previous individual gliding sporozoites were imaged to come in close contact. Unlike vortices forming a circular structure, swarm sporozoites would laterally attach to each other, remain in close contact and contain a rather small number of two to seven sporozoites. Despite single sporozoites occasionally joining or leaving a swarm the initial formation was imaged to appear at once. Both phenomena show distinct characteristics, which will be further explained in the following sections.

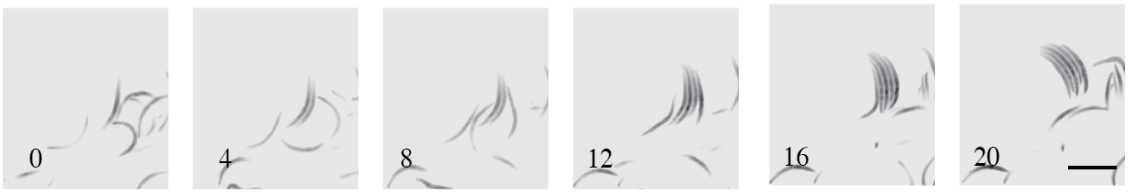

Fig. 4.9 Swarm formation at basal membrane of infected salivary gland. Time series of sporozoite swarm forming over period of 20 s. Images show five individually gliding sporozoites getting laterally attached to each other (0-16 s) and continues to move in a swarm formation afterwards (16-20 s). Scale bar corresponds to 10 µm.

4.1.3 Vortices and swarms form at the basal membrane surrounding the salivary gland

To deepen our understanding of the surrounding space of vortices and swarms, confocal z-stacks of infected salivary glands were imaged after preparation (Fig. 4.10). Reassembling of the images allowed for a three-dimensional analysis of the gland. As mentioned previously, vortices were appearing in the gland periphery after disruption of acinar cells and redistribution of sporozoites inside the gland. Vortices were localized in close contact to the basal membrane surrounding the lobe. In contrast to individual sporozoites which were distributed in the whole gland, vortices were clearly located in between the constrained space between basal membrane and plasma membrane of the acinar cells (Fig. 4.10 B-C). In addition, small vortices in the range of five to ten sporozoites could also exist in areas where the basal membrane detached strongly from the underlying cells such that these vortices would only have contact to the basal membrane (Fig. 4.11). However, larger vortices (>ten sporozoites) were so far only observed in areas of constrained space.

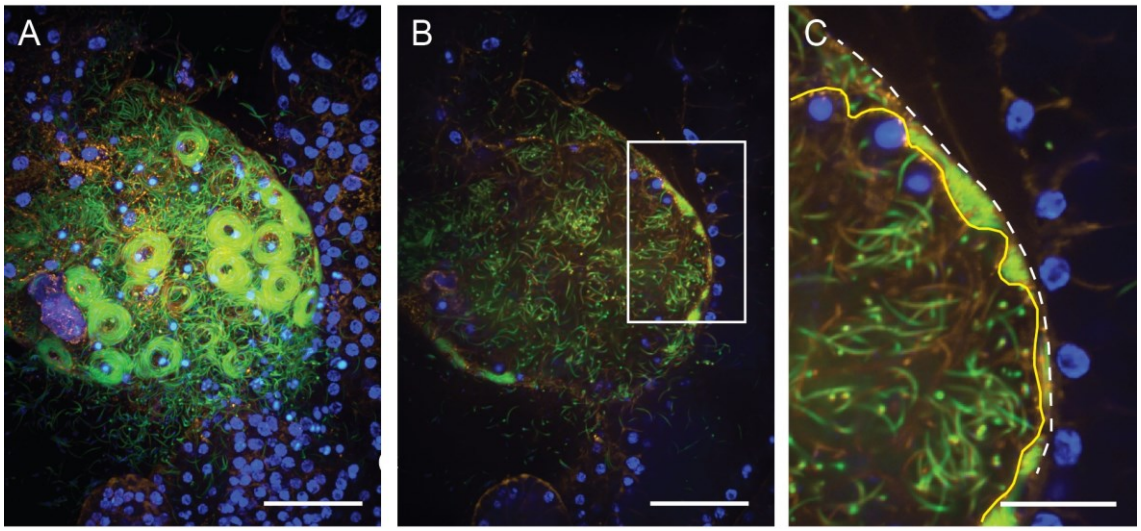

Fig. 4.10 Vortices form in the narrow space between acinar cells and basal membrane in the gland periphery. (A-C) Spinning disc confocal images of a lateral lobe infected with GFP expressing sporozoites (green). Staining with wheat germ agglutinin-594 (WGA-594) was used to visualize membranes (yellow). Hoechst (10 µg/ml) was used to visualize the nuclei (blue). (A) Z-projection of highly infected lateral lobe. Vortices are located at the gland periphery. Scale bar: 50 µm (B) Single z-slice from (A) shows distribution of sporozoites inside the gland and an accumulation of sporozoites in the gland periphery. White box is magnified in (C). Scale bar: 50 µm (C) Magnification of (B) shows lateral view of vortex located in between plasma membrane of acinar cells (yellow) and basal membrane (white dotted line). Scale bar: 20 µm

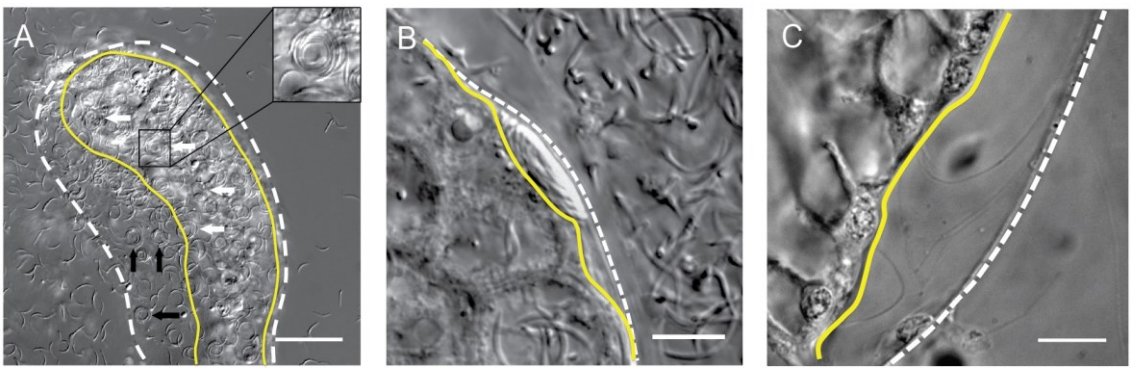

Fig. 4.11 Differential interference contrast images of vortices. (A) Image of infected lateral lobe. The basal membrane (white dotted line) is partly detached from acinar cells (yellow line) on the left side of the gland. Vortices are marked in between acinar cells and basal membrane (white arrows) as well as in areas where the basal membrane detached form the gland (black arrows). Magnified vortex is shown in upper right corner. Scale bar: 50 µm. **(B)** Lateral view of vortex located in between acinar cells and basal membrane. Scale bar: 10 µm. **(C)** Image shows strong detachment of basal membrane from underlying acinar cells. Scale bar: 10 µm.

Computational simulations of vortices by Dr. Anna Battista (Battista 2015) predicted that vortices would be more stable over time if the individual sporozoites would be allowed to overlap with each other. Consistently, three-dimensional image reconstructions revealed vortices to consist of one up to six sporozoite layers stacked on top of each other (Fig. 4.12). In contrast, swarms have so far been imaged to only consist of one single layer.

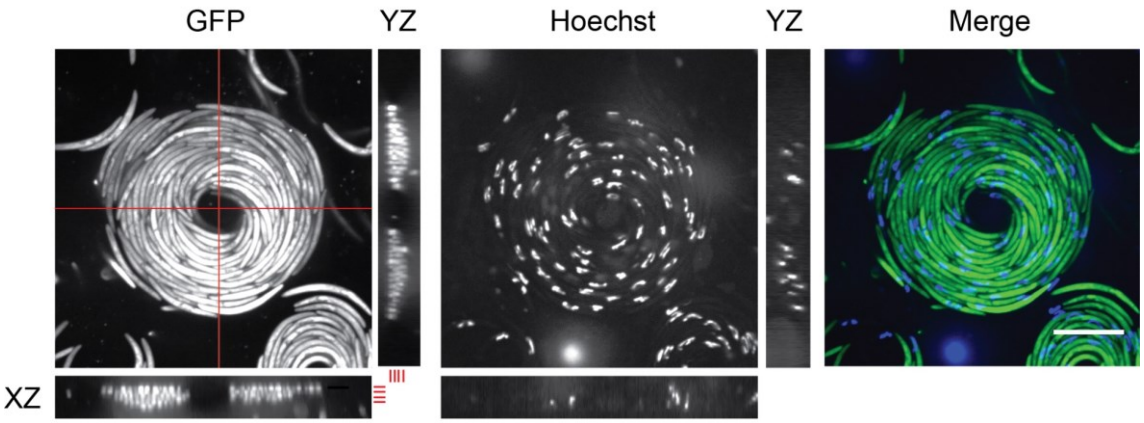

Fig. 4.12 Vortices can consist of multiple layers in z-dimension. Large vortex of GFP expressing sporozoites after fresh preparation of *Anopheles stephensi* salivary glands (SG). Hoechst (10 µg/ml) was used to visualize the nuclei. Crossing red lines indicate position of XZ and XY images showing sporozoites arranged in up to four layers (indicated by short red lines). Scale bar corresponds to 10 µm.

4.1.4 Swarms

As mentioned in the previous section, swarms are observed to move at the basal membrane of infected salivary glands. Sporozoites inside a swarm remain closely attached to each other for several minutes and therefore move with a similar speed (Fig. 4.13). The average speed of a swarm varies in a range of about 1-3 µm/s which is similar to speeds of individual moving sporozoites migrating at the basal membrane. In contrast to individually gliding sporozoites, swarms appear to be highly dynamic formations and demonstrate varying and complex gliding patterns (Fig. 4.13). As described, they form out of individual sporozoites (Fig. 4.9). Also, individual sporozoites can join a swarm (Fig. 4.13 A) and reorient themselves within a swarm (Fig. 4.13 B). Furthermore, swarms can rapidly break up (Fig. 4.13 C). In contrast to vortices, which were observed to be stable for hours, swarms could already disintegrate after

30 seconds. However, some of the swarms were continuously gliding for more than 10 minutes. The number of sporozoites inside a swarm was variable as sporozoites were observed to join or leave a swarm (Fig. 4.13 A). Once, even two swarms were observed to merge into one larger swarm (Fig. 4.13 D). In the illustrated case, a swarm consisting of two sporozoites is merging with a swarm of three sporozoites. Curiously, the smaller swarm is completely changing its direction by making a complete turn after encountering the larger swarm. In this case, both swarms end up facing the same direction and continue to glide laterally aligned as one unit. This form of side by side migration seems to be the most favourable position as it occurs for the majority of the observed time. However, sporozoites inside a swarm occasionally rearrange (e.g. after encountering some obstacle) in a way that single or several sporozoites advance or lag behind the swarm and then realign again afterwards (Fig. 4.13 B).

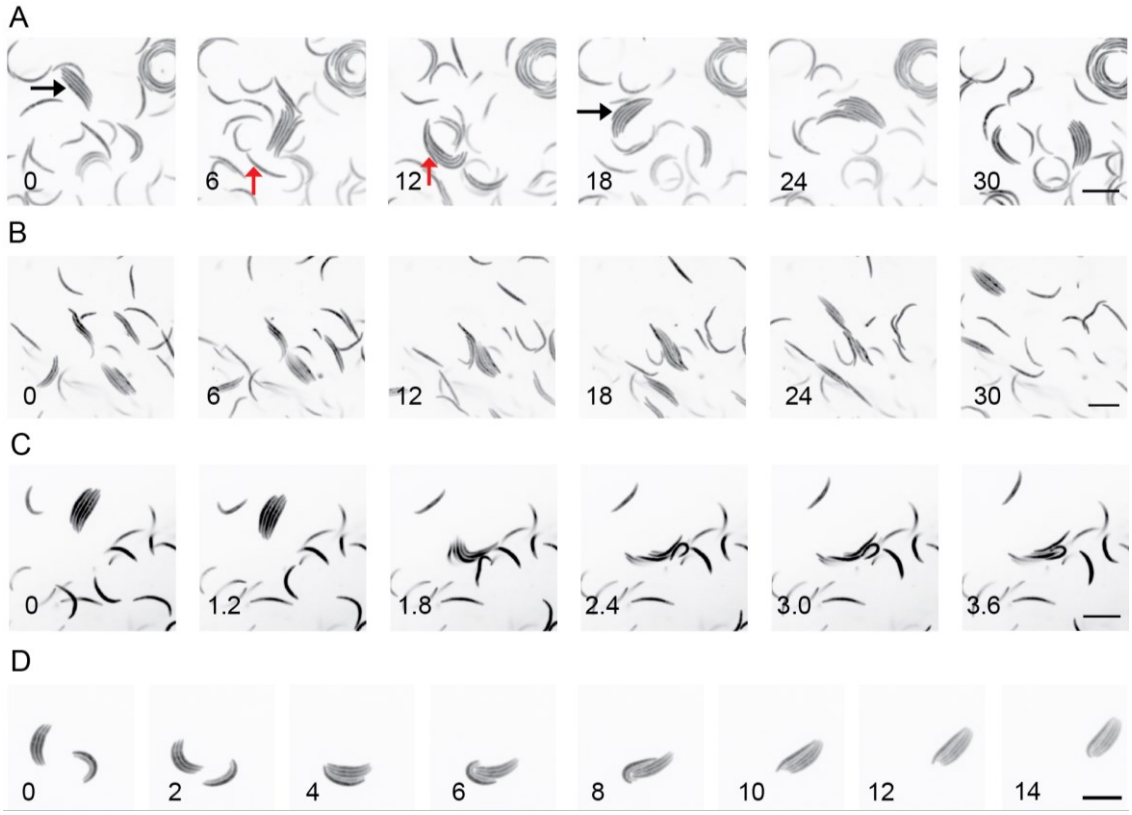

Fig. 4.13 Examples of swarm behavior. Swarm motility was imaged at the basal membrane of infected glands after preparation in 3% BSA/ RPMI. Scale bars correspond to 10 µm. **(A)** Single sporozoite (red arrow) joining an already existing swarm of four sporozoites (black arrows mark swarm before and after joining). (30 s) **(B)** Reorientation of several sporozoites inside a swarm (30 s). Temporary elongation of swarm between 12 and 24 s. **(C)** Swarm of five sporozoites rapidly breaking up into individually gliding sporozoites (3.6 s). **(D)** Two independent swarms of three and two sporozoites merging into one single swarm.

4.1.5 Peripheral and central vortex sporozoites differ in curvature and angular speed

More detailed characterization of vortices was achieved by measuring the length, speed and curvature of individual sporozoites within the vortices. Individual migrating sporozoites on glass and basal membrane were compared with sporozoites gliding as part of a vortex. To reveal any potential differences within vortices, we distinguished between all vortex sporozoites (vortex average), sporozoites moving in the outer vortex orbitals (vortex peripheral) and sporozoites moving close to the vortex centre (vortex central) (Fig. 4.14). Comparison of the length showed a slight increase in average length of peripheral sporozoites (~12 µm) compared to central vortex sporozoites (~11 µm) (Fig. 4.14 A). However, the difference could be also due to measuring errors as sporozoites have the tendency to overlap more frequently in the centre of the vortex. For both groups, the sporozoite length varied in the range of about 9 - 14 µm. Analysing the speed of sporozoites migrating on glass and basal membrane showed that sporozoites were significantly slower when moving on the basal membrane (Fig. 4.14 B). Individual sporozoites migrate on glass with an average speed of ~2.2 µm/s within a range of about 1-3 µm/s. In comparison, they were migrating with about ~1.7 µm/s at the basal membrane. Vortex sporozoites were migrating with similar speeds as individual sporozoites at the basal membrane. Interestingly, also central and peripheral sporozoites were migrating with approximately the same average speed of ~1.5-1.6 µm/s. Curvatures varied between 0.1 μm^{-1} and 0.3 μm^{-1} (Fig. 4.14 C). Individual migrating sporozoites on glass had an average curvature of 0.2 μm^{-1}. Sporozoites at the basal membrane had a slightly lower average curvature of 0.18 μm^{-1} and were migrating in larger circular trajectories. Sporozoites inside vortices had an even lower average curvature of 0.15 μm^{-1}. Sporozoites in the centre of vortices had far higher curvatures of 0.1 μm^{-1} when compared to peripheral sporozoites of 0.22 μm^{-1}. In summary, the obtained data suggests that sporozoites are flexible enough to adapt their curvature as well as their speed to different environments and constraints.

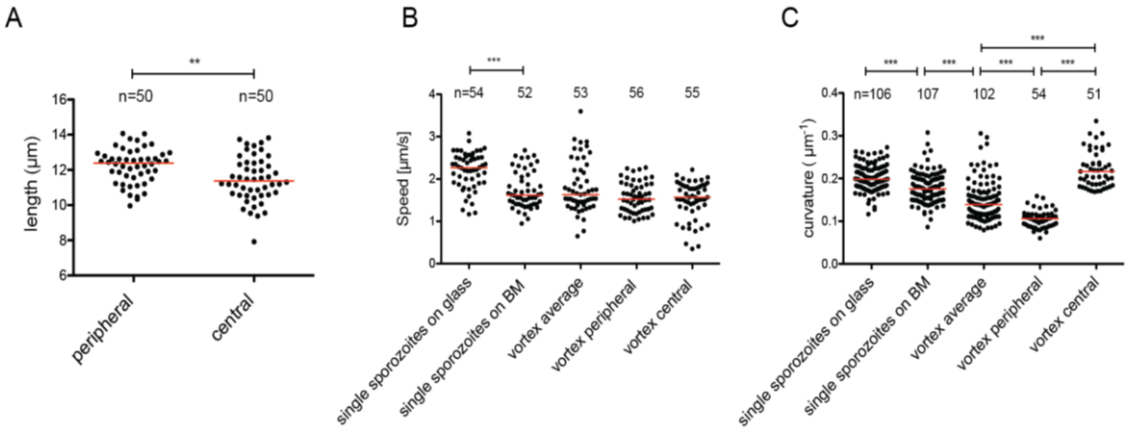

Fig. 4.14 Length, speed and curvature of peripheral and central vortex sporozoites. **(A-C)** Salivary glands of mosquitoes infected with CSGFP sporozoites were imaged in 3% BSA/RPMI on day 17-20 post infection using the spinning disc confocal microscope. Sporozoites gliding in the vortex periphery (outer two vortex orbitals) were compared with sporozoites gliding in the centre (inner two vortex orbitals) in respect of length **(A)**, average gliding speed (measured for 30 s) **(B)** and curvature **(C)** (11 vortices were analysed in total). In addition, speed and curvature of individually gliding sporozoites (single sporozoites) on glass, basal membrane (BM) of salivary glands and average vortex sporozoites (all sporozoites out of four vortices) are shown. (n) indicates the number of analysed sporozoites. Red line indicates the median for each dataset. Data was analysed using the one-way ANOVA and Kruskal-Wallis test (a p-value of $p < 0.05$ was considered significant, *** refers to a p-value ≤ 0.001, ** refers to a p-value ≤ 0.01).

Besides the absolute speeds, we were further interested in the angular speed of sporozoites inside a vortex. Analysis of the angular speed provides an indication if sporozoites inside a vortex interact with each other or glide alongside each other. The angular speed or rotational speed (ω) is defined as the angular change of a rotating object in a certain amount of time. It can be calculated as the ratio of the speed of an object to the radius of the circular path on which the object moves. Again, we compared sporozoites migrating in the outer orbitals of a vortex to sporozoites in the vortex centre and analysed medium sized (10-20 sporozoites) as well as large vortices (25-50 sporozoites). If two sporozoites would migrate with the same angular speed they would move in parallel to each other despite having a different radius to the vortex centre. In any other case the sporozoite with the higher angular speed would “overtake” the slower one with time. Our results indicate that central vortex sporozoites have a higher angular speed as peripheral sporozoites in medium sized vortices (Fig. 4.15 A). This trend was even more pronounced when observing large

vortices. Consequently, central sporozoites do not migrate in parallel with peripheral sporozoites but tend to overtake them. Again, central and peripheral sporozoites were measured to migrate with similar absolute speeds of 1.5 µm/s (Fig. 4.15 B). This suggests that sporozoites inside a vortex do not interact with each other as much as observed for swarm sporozoites.

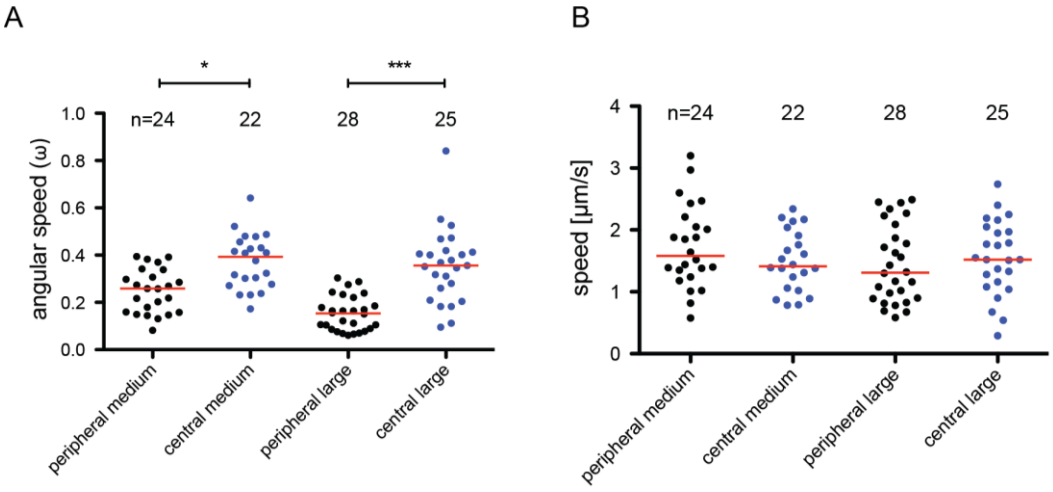

Fig. 4.15 The angular speed of central vortex sporozoites is higher compared to peripheral vortex sporozoites. Medium sized vortices containing 10-25 sporozoites and large vortices containing 25-50 sporozoites were analysed. **(A)** Angular speed was calculated based on average sporozoite speed within 3 s and distance of sporozoites to the vortex centre. Combined data shows higher angular speed of central sporozoites compared to peripheral sporozoites, whereas there was no difference in the average speed **(B)** of the same sporozoites. Data was analysed using the one-way ANOVA and Kruskal-Wallis test (a p-value of $p < 0.05$ was considered significant, *** refers to a p-value ≤ 0.001, * refers to a p-value ≤ 0.05).

4.1.6 Effect of cytochalasin D and jasplakinolide

To test the effect of the cytochalasin D (cyto D) and jasplakinolide (Jas) on vortices, salivary glands infected with the CSGFP line were prepared for imaging as previously described in section 3.2.14. Cyto D and Jas are actin-interacting drugs and were shown to inhibit sporozoite gliding motility in a dose dependent manner (Münter et al. 2009; Hegge et al. 2010). Cyto D inhibits actin polymerisation whereas jasplakinolide inhibits actin depolymerisation and leads to accumulation of actin filaments (Cooper 1987; Cramer 1999; Bubb et al. 2000). Shortly before imaging, varying concentrations of cyto D (final concentration: 50 and 100 nM) or Jas (final concentration: 50, 100 and 200 nM)

were added to the sample. Images were taken at the Zeiss microscope for up to 60 minutes after the drug was added. Sporozoite vortices, swarms as well as individual sporozoites gliding at the basal membrane were observed to pause more frequently moving back and forth until stopping completely. The overall structure of the vortices was unchanged and pausing and stopping of the sporozoites did not cause vortices or swarms to disintegrate. However, the retrieved image data was highly inconsistent as the time until sporozoites started to be affected and completely stopped moving was highly variable (between 5 and 30 minutes). Further, sporozoites of several salivary glands seemed to be unaffected by the drug treatment and kept migrating continuously even after 60 minutes.

4.1.7 Characterisation of mutant lines

To further investigate vortex and swarm behavior we observed salivary glands infected with two parasite lines with altered gliding motility due to genetic alterations. First, we observed a parasite line lacking the actin binding protein coronin. Coronin-KO sporozoites show inefficient gliding motility on glass and migrate with strongly reduced speeds (Bane et al. 2016). In contrast, they show similar gliding speeds to wild type after transmission into the host skin. Furthermore, there is no difference observed in curvature compared to wild type sporozoites (Bane et al. 2016). The other investigated mutant line lacks the HSP20 chaperone (Montagna et al. 2012). HSP20-KO sporozoites were shown to migrate with strongly reduced speeds *in vivo* and *in vitro* and are less curved compared to wild type sporozoites (Montagna et al. 2012). For both mutant lines, we were interested if they would still be capable of forming vortices as well as swarms and if their appearance or physical parameters would be affected.

4.1.7.1 Coronin-KO sporozoites show vortex and swarm formations

Our results show that coronin-KO sporozoites are still capable of forming stacks, vortices as well as swarms appearing similar to wild type sporozoites (Fig. 4.16 A-D).

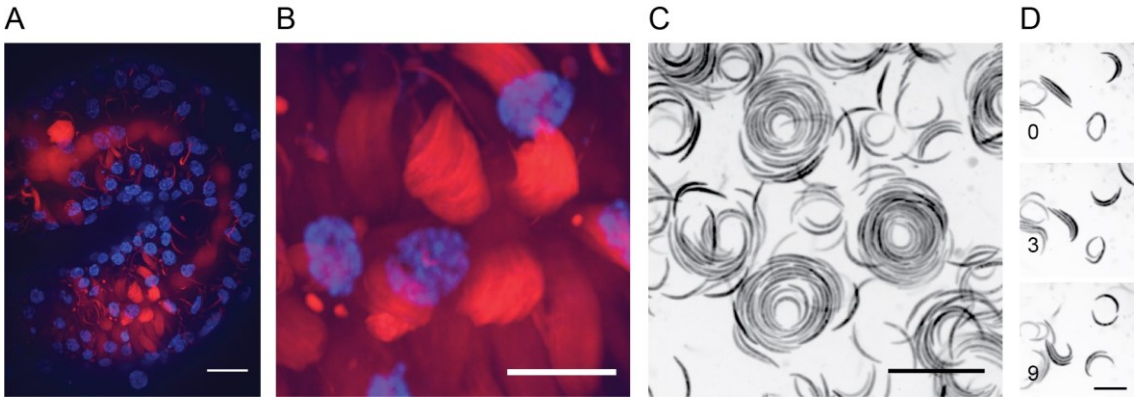

Fig. 4.16 Coronin-KO sporozoites are capable of forming stacks, vortices and swarms. **(A)** Salivary gland infected with coronin-KO sporozoites expressing mCherry (red). Hoechst (10 µg/ml) was used to stain the nuclei of the acinar cells (blue). **(B)** Magnified image of (A) showing sporozoite stacks in the gland cavities. Coronin-KO sporozoites were observed to form vortices **(C)** and swarms **(D)** at the basal membrane of the gland (0-9 sec). Scale bars correspond to 20 (A-C) and 10 µm (D).

We further compared the speeds of coronin-KO sporozoites individually migrating on glass, at the basal membrane and in vortices. As before, CSGFP sporozoites served as a control. Coronin-KO sporozoites on glass showed the previously described strong reduction in speed (~0.2 µm/s) compared to WT sporozoites (~2.2 µm/s) (Fig. 4.17). The average speed of coronin-KO sporozoites gliding at the basal membrane (~1.0 µm/s) was still reduced when compared to the WT control (~1.7 µm/s). However, coronin-KO sporozoites were migrating distinctly faster when compared with migration speeds on glass indicating that the speed reduction is to some extent compensated in this environment. This was also the case for sporozoites migrating as part of a vortex. The average speeds of coronin-KO sporozoites in vortices (~0.6 µm/s) was again lower when compared to WT speeds inside a vortex (~1.6 µm/s). Yet, they were still faster in comparison to Coronin-KO speeds on glass (0.2 µm/s).

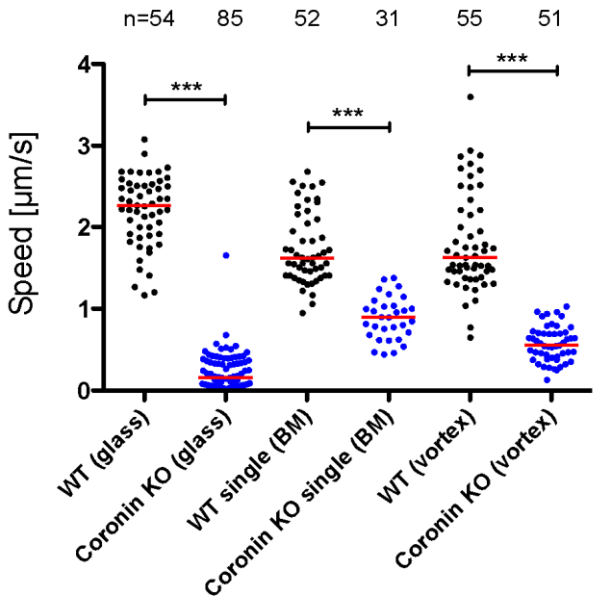

Fig. 4.17 Speed reduction of coronin-KO sporozoites is compensated at the basal membrane and in vortices. Average speeds of CSGFP wild type (WT) and coronin-KO sporozoites gliding individually on glass, at the basal membrane of salivary glands (BM) and in vortex formations. Data of coronin-KO on glass was obtained by Kartik Bane. Sporozoite speed was measured for a minimum of 45 s. The red line indicates the median. (n) indicates the number of observed sporozoites. Data was analysed using the one-way ANOVA and Kruskal-Wallis test (a p-value of $p < 0.05$ was considered significant, *** refers to a p-value ≤ 0.001).

When closely observing coronin-KO sporozoites in vortices we noticed that sporozoites would occasionally reverse for several µm and continue gliding in the same direction as before afterwards (Fig. 4.18 A). Observing about 100 coronin-KO vortex sporozoites revealed that about 80% reversed their direction of gliding at least one up to five times during a period of 100 s. These “reversing events” were never observed for wild type vortex sporozoites (Fig. 4.18 B). In summary, coronin-KO sporozoites are still capable of vortex formations despite an altered migration phenotype and reduced speeds.

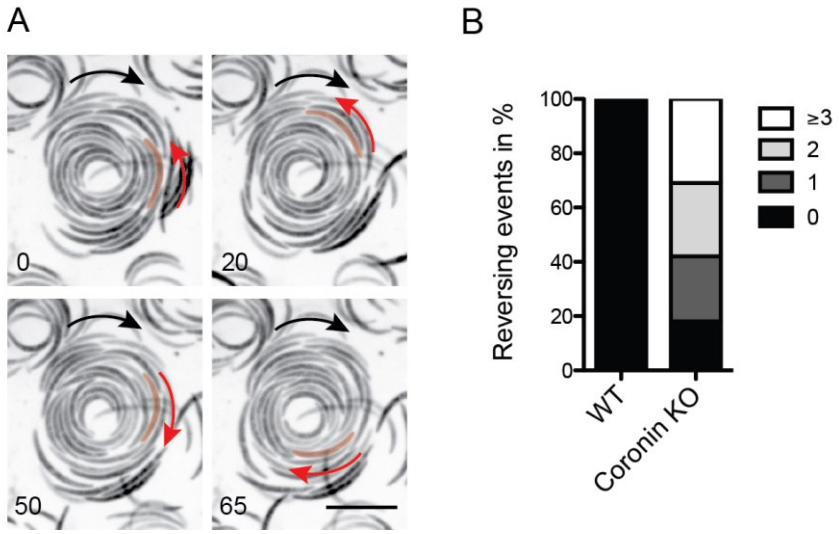

Fig. 4.18 Coronin-KO sporozoites show "Reversing events" inside vortex formations. **(A)** Sporozoite (marked in light red) inside a clockwise rotating vortex reverses and continues to glide in the previous clockwise direction afterwards. Black arrows indicate the direction of the vortex (clockwise). Red arrows indicate migration direction of single marked sporozoite. Time scale: 65 s. Scale bar corresponds to 10 µm. **(B)** Number of "reversing events" of GFP expressing wild type (WT) sporozoites inside vortices was compared to "reversing events" of coronin-KO sporozoites inside vortices. A total number of 100 sporozoites each were observed for a period of 100 s.

4.1.7.2 HSP20-KO sporozoites fail to form vortices and swarms

In contrast to coronin-KO sporozoites and despite high sporozoite densities, neither vortices nor swarms or sporozoite stacks were observed in HSP20-KO infected salivary glands (Fig. 4.19 A). As before, infected glands were freshly dissected in PBS, transferred to 3% BSA/RPMI and imaged using the spinning disc confocal microscope. HSP20-KO sporozoites were gliding with an average speed of ~0.25 µm/s at the basal membrane which was slightly higher compared to speeds of HSP20-KO sporozoites on glass (~0.1 µm/s) yet much lower in comparison to wild type sporozoites migrating on glass (~2.1 µm/s) and basal membrane (~1.7 µm/s) (Fig. 4.19 B). Furthermore, HSP20-KO sporozoites were either gliding in larger circles or showed more linear trajectories compared to wild type sporozoites. This resulted in a higher average meandering index (displacement rate/ speed) of HSP20-KO sporozoites on glass as well as basal membrane compared to wild type sporozoites (Fig. 4.19 C). In contrast to coronin-KO sporozoites, HSP20-KO sporozoites were not capable to form vortices and swarms.

Both the strongly reduced speeds as well as the altered curvature and trajectories of HSP20-KO sporozoites might be critical factors in initial vortex and swarm formation. In addition, the absence of HSP20 could lead to misfolded proteins on the sporozoite surface which could disable potential sporozoite-sporozoite interactions.

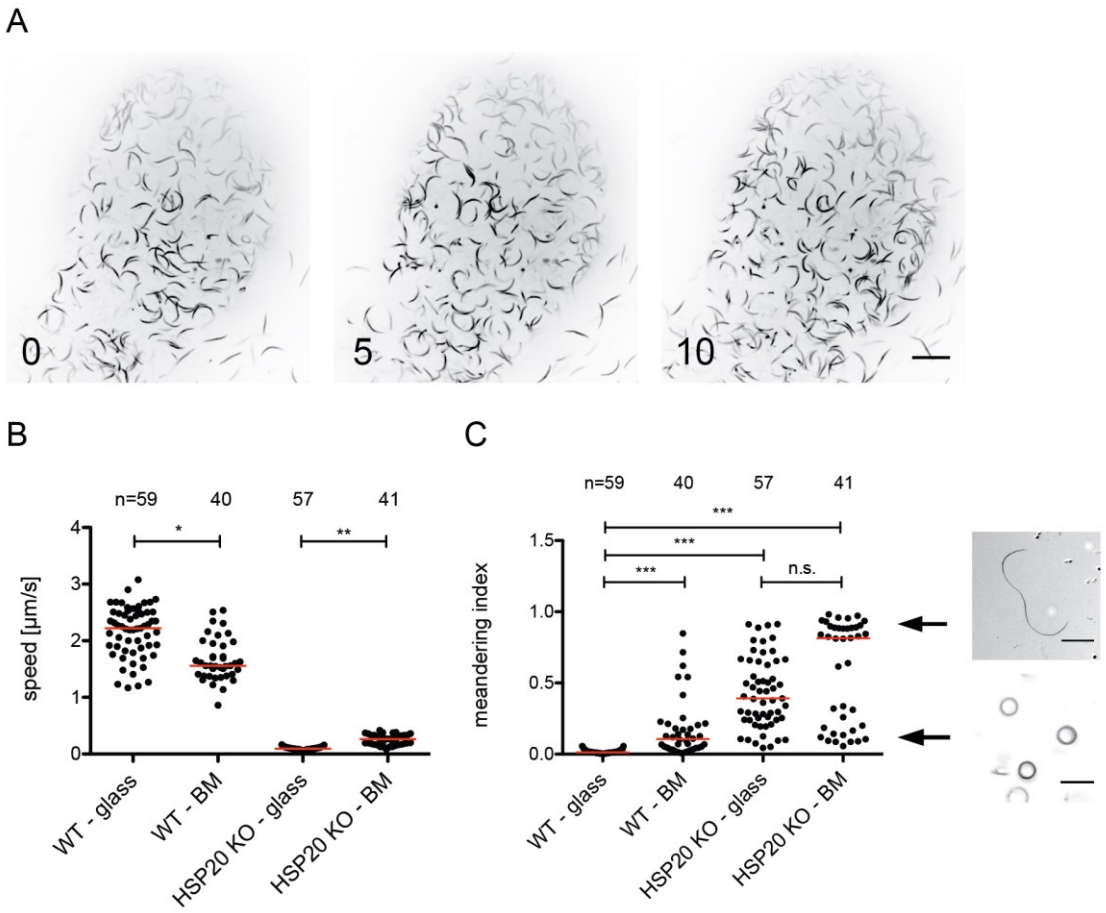

Fig. 4.19 HSP20-KO sporozoites do not form vortices and swarms. (A) Time series of HSP20-KO sporozoites gliding at the basal membrane of an infected salivary gland (0- 10 min). Sporozoites show no formation of vortices and swarms despite high numbers of gliding sporozoites at the basal membrane. Scale bar corresponds to 20 µm. **(B)** Average speed of wild type CSGFP (WT) and HSP20-KO sporozoites on glass and basal membrane (BM). **(C)** Meandering index of wild type CSGFP (WT) and HSP20-KO sporozoites on glass and basal membrane (BM). Values close to zero reflect gliding in a circle whereas values close to one would refer to gliding in a straight line. Images show example trajectories of sporozoites with meandering index close to one (upper image) and zero (lower image). Scale bar corresponds to 20 µm. Red lines indicate the median. HSP20-KO sporozoites were observed for a period of 15 min. Data was analysed using the one-way ANOVA and Kruskal-Wallis test (a p-value of $p < 0.05$ was considered significant, ** refers to a p-value ≤ 0.01, * refers to a p-value ≤ 0.05, n.s. - non significant).

4.2 Characterisation of adhesin double and triple knockouts

4.2.1 Quantification of oocyst numbers revealed unexpected reduction

To characterize the generated parasite lines, oocysts of infected mosquitoes were quantified on day 12-13 post infection. All generated mutants were expressing mCherry under control of the CSP promoter allowing for pre-selection of infected mosquito midguts with a stereomicroscope. The *P. berghei* ANKA line served as control and oocysts were counted after mercurochrome staining.

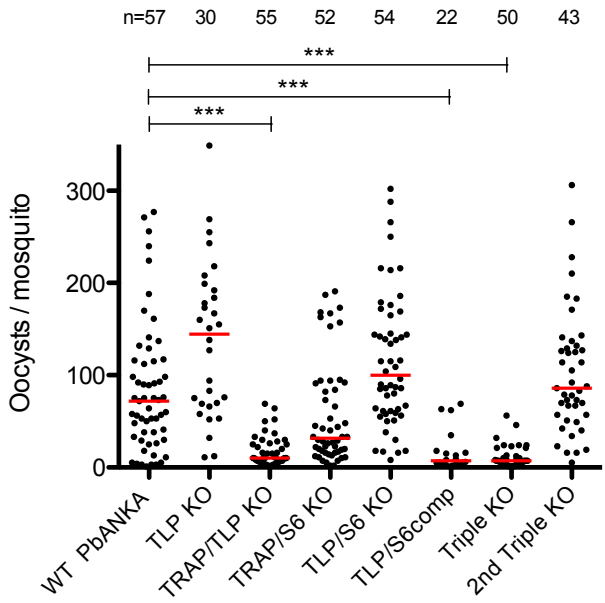

Fig. 4.20 Comparison of oocyst numbers of infected mosquito midguts (day 12-13 post-infection). Midguts of mosquitoes pre-selected for fluorescence were counted under the binocular (SMZ 1500, Nikon). The data represents at least two independent countings of two selected feeding experiments (one feeding experiment in case of TLP KO and TLP/S6comp). Each data point corresponds to the number of oocysts in a single mosquito midgut. The red horizontal line indicates the median. (n) - refers to the number of observed midguts. Data was analysed using the one-way ANOVA and Kruskal-Wallis test (a p-value of $p \leq 0.05$ was considered to be significant, *** refers to a p-value ≤ 0.001).

The results of the oocyst countings are shown in Fig. 4.20. Approximately 80 oocysts per infected midgut on average were counted for *Pb*ANKA wild type (Vincke and Lips 1948). The TLP KO, TLP/S6 KO, TRAP/S6 KO and the 2nd Triple KO line showed similar oocyst numbers varying between 60 and 140 oocysts on average. Statistical analysis showed no significant difference for the mentioned lines (ΔTLP, ΔTLP/ΔS6, ΔTRAP/S6

and ΔTLP/ΔTRAP/ΔS6). In contrast, the total number of oocysts in the TRAP/TLP KO, the 2nd TLP/S6 clone (TLP/S6comp) as well as the 1st triple KO showed significantly reduced oocyst numbers compared to wild type. Oocyst numbers were reduced to about 10-20 oocysts in average per midgut. The oocyst and midgut sporozoite morphology of all generated lines showed no altered phenotype in comparison to the wild type control.

4.2.2 Sporozoite numbers reflect a dominant phenotype of TRAP and S6 knockouts

For further characterization of the knockout lines salivary gland (SG), hemolymph (HL) and midgut (MG) sporozoite numbers were determined on two different days between day 14 and 16 post infection. The ratio of HL and MG sporozoites as well as SG and MG sporozoites was calculated to detect possible salivary gland invasion and oocyst egress phenotypes (Fig. 4.21).

MG, SG and HL sporozoite numbers are shown in Table 7. The MG sporozoite numbers of the generated parasite lines reflect the oocyst numbers observed on day 12-13. The HL/MG ratios of the double and triple KO lines were varying in a normal range between 0.05 and 0.2 comparable to the wild type ratio of 0.1 (Fig. 4.21 A). Besides the 2nd triple KO, all the mutant lines showed a slightly increased HL/MG ratio. Except for the TLP KO line, salivary gland invasion was strongly affected in the generated mutant lines (Fig. 4.21 B). Wild type as well as the TLP KO showed a normal SG/MG ratio of 0.2 to 0.3 respectively. Salivary gland invasion of the two TLP/S6 KO mutants (TLP/S6 KO and TLP/S6 comp) was strongly impaired as the SG/MG ratio was decreased to 0.01 and 0.04. Most drastically, no salivary gland sporozoites were found in the TRAP double KOs (TRAP/S6 and TRAP/TLP) and the triple KO (TRAP/TLP/S6) lines.

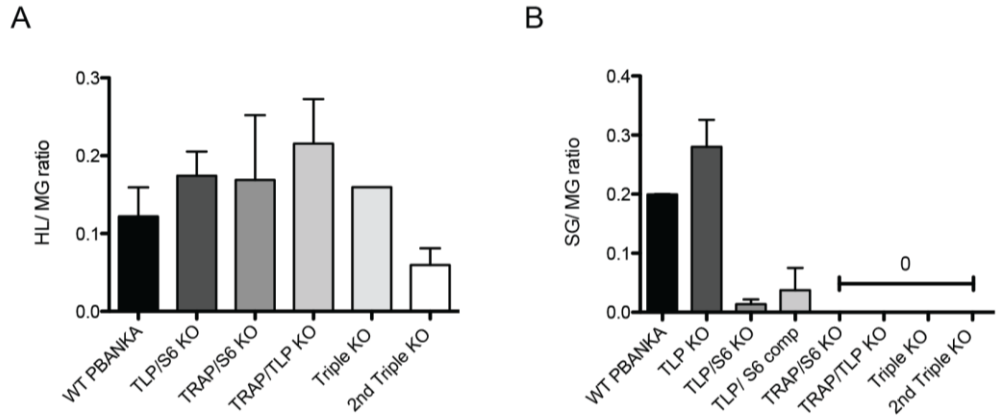

Fig. 4.21 Ratios of midgut (MG), hemolymph (HL) and salivary gland (SG) sporozoites. Each graph represents data from at least two independent countings of two selected feeding experiments (one feeding experiment in case of triple KO). Sporozoite numbers were counted on two days between 14 and 16 post infection. **(A)** Hemolymph to midgut sporozoite ratios of double and triple knockout mutants. **(B)** Salivary gland to midgut ratio of TLP-KO, double and triple knockout sporozoites. 0 - indicates that no salivary gland sporozoites were found in the TRAP double and triple KOs.

(day 14-16)	MG	HL	SG	SG/MG Ratio
Wild type *Pb*ANKA	31.000 ± 12.000	3.500 ± 100	6.300 ± 2.400	0.2
TLP KO	74.000 ± 35.000	/	19.400 ± 5.000	0.28
TLP/S6 KO	100.000 ± 62.000	16.000 ± 6.500	750 ± 200	0.01
TLP/S6 comp KO	2.000 ± 1.000	/	100	0.04
TRAP/S6 KO	34.000 ± 29.000	3.500 ± 700	0	0
TLP/TRAP KO	6.000 ± 6.000	800 ± 300	0	0
Triple KO	5.000	750	0	0
2nd Triple KO	93.000 ± 36.000	5.000 ± 1600	0	0

Table 7 Numbers of midgut (MG), hemolymph (HL) and salivary gland (SG) sporozoites. Mosquitoes of wild type (*Pb*ANKA) and the respective mutant lines were dissected on two days between day 14 and 16 post infection. Each time ten Mosquitoes were pre-selected for midgut fluorescence, dissected and sporozoite numbers were counted using a haemocytometer.

4.2.3 Triple adhesin KO hemolymph sporozoites are capable of patch gliding behavior

I was interested in the gliding behavior of the sporozoites. Therefore, gliding assays of hemolymph and salivary gland sporozoites of each of the lines were performed. Ten infected mosquitoes of each mutant line were pre-selected for midgut fluorescence with a stereomicroscope, dissected and hemolymph as well as salivary gland sporozoites were collected in different plastic reaction tubes (Eppendorf). The sporozoites were activated in RPMI medium containing 3% BSA, transferred to a 96 - well plate and imaged at the Axiovert 200M (Zeiss) using 10x (NA 0.5, air) and 25x (NA 0.8, water) objectives. Gliding assays with hemolymph sporozoites were performed between day 14 and 16 post infection. Sporozoites were imaged for three minutes with an image acquisition rate of three seconds. Sporozoites were categorized into drifting, attached, circular gliding and patch gliding sporozoites – a form of undirected back and forth movement over a single adhesion site (Fig. 4.22 A-C) (Münter et al. 2009).

About 70% of wild type hemolymph sporozoites were non-attached, 19% moved in circles and the minority of sporozoites were either attached (6%) or demonstrated patch gliding behavior (5%). All generated double and triple knockout lines showed a uniform outcome. Again, the majority of sporozoites (65 – 85%) were drifting and did not attach during the observed time of three minutes. However, none of the knockout hemolymph sporozoites showed productive circular gliding. Between 10% and 30% of the sporozoites remained attached to the glass surface during the observed time and about 1-5% was showing patch gliding behavior. Strikingly, patch gliding was also observed in the generated triple KO sporozoites lacking all three known adhesins. To investigate if patch gliding of the triple KO mutant still depends on the actin-myosin motor 1 µM cytochalasin D (cyto D) – a cell permeable inhibitor of actin polymerization - was added in an independent hemolymph assay. One micromolar cyto D should result in a complete block of actin polymerization (Hellmann et al. 2011). Addition of cyto D resulted in about 50% drifting and 50% attached triple KO sporozoites. Thus, there were slightly more sporozoites attached under cyto D than in its absence which indicates that actin filaments might link to receptors other than TRAP family adhesins to pull sporozoites of the substrate. Furthermore, no patch gliding sporozoites were

observed indicating that patch gliding of the triple KO still depends on the sporozoite actin-myosin motor. Similar to the hemolymph gliding assay, salivary gland gliding assays of the TLP/S6 KO sporozoites were performed (Fig. 4.23). About 35% of the TLP/S6 KO sporozoites were observed to undergo circular gliding whereas about 63% of wild type SG sporozoites were gliding in circles. The rest of the sporozoites were either attached or drifting (Fig. 4.23 A). TLP/S6 KO sporozoites were gliding with a slightly reduced speed of on average 1,5 µm/s in comparison to wild type sporozoites gliding with about 2,2 µm/s (Fig. 4.23 B).

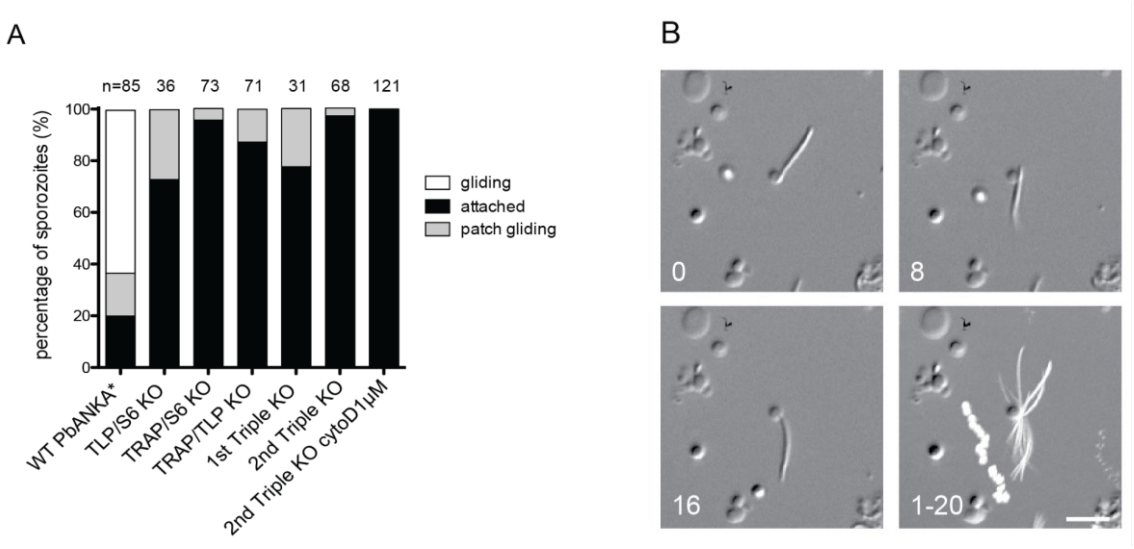

C

(day 14-16)	drifting (%)	attached (%)	gliding (%)	patch gliding (%)	total spz. number
Wild type *Pb*ANKA	70	6	19	5	282
TLP/S6 KO	85	11	0	4	238
TRAP/S6 KO	75	24	0	1	296
TLP/TRAP KO	65	31	0	4	201
Triple KO	86	11	0	3	225
2nd Triple KO	67	32	0	1	207
2nd Triple KO cyto D (1 µM)	51	49	0	0	249

Fig. 4.22 Hemolymph gliding assay of double and triple knockout mutants. (A) Comparison of hemolymph gliding patterns of double and triple KO mutants (day 14-16 post

infection). Hemolymph of ten infected mosquitoes per line was collected, sporozoites were activated with 3% BSA in RPMI and imaged using the 10x objective (NA 0.5, air) of a Axiovert 200M (Zeiss). Bar graphs show percentage of attached (black), patch gliding (light grey) and circular gliding (white) sporozoites. Corresponding results including drifting sporozoites and total number of observed sporozoites are shown in the table below **(C)**. * Sporozoite numbers for wild type (*Pb*ANKA) were obtained by Dennis Klug. The number of analyzed sporozoites (n) is depicted above each bar graph or on the right side of the table. **(B)** Image sequence and maximum projection of a patch gliding triple KO sporozoite isolated from hemolymph. Time is indicated in lower left corner of the image (1 – 20 seconds). Scale bar corresponds to 10 µm.

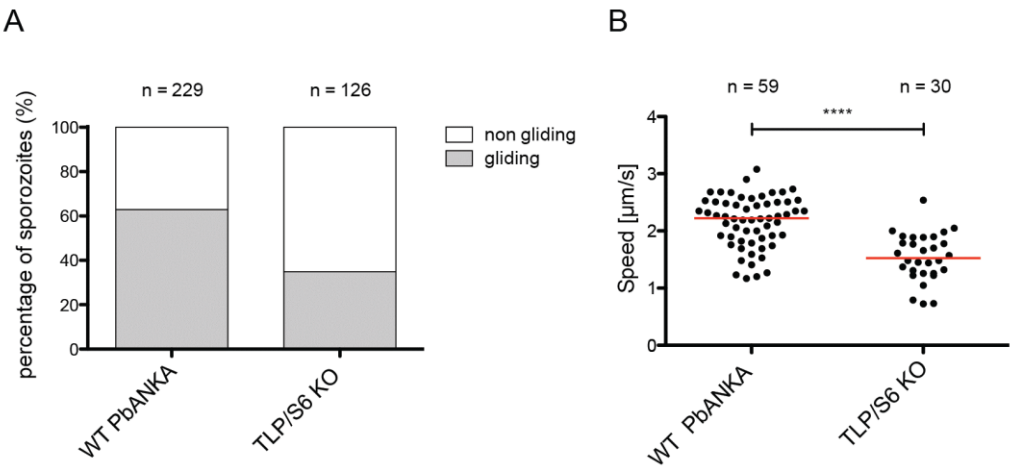

Fig. 4.23 Gliding assay of TLP/S6 KO salivary gland sporozoites in comparison to wild type. Salivary gland sporozoites of ten infected mosquitoes each were activated with 3% BSA in RPMI and imaged using the 25x objective (NA 0.8, water) on an Axiovert 200M (Zeiss) on day 17-20 post infection. The number of analyzed sporozoites (n) is depicted above each bar graph. Sporozoites were considered when gliding consciously for at least 30s. **(A)** Percentage of circular gliding and non-gliding (attached/drifting) salivary gland sporozoites of wild type and TLP/S6 KO sporozoites. **(B)** Gliding speed of wild type and TLP/S6 KO salivary gland sporozoites. Red line indicates the median. Data was analysed using the one-way ANOVA and Kruskal-Wallis test (a p-value of $p \leq 0.05$ was considered to be significant, **** refers to a p-value ≤ 0.0001).

4.2.4 In vivo experiments reveal delay in infectivity of TLP/S6 knockout

Analysis of the *in vitro* gliding assays revealed that only salivary gland derived TLP/S6 KO sporozoites were capable to perform circular gliding. This result was confirmed by the 2nd independent TLP/S6 KO line (TLP/S6 comp) which was also capable of productive gliding motility. However, both lines showed strongly diminished sporozoite numbers in the salivary gland (<1 000 sporozoites/ infected mosquito). To address the question if TLP/S6 KO sporozoites are still capable of natural transmission

back to the mammalian host re-infection experiments with infected mosquitoes were performed. Pre-selected mosquitoes infected with the TLP/S6 KO lines were allowed to bite naive C57BL/6 mice. Post bite the parasitemia of the mice was monitored daily. As sporozoite motility is crucial for skin transmission a defect can result in either a delay in parasitemia or even lead to a complete block of infection (Sultan et al. 1997; Heiss et al. 2008; Moreira et al. 2008; Morahan et al. 2009). Furthermore, 10.000 hemolymph or 100 salivary gland sporozoites were injected i.v. and the parasitemia was monitored. As the host skin is bypassed during i.v. injection, any delay in parasitemia would indicate a potential problem in liver entry or a delay in liver-stage development. The redgreen line (PbANKA-ef1αeGFPCSmCherry) – a fluorescent and marker free line – served as a control for all *in vivo* experiments (Klug and Frischknecht 2017). Mice bitten by infected mosquitoes showed a clear delay in the prepatent period of the TLP/S6 KO line (Fig. 4.24 A). Two out of four mice became positive on day six, whereas all four control mice became positive with a prepatent period of three days (Table 8). In contrast, there was no delay when mice were injected i.v. with 100 SG sporozoites (Fig. 4.24 B). Here, the control line showed a prepatency of 4.5 days and the TLP/S6 KO had a similar prepatency of 4.3 days. However, TLP/S6 comp showed a delay of 1.5 days compared to the control with a prepatent period of six days. All four control mice became infected, whereas three out of four mice injected with TLP/S6 KO sporozoites and two out of four TLP/S6 comp mice became infected. Injection of 10.000 hemolymph sporozoites i.v. resulted in a delay in prepatency of 1.5 days (Fig. 4.24 C). Here, the control mice had a prepatent period of 3.5 day, whereas the mice injected with TLP/S6 KO sporozoites had a prepatency of 5 days.

The results show that the TLP/S6 KO line is still capable of host skin traversal, although it is lacking two of the three major sporozoite adhesins. However, the TLP/S6 KO sporozoites show a potential skin traversal phenotype as the prepatent period was delayed by three days. This skin delay could also be due to a smaller number of sporozoites in the skin. Furthermore, i.v. injections of salivary gland TLP/S6 KO sporozoites indicate that this delay is completely resulting from a skin traversal defect as no delay in prepatency could be detected. However, only three out of four injected mice became positive whereas all four injected wild type mice became positive. In contrast, i.v. injection of 10.000 hemolymph sporozoites resulted in a 1.5 day

prepatency delay of the TLP/S6 KO line which either indicates a potential phenotype in liver stage development or a reduced liver invasion rate. All mice injected with TLP/S6 KO hemolymph sporozoites became positive.

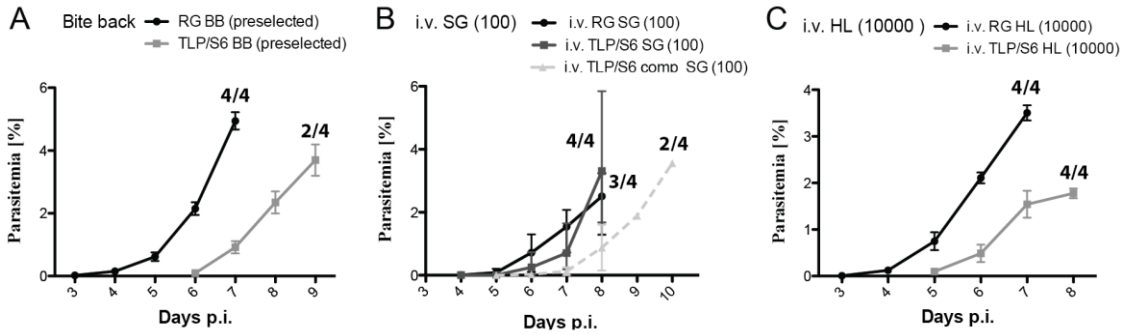

Fig. 4.24 Parasitemia of mice infected by mosquito bites or by i.v. injection of hemolymph or salivary gland sporozoites. (A-C) Each graph shows the mean parasitemia ±SD of four naive C57BL/6 mice infected via mosquito bites or intravenous injection of sporozoites. Number ratio shows how many mice out of four inoculated mice became infected. The redgreen (RG) line – a marker free, fluorescent *Pb*ANKA line - served as control. Mice were monitored for at least 4 consecutive days after blood stages were detected. (A) Graph shows parasitemia of mice infected with mosquito bites. Ten infected mosquitoes were pre-selected in cups prior to the experiment. (B) Graph shows the parasitemia of mice after i.v. injection with 100 salivary gland (SG) sporozoites. (C) Graph shows the parasitemia of mice after i.v. injection of 10.000 hemolymph (HL) sporozoites.

Parasite line	Route of inoculation	Infected /inoculated mice	Prepatency	Parasitemia day 6 (%)
WT (RG-line)	by bite	4/4	3.0	2.15
TLP/ S6 KO	by bite	2/4	6.0	0.1
WT (RG-line)	10.000 HL i.v.	4/4	3.5	2.1
TLP/ S6 KO	10.000 HL i.v.	4/4	5.0	0.5
WT (RG-line)	100 SG i.v.	4/4	4.5	0.7
TLP/ S6 KO	100 SG i.v.	3/4	4.3	0.25
TLP/ S6 comp	100 SG i.v.	2/4	6	0.02

Table 8 Prepatent period and parasitemia in mice infected by mosquito bites or intravenously (i.v.). Mice were infected either with mosquito bites (by bite) of pre-selected, infected mosquitoes or via intravenous (i.v.) injection of 10.000 hemolymph (HL) or 100 salivary gland (SG) sporozoites. The redgreen (RG) line – a marker free, fluorescent PbANKA line - served as control. Four naive C57BL/6 mice were used for each experiment.

5 Discussion

5.1 Categorisation of sporozoite collective motion behavior

As this thesis is the first attempt to characterize the collective behavior of sporozoites, I first categorized the observed collective migration phenomena. Looking through the scientific literature for collective motion phenomena revealed a varying application of behavioral terms like “schools” or “swarms” and given definitions do usually not allow for comparison of different studies (Delcourt and Poncin 2012). Two phenomena of collective motion are described in this study – sporozoite swarms and vortices. Sporozoite swarms consist of two to seven sporozoites, which remain closely attached to each other for most of the observed time and migrate with about the same speed (1-3 µm/s). Further, sporozoites inside a swarm are observed to face the same direction and migrate as one unit, despite allowing individual sporozoites to join or leave the swarm. Relating to recent studies, sporozoite swarms show all characteristics of “polarized schools” as they show a high degree of alignment, which results in an overall synchronization of the group as well as directed movement (Delcourt and Poncin 2012; Delcourt et al. 2016). Sporozoite vortices consist of five up to 100 sporozoites facing the same direction migrating with speeds of 1-3 µm/s. In the literature vortices are described as “systems (groups of animals) in which there is a correlated radial motion of components of this system (individuals) around a common center” (Ben-Jacob et al. 1997; Delcourt et al. 2016). The term “vortex” therefore applied to the observed circling behavior of sporozoites in the mosquito salivary gland. In this context, sporozoite vortices can be categorized as a specific case of polarized schools as they show a high degree of movement synchronization and alignment of nearby individuals towards each other (Delcourt and Poncin 2012).

5.2 Vortex and swarm behavior

The first part of my thesis aimed to reach a better understanding of the characteristics of collective movement of sporozoites observed inside the mosquito salivary gland. First, I was interested how these formations arrange over time and where they localize. Second, I was curious to analyze the basic physical parameters of vortices (e.g.

size, speed, curvature and angular speed). Third, I was interested if the collective behavior would change using two genetically modified parasite lines (*hsp20(-)* and *coronin(-)*) known to show altered motility *in vitro* (Montagna 2012; Bane et al. 2016).

Spinning disc confocal microscopy, epifluorescence and differential interference contrast (DIC) imaging in combination with the use of a GFP expressing parasite line (CSGFP) and DNA as well as membrane dyes enabled us to get detailed images of vortex and swarm formations. Both phenomena appeared to localize in close contact to the apical site of the basal lamina in the periphery of mosquito salivary glands. Image series allowed me to observe the formation of sporozoite vortices and swarms revealing that sporozoites in the center of the gland redistribute to the periphery after swelling of the gland and rupture of acinar cells. Once in contact with the basal membrane sporozoites were observed to move at high speeds of 1 - 3 µm/s and eventually to form vortices over the cause of minutes. In contrast, sporozoite swarms were observed to form in the range of several seconds but were also migrating in close contact to the basal membrane. Analysis of the image data allowed for extraction of basic physical parameters. Vortices were not only observed to vary in diameters of 10 – 30 µm and number of sporozoites (5 – 100 individuals) but also to contain up to six layers of sporozoites. In contrast, sporozoites migrating in a swarm formation were consisting of a lower number of parasites (two to seven sporozoites) remaining closely attached to each other in a single layer for most of the observed time. Comparison of sporozoites in the center and the periphery of vortices revealed that sporozoites in the center were migrating with a similar average speed as sporozoites in the periphery despite being more curved. Further, our data indicates that central vortex sporozoites migrate with a higher angular speed compared to peripheral vortex sporozoites.

To our knowledge, sporozoite vortices and swarms are the only observed examples of collective motion of apicomplexans. However, other examples of collective motion including vortices and swarms of unicellular, self-propelled cells such as bacteria (e.g. *Bacillus subtilis, Bacillus circulans, Paenibacillus vortex, Myxococcus Xanthus*) and slime molds (e.g. *Dictyostelium discoideum*) are described in the literature. For example, hundreds to millions of swarming bacteria (*Bacillus subtilis)* are described to circle around common centers during colony formation on agar plates at average speeds of 10 µm/s (Ben-Jacob et al. 1997). Due to these numbers, bacterial vortices exceed

vortices formed by sporozoites (up to 100 individuals) by a factor of up to 10.000. Despite these differences in scale and speed, swarming of colony forming bacteria show some fascinating similarities to collective motion of sporozoites. Like sporozoite vortices, bacterial vortices are known to consist of single or multiple cell layers and are occasionally observed to possess an empty core similar to vortices referred to as “bagel shape” (Ben-Jacob et al. 1997). *In silico* simulations of sporozoite vortices suggest that overlapping of sporozoites might be an important factor to ensure vortex stability over time (Battista 2015). This hypothesis is yet to be confirmed by quantitative analysis of three-dimensional vortex data, which is beyond the scope of this thesis. Another interesting aspect is the directionality of vortices. Bacterial vortices are observed to turn either clockwise or counterclockwise whereas sporozoite vortices are observed to turn solely in clockwise direction for so far unknown reasons. Sporozoite vortices seem to be an exception in this behaviour, as all so far reported vortex examples are observed to move in both directions (Delcourt et al. 2016). This might be due to the chiral architecture of sporozoites (Kudryashev et al. 2012) that favors one gliding direction. Curiously, the majority (> 90%) of individual migrating sporozoites are gliding counterclockwise at the basal membrane as well as on glass. The preferred clockwise migration of sporozoites within vortices might be related to the structural consistency of the basal membrane and the spatial constraints sporozoites are facing when migrating in a dense collective inside the limited space between basal membrane and the underlying acinar cells. Comparison of bacterial and sporozoite vortices revealed another major difference. Bacterial vortices are described to translocate as one unit when observed in culture. In contrast, sporozoite vortices show only minor center displacements. This might be related to the constrained space in which sporozoite vortices are located or due to the absence of chemotactic signals suggested to be involved in formation and translocation of bacterial vortices (Ben-Jacob et al. 1997). Groups of cells, which are left behind in the trails from such translocating bacterial vortices, are reported to show complex dynamics similar to the described dynamics of sporozoite swarms. The bacterial trails consist of “wetting fluid”, which is secreted to allow for collective colonialization of hard surfaces. Collective movement of bacterial swarms is observed to be restricted to these trails (Ben-Jacob et al. 1997). Despite containing thousands of cells compared to sporozoites

swarms with only two to seven individuals, bacterial swarms show similarities to sporozoite swarms as they move in various directions and abruptly change their direction. Further they merge with other groups or pass along each other without joining into one group, which we also observed in sporozoite swarms.

The results of this thesis did not reveal the cause of the observed collective motion phenomena. In theory, there might be one or several causes for collective motion of sporozoites. As described in the introduction of this thesis there is a large variety of potential causes involved in vortex formations reaching from environmental constraints and steric interactions to attractive and repulsive stimuli and social interactions (section 1.5). Recent studies showed that confinement of self-propelled, swarming bacteria (e.g. *Bacillus subtilis*) in flattened drops with a diameter of 30 – 70 µm was leading to self-organization of stable spiral vortex formations (Wioland et al. 2013; Lushi et al. 2014). In this case, spatial confinement in combination with steric cell-cell interactions was sufficient for vortex formations to emerge. This might also be the case for sporozoites inside vortices as they are confined in space and undergo steric interactions with each other. However, the quality of the experimental image data did not allow for a detailed analysis of the given confinement of basal membrane and acinar cells. Improved membrane staining in combination with three-dimensional analysis of vortex environments could potentially lead to further insights.

Another recent study investigated the self-organization of a curved marine flatworm species (*Symsagittifera roscoffensis*) (Franks et al. 2016). They observed these self-propelled worms to actively interact with each other and to organize in small polarized groups as well as large vortices. Further, they demonstrated experimentally as well as in computer simulations that vortex formations appear more likely at higher densities. Interestingly, vortex formation of marine flat worms was suggested to be purely based on density and local interactions and not on spatial confinements as the tank size was large enough and vortices rather appeared in the center of the tanks (Franks et al. 2016). Even if we never quantified sporozoite densities inside salivary glands, vortices and swarms were observed to emerge more likely in well-infected glands leading to high sporozoite densities of migrating sporozoite at the basal membrane after preparation. This indicates that density might be a crucial factor for collective migration of sporozoites. Another factor with potential influence on vortex formation

could be the curvature of individuals. The described marine flat worms (*Symsagittifera roscoffensis)* as well as a colony forming strain of flagellated bacteria (*Paenibacillus vortex)* are known examples of curved cells observed to form vortices and polarized groups (Ingham et al. 2008; Franks et al. 2016). However, none of these studies investigated the relevance of curvature in further detail. Our data show that sporozoites have an average curvature of 0.2 μm^{-1} when individually gliding on glass and about 0.18 μm^{-1} when gliding at the basal membrane. As sporozoites were observed to have a high degree of flexibility, they were observed to be more curved when gliding in the center of a vortex (up to 0.3 μm^{-1}) and less curved when gliding in the vortex periphery (~ 0.1 μm^{-1}) adapting to the constraints of other nearby sporozoites. The intrinsic curvature in combination with flexibility could facilitate better alignment of sporozoites and therefore contribute to vortex formations. Computer simulations performed by Dr. Anna Battista indicate that the curvature of sporozoites might be crucial for vortex formations of sporozoites (Battista 2015). This hypothesis is further supported by observations of the HSP20 knockout line (Montagna 2012) as we observed *hsp20 (-)* sporozoites to undergo less curved trajectories when gliding on glass as well as on the basal membrane and to be completely uncapable to form vortices despite glands were well infected. However, the absence of vortices might result from other factors such as the reduced average gliding speed of *hsp20 (-)* sporozoites (~ 0.2 µm/ s). As HSP20 is a chaperone, misfolding of surface proteins might have caused disabled sporozoite-sporozoite interactions which in turn prevented the formation of stacks, swarms and vortices. Finally, chemotactic signals secreted by sporozoites could be involved in vortex and swarm formations, which might cause sporozoites to concentrate in a small area. Chemotactic signals are already known to be involved in collective motion of slime molds (e.g. *Dictyostelium discoideum*) during fruiting body formation and are suggested to play a role in the formation of bacterial vortices (e.g. *Paenibacillus vortex, Bacillus subtilis*) (Rappel et al. 1999; Ben-Jacob 2003; Ingham et al. 2008). *D. discoideum* amoeba secrete cyclic adenosine monophosphate (cAMP) to attract other nearby cells to initiate aggregation (Dusenbery 1996). Although we cannot exclude their existence, there is no evidence on the secretion of similar chemotactic attractants or repellents of sporozoites throughout the literature. In this respect, a closer look on the proteins known to be

released by secretory organelles of sporozoites (e.g. micronemes and rhoptries) might lead to the identification of potential candidates (Lindner et al. 2013). One of these candidates is LIMP, which is a soluble protein lacking a transmembrane domain that is suggested to be secreted to the sporozoite surface (see section 1.4) (Santos et al. 2017).

Similar to the variety of causes, there are multiple functions of collective phenomena. In most cases, the formation of vortices and swarms has energy or survival benefits to the individual (e.g. predator avoidance, better access to food sources, collision avoidance and translocation) (Delcourt et al. 2016). In contrast, there are also maladaptive examples of collective motion providing no benefit (e.g. circular trails of army ants and caterpillars) (Fabre 1879; Wheeler 1910; Schneirla 1944). There seems to be no obvious function for vortex or swarm formations of sporozoites as they are only observed *ex vivo* after preparation of infected salivary glands, disruption of acinar cells and reorientation of sporozoites to the basal membrane thus unlikely to happen inside the mosquito. However, the dense alignment of sporozoites in swarms and vortices is reminiscent of non-motile stack formations inside the gland cavity. Especially the lateral alignment of swarms is highly similar to sporozoite alignment inside stacks indicating that the observed collective phenomena might play a role during formation of these structures. There is no information on formation and purpose of sporozoite stacks. Sporozoites might have evolved to form stacks to not be released at once during a mosquito bite or to prevent the salivary duct from clogging. Further analysis of vortices and swarms might provide insights that deepen our understanding of sporozoite stacks. A recent study showed that active collective-like motility of sporozoites can also occur in oocysts prior to the release of sporozoites into the mosquito hemolymph (Klug and Frischknecht 2017). Here, they imaged over 800 wild type oocysts and observed intra-oocyst motility in 5-6% of them. They suggest that this form of sporozoite motility might be essential for sporozoite release. Similar to vortices and swarms, sporozoites inside oocysts were observed to move in a highly constrained space. In contrast however, sporozoites were completely surrounded by an oocyst wall, whereas sporozoites in vortices and swarms appear to be constrained by the basal membrane as well as acinar cells but are not fully enclosed. A further major difference is the spherical setting of an oocyst compared to the single or multi-

layered appearance of vortices as well as the number of sporozoites as an oocyst contains up to a thousand sporozoites whereas vortices were observed to consist of up to a hundred sporozoites and swarms only up to seven sporozoites.

Despite the fundamental characterization of sporozoite vortices and swarms achieved in this thesis, there are still many questions to answer. What factors cause sporozoites to form vortices and swarm? Do sporozoites inside vortices and swarms interact with each other and what are the mechanisms involved? Are vortices and swarms related to each other or rather distinct phenomena? What are the limitations regarding number of individuals as well as size and what causes most sporozoites inside vortices to migrate clockwise instead of counterclockwise? The study of sporozoite vortices and swarms was mainly limited by the observation of *ex vivo* preparations, which did not allow for controlled experimental conditions (e.g. concentration of sporozoites, constraints). The establishment of an *in vitro* collective motion assay on glass in combination with further computer simulations would allow an in-depth examination of confinement and other defined experimental parameters on vortex and swarm formations (e.g. environmental components, potential chemotactic signals, sporozoite densities etc.). In addition, an improved staining of the surrounding gland environment (e.g. cells, debris) would allow for a more detailed analysis of the given constraints.

The characterization of *Plasmodium* vortices and swarms adds another example to the list of collective movements observed throughout nature and is the only reported parasitic example so far. Whether such formations might emerge during the invasion process of the salivary glands cannot be answered yet. Further investigation of these phenomena might lead to a better understanding of sporozoite migration as well as stack formation during salivary gland invasion. In future studies, sporozoite vortices might be used as a model system for collective, radial motion of self-propelled cells, which could lead to further insights in origin and stability of these complex structures. In addition, investigation of the transition of individual migrating sporozoites into swarms and vortices as well as observation of sporozoites leaving a swarm or vortex might lead to insights about potential sporozoite interactions.

5.3 Characterisation of adhesin double and triple knockouts

In the second part of my thesis I characterized double and triple knockouts of the three TRAP family adhesins - TRAP, S6 and TLP - expressed in the sporozoite stage of *Plasmodium*. As they have already been investigated individually and are known to play a major role in invasion and gliding motility of sporozoites I was interested how they act in concert to ensure efficient gliding motility and infective capacity. First, I generated the respective double knockouts (ΔTRAP/ΔS6, ΔTLP/ΔTRAP and ΔTLP/ΔS6) and the triple knockout line (ΔTRAP/ΔTLP/ΔS6) as well as an independent ΔTLP/ΔS6 KO and triple KO line. Subsequently, I analysed the generated knockout lines *in vitro* and *in vivo* to detect potential synergistic or antagonistic effects, which would potentially lead to insights into the type and degree of interaction.

During characterisation of the double and triple knockout lines we noticed that the ΔTLP/ΔTRAP line and the subsequently generated triple knockout as well as the complemented ΔTLP/ΔS6 had strongly reduced oocyst numbers in mosquito midguts (~10 oocysts/midgut). This was surprising, as all other knockout lines (single as well as double KO lines) did not show a phenotype (~ 100 oocysts/midgut). Further, the TLP KO line used to generate the TLP/TRAP KO had normal oocyst numbers and none of the previous TRAP KO studies stated such a reduction in oocyst numbers before (Sultan et al. 1997; Kappe et al. 1999; Wengelnik et al. 1999). One explanation would be that TRAP and TLP play an unknown role during ookinete or oocyst formation only revealed when parasites are lacking both adhesins. However, this is unlikely as only very low quantities of TRAP and TLP are expressed in ookinetes (Mirko Singer, unpublished qPCR data). Another more likely explanation would be that the parasite genome was altered in an inadvertent manner during transfection of the TRAP KO construct into the ΔTLP KO line. Further, the selection of a clone with a low capacity to generate oocyst independent of genetic alterations could have caused the low oocyst numbers. These hypotheses are further endorsed by the 2nd independently generated Triple KO, which showed no reduction in oocyst numbers. Clarification might result from sequence analysis of the TRAP loci and the neighboring genes of the respective TRAP/TLP KO and triple KO lines (ΔTRAP/ΔTLP/ΔS6) as mutations resulting from the recombination process could have affected them causing the low oocyst numbers.

One of our key questions was if the generated TRAP KO lines (ΔTRAP/ΔS6, ΔTLP/ΔTRAP and ΔTRAP/ΔTLP/ΔS6) would be able to enter the salivary glands even though there was no salivary gland invasion observed for the TRAP single KO (Sultan et al. 1997; Kappe et al. 1999; Morahan et al. 2009). In addition, we were interested if salivary gland invasion of the ΔS6/ΔTLP KO would be altered compared to the strongly reduced salivary gland numbers of the ΔS6 KO (Combe et al. 2009; Steinbuechel and Matuschewski 2009). Counting sporozoite numbers of mosquito midgut, hemolymph and salivary glands revealed a complete block of salivary gland invasion whenever the parasite line was lacking TRAP. Further, the ΔS6/ΔTLP KO showed strongly reduced salivary gland numbers (<1000 sporozoites/mosquito) similar to the salivary gland numbers reported for the ΔS6 KO (Combe et al. 2009; Steinbuechel and Matuschewski 2009). This was also the case after complementation of the triple KO line with the TRAP gene (ΔTLP/ΔS6 comp) resulting in about 100 salivary gland sporozoites per mosquito. The hemolymph/midgut sporozoite ratio of all generated lines except the 2nd triple knockout was slightly increased indicating an accumulation of sporozoites within the hemolymph. No antagonistic or synergistic effects were observed comparing midgut, hemolymph and salivary gland sporozoite numbers of all generated knockout lines. Instead, our results corroborate the existing KO studies and confirm a dominant role in the order TRAP > S6 > TLP.

An interesting observation resulted from the investigation of gliding patterns of hemolymph sporozoites. Strikingly, a small percentage (1-3%) of the hemolymph sporozoites of the generated independent triple knockout lines were demonstrating patch gliding behavior – a form of unproductive back and forth movement over one single adhesion spot (Münter et al. 2009) - even though the observed sporozoites were lacking all the three known sporozoite surface adhesins. When performing the experiment in the presence of high concentrations of cytochalasin D (1 µM) - a drug that prevents actin polymerization - no patch gliding sporozoites were observed. Taken together these results demonstrate, that parasites are able to convey force produced by the actin-myosin motor to the surface completely independent of TRAP, TLP and S6. Thus, there might exist one or several currently unknown surface adhesins involved in gliding. One potential candidate is the recently described thrombospondin-related protein 1 (TRP1) (Klug and Frischknecht 2017). TRP1 belongs to the family of TRAP

related proteins as it shares common features of TRAP such as the transmembrane domain (TMD), a thrombospondin type-I repeat domain (TSR) and a cytoplasmic tail domain (CTD). However, it lacks the conserved penultimate tryptophan residue, which is found at the C-terminus of TRAP family proteins (Klug and Frischknecht 2017) and was shown to be important for TRAP function (Kappe et al. 1999). Furthermore, TRP1 lacks the von Willebrandt factor like A-domain known to be important for TRAP during sporozoite invasion (Matuschewski, Nunes, et al. 2002). TRP1 KO sporozoites show no obvious migration defect *in vitro* suggesting TRP1 to have no function in gliding motility (Klug and Frischknecht 2017). However, TRP1 could still bind to the surface via its TSR domain and act in concert with other proteins to enable patch gliding behavior. Further, the mentioned intra-oocyst motility (section 5.2) was only observed in wild type oocysts and not for sporozoites lacking TRP1 suggesting an essential role for TRP1 in sporozoite movement prior to oocyst release. Another potential candidate is the sporozoite surface protein 3 (SSP3), which has been recently described for *P.yoelii* parasites and is known to have orthologs in all *Plasmodium* species (Harupa et al. 2014). Like TRP1 and TRAP, SSP3 has a TSR domain although in close proximity to its transmembrane domain. Parasites lacking SSP3 are capable of initial adhesion *in vitro* but fail to undergo productive gliding (Harupa et al. 2014). In this respect, it would be interesting to investigate if SSP3-KO sporozoites can still undergo patch gliding. Besides TRP1 and SSP3, there are several other sporozoite surface antigens with yet unknown function, which might turn out to be involved in patch gliding as well as in productive gliding (Bottius et al. 1996; Chattopadhyay et al. 2003; Currà et al. 2013).

Finally, I investigated the ΔTLP/ΔS6 KO sporozoites, which are able to invade the mosquito salivary gland although in strongly reduced numbers. Gliding assays revealed that ΔTLP/ΔS6 KO sporozoites are still capable of continuous gliding at almost normal speeds. Further, *in vivo* experiments showed that ΔTLP/ΔS6 KO sporozoites are able to be naturally transmitted back to the mammalian host. However, transmission of ΔTLP/ΔS6 KO parasites via mosquito bites resulted in a delay in prepatency of three days. Both, TLP and S6 KO parasites are reported to be infectious to the mammalian host after natural transmission (Heiss et al. 2008; Combe et al. 2009). Our results extend these findings, as parasites lacking both adhesins are still able of natural transmission despite strongly reduced salivary gland numbers indicating that ΔTLP/ΔS6

KO sporozoites migrate inside the host skin and invade blood capillaries after transmission via the mosquito bite. Further, we detected a prepatency delay of three days of the TLP/ S6 KO compared to wild type. This result agrees with the literature, as prepatency of S6 KO parasites was previously monitored in Sprague/Dawley rats to be delayed by ~2.5 days (Steinbuechel and Matuschewski 2009). Further, TLP was suggested to have a role during host skin traversal as liver burden in mice infected with TLP KO parasites was found to be reduced by 95% after intradermal sporozoite injection (Moreira et al. 2008) and blood prepatency was delayed by 0.5 days when injected via mosquito bite (Heiss et al. 2008; Hellmann et al. 2011). These results agree with our results and show that the delay could be either caused by a defect during migration in the skin or by a cumulative delay resulting from a low number of inoculates sporozoites.

S6 KO sporozoites isolated from the hemolymph have been reported to adhere less and to be strongly impaired in productive gliding *in vitro* as they undergo incomplete circular movements (Combe et al. 2009; Steinbuechel and Matuschewski 2009). S6 KO sporozoites extracted from the salivary gland were observed to adhere less and to undergo less circular gliding when compared to WT (Hegge et al. 2010). TLP KO sporozoites were observed to undergo normal but less continuous circular gliding compared to WT (Heiss et al. 2008; Hegge et al. 2010). Surprisingly, our results show that ΔTLP/ ΔS6 KO salivary gland sporozoites were capable to glide continuously when observed *in vitro* with only slightly reduced speeds compared to wild type sporozoites. In contrast to previous studies, this would either indicate that TLP and S6 are mostly obsolete for continuous gliding *in vitro* or that TLP and S6 interact with each other and lead to less continuous gliding only when parasites are lacking one but not both adhesins. Clarification might result from further investigation of the gliding patterns of the TLP KO and S6 single KO lines. Both lines could be generated by complementation of the generated TLP/S6 KO lines. Further, it would be interesting to measure the forces transduced by the generated double and triple KO lines. Trapping experiments of individual sporozoites with laser tweezers already showed that S6 and TRAP play critical roles in initial adhesion site formation, as sporozoites lacking S6 or TRAP adhere less well to the substrate than wild type (Hegge et al. 2012). They also revealed that patch gliding hemolymph sporozoites of these mutant lines are readily trapped

compared to wild type sporozoites suggesting that the transduced force is weaker compared to wild type sporozoites (Hegge et al. 2012). They further found that S6 and TRAP-KO hemolymph sporozoites show distinct defects in their initial adhesion. TRAP-KO sporozoites were shown to adhere mainly with their front end while sporozoites lacking S6 show no preference in their adhesion site (Hegge et al. 2012). Investigating the transduced forces of the generated double and triple knockout lines as well as observation of their initial adhesion sites could potentially reveal synergistic or antagonistic effects which could not be observed with the methods applied in this thesis and might lead to further insights regarding their functional interplay.

In conclusion, the characterization of the generated adhesin double and triple knockout lines confirmed the dominant role of TRAP and S6 in the order TRAP > S6 > TLP which resulted in a complete block of salivary gland invasion whenever TRAP was missing and a strong reduction in salivary gland invasion when sporozoites were lacking S6. The results of this thesis revealed no synergistic or antagonistic effects between the three adhesins. Instead, I found that sporozoites that lack the TLP and S6 adhesin can still undergo natural transmission into the host and discovered that sporozoites which lack all three adhesins are still capable to undergo “patch gliding” motility indicating the existence of at least one further adhesin involved in gliding motility.

6 Bibliography

Aikawa M, Atkinson CT, Beaudoin LM, Sedegah M, Charoenvit Y, Beaudoin R. 1990. Localization of CS and non-CS antigens in the sporogonic stages of Plasmodium yoelii. Bull. World Health Organ. 68:165–71.

Aly ASI, Matuschewski K. 2005. A malarial cysteine protease is necessary for Plasmodium sporozoite egress from oocysts. J. Exp. Med. 202:225–30.

Amino R, Thiberge S, Shorte S, Frischknecht F, Ménard R. 2006. Quantitative imaging of Plasmodium sporozoites in the mammalian host. Nature Medicine 12:220-224.

Angrisano F, Tan Y-H, Sturm A, McFadden GI, Baum J. 2012. Malaria parasite colonisation of the mosquito midgut – Placing the Plasmodium ookinete centre stage. Int. J. Parasitol. 42:519–527.

Baer K, Klotz C, Kappe SHI, Schnieder T, Frevert U. 2007. Release of hepatic Plasmodium yoelii merozoites into the pulmonary microvasculature. PLoS Pathog. 3:e171.

Bane KS, Lepper S, Kehrer J, Sattler JM, Singer M. 2016. The actin filament-binding protein coronin regulates motility in Plasmodium sporozoites. PLoS Pathog. 12:e1005710.

Battista A. 2015. Physical models for the motility of malaria parasites. http://archiv.ub.uni-heidelberg.de/volltextserver/18742.

Baum J, Gilberger T-W, Frischknecht F, Meissner M. 2008. Host-cell invasion by malaria parasites: insights from Plasmodium and Toxoplasma. Trends Parasitol. 24:557–63.

Bazazi S, Pfennig KS, Handegard NO, Couzin ID. 2012. Vortex formation and foraging in polyphenic spadefoot toad tadpoles. Behav. Ecol. Sociobiol. 66:879–889.

Beebe W. 1921. Edge of the jungle. H. Holt and Company.

Beier JC. 1998. Malaria parasite development. Annu. Rev. Entomol. 43:519–43.

Ben-Jacob E. 2003. Bacterial self-organization: co-enhancement of complexification and adaptability in a dynamic environment. Philos. Trans. A. Math. Phys. Eng. Sci. 361:1283–312.

Ben-Jacob E, Cohen I, Czirók A, Vicsek T, Gutnick DL. 1997. Chemomodulation of cellular movement, collective formation of vortices by swarming bacteria, and colonial development. Phys. A Stat. Mech. its Appl. 238:181–197.

Bergman LW, Kaiser K, Fujioka H, Coppens I, Daly TM, Fox S, Matuschewski K, Nussenzweig V, Kappe SHI. 2003. Myosin A tail domain interacting protein (MTIP) localizes to the inner membrane complex of Plasmodium sporozoites. J. Cell Sci. 116:39–49.

Blair DL, Neicu T, Kudrolli A. 2003. Vortices in vibrated granular rods. Physical Review 67:031303.

Bode NWF, Delcourt J, Czirok A, Vicsek T, Gutnick D. 2013. Individual-to-resource landscape interaction strength can explain different collective feeding behaviours. PLoS One 8:e75879.

Bottius E, BenMohamed L, Brahimi K, Gras H, Lepers JP, Raharimalala L, Aikawa M, Meis J, Slierendregt B, Tartar A. 1996. A novel Plasmodium falciparum sporozoite and liver stage antigen (SALSA) defines major B, T helper, and CTL epitopes. J. Immunol. 156:2874–84.

Boucher LE, Bosch J. 2015. The apicomplexan glideosome and adhesins – Structures and function. J. Struct. Biol. 190:93–114.

Braks JAM, Franke-Fayard B, Kroeze H, Janse CJ, Waters AP. 2006. Development and application of a positive-negative selectable marker system for use in reverse genetics in Plasmodium. Nucleic Acids Res. 34:e39.

Bubb MR, Spector I, Beyer BB, Fosen KM. 2000. Effects of jasplakinolide on the kinetics of actin polymerization. An explanation for certain in vivo observations. J. Biol. Chem. 275:5163–70.

Bullen HE, Tonkin CJ, O'Donnell RA, Tham W-H, Papenfuss AT, Gould S, Cowman AF, Crabb BS, Gilson PR. 2009. A novel family of Apicomplexan glideosome-associated proteins with an inner membrane-anchoring role. J. Biol. Chem. 284:25353–63.

Calovi DS, Lopez U, Ngo S, Sire C, Chaté H, Theraulaz G. 2014. Swarming, schooling, milling: phase diagram of a data-driven fish school model. New J. Phys. 16:15026.

Chattopadhyay R, Rathore D, Fujioka H, Kumar S, de la Vega P, Haynes D, Moch K, Fryauff D, Wang R, Carucci DJ. 2003. PfSPATR, a Plasmodium falciparum protein containing an altered thrombospondin type I repeat domain is expressed at several stages of the parasite life cycle and is the target of inhibitory antibodies. J. Biol. Chem. 278:25977–25981.

Combe A, Moreira C, Ackerman S, Thiberge S, Templeton TJ, Ménard R. 2009. TREP, a novel protein necessary for gliding motility of the malaria sporozoite. Int. J. Parasitol. 39:489–496.

Cooper JA. 1987. Effects of cytochalasin and phalloidin on actin. J. Cell Biol. 105:1473–8.

Coppi A, Natarajan R, Pradel G, Bennett BL, James ER, Roggero MA, Corradin G, Persson C, Tewari R, Sinnis P. 2011. The malaria circumsporozoite protein has two functional domains, each with distinct roles as sporozoites journey from mosquito to mammalian host. J. Exp. Med. 208:341–56.

Couzin ID, Krause J. 2003. Self-organization and collective behavior in vertebrates. Adv Study Behav 32:1–75.

Couzin ID, Krause J, James R, Ruxton GD, Franks NR. 2002. Collective memory and spatial sorting in animal groups. J. Theor. Biol. 218:1–11.

Cramer LP. 1999. Role of actin-filament disassembly in lamellipodium protrusion in motile cells revealed using the drug jasplakinolide. Curr. Biol. 9:1095–105.

Crawley J, Chu C, Mtove G, Nosten F. 2010. Malaria in children. Lancet 375:1468–1481.

Currà C, Di Luca M, Picci L, de Sousa Silva Gomes dos Santos C, Siden-Kiamos I, Pace T, Ponzi M. 2013. The ETRAMP family member SEP2 is expressed throughout Plasmodium berghei life cycle and is released during sporozoite gliding motility. PLoS One 8:e67238.

Czirók A, Matsushita M, Vicsek T. 2001. Theory of periodic swarming of bacteria: application to Proteus mirabilis. Phys. Rev. E. Stat. Nonlin. Soft Matter Phys. 63:31915.

Delcourt J, Bode NWF, Denoël M. 2016. Collective vortex behaviours: diversity, proximate, and ultimate causes of circular animal group movements. Quarterly Rev. of Biol. 91:1–24.

Delcourt J, Poncin P. 2012. Shoals and schools: back to the heuristic definitions and quantitative references. Rev. Fish Biol. Fish. 22:595–619.

Douglas RG, Amino R, Sinnis P, Frischknecht F. 2015. Active migration and passive transport of malaria parasites. Trends Parasitol. 31:1–6.

Douradinha B, Augustijn KD, Moore SG, Ramesar J, Mota MM, Waters AP, Janse CJ, Thompson J. 2011. Plasmodium cysteine repeat modular proteins 3 and 4 are essential for malaria parasite transmission from the mosquito to the host. Malar. J. 10:71.

Dusenbery DB. 1996. Life at small scale: the behavior of microbes. Scientific American Library.

Ejigiri I, Ragheb DRT, Pino P, Coppi A, Bennett BL, Soldati-Favre D, Sinnis P. 2012. Shedding of TRAP by a rhomboid protease from the malaria sporozoite surface is essential for gliding motility and sporozoite infectivity. PLoS Pathog 8:e1002725.

El-Manzalawy Y, Munoz EE, Lindner SE, Honavar V. 2016. PlasmoSEP: Predicting surface-exposed proteins on the malaria parasite using semisupervised self-training and expert-annotated data. Proteomics 16:2967–2976.

Fabre J-H. 1879. Souvenirs entomologiques: études sur l'instinct et les moeurs des insectes.

Franks NR, Worley A, Grant KAJ, Gorman AR, Vizard V, Plackett H, Doran C, Gamble ML, Stumpe MC, Sendova-franks AB. 2016. Social behaviour and collective motion in plant-animal worms. Proc. R. Soc. B. 283:20152946.

Frénal K, Polonais V, Marq J-B, Stratmann R, Limenitakis J, Soldati-Favre D. 2010. Functional dissection of the Apicomplexan glideosome molecular architecture. Cell Host Microbe 8:343–357.

Frischknecht F, Baldacci P, Martin B, Zimmer C, Thiberge S, Olivo-Marin JC, Shorte SL, Ménard R. 2004. Imaging movement of malaria parasites during transmission by Anopheles mosquitoes. Cell. Microbiol. 6:687–694.

Frischknecht F, Matuschewski K. 2017. Plasmodium sporozoite biology. Cold Spring Harb. Perspect. Med. 7:a025478.

Gaskins E, Gilk S, DeVore N, Mann T, Ward G, Beckers C. 2004. Identification of the membrane receptor of a class XIV myosin in Toxoplasma gondii. J. Cell Biol. 165:383–93.

Ghosh A, Jacobs-Lorena M. 2009. Plasmodium sporozoite invasion of the mosquito salivary gland. Curr. Opin. Microbiol. 12:394–400.

Ghosh AK, Devenport M, Jethwaney D, Kalume DE, Pandey A, Anderson VE, Sultan AA, Kumar N, Jacobs-Lorena M. 2009. Malaria parasite invasion of the mosquito salivary gland requires interaction between the Plasmodium TRAP and the Anopheles saglin proteins. PLoS Pathog. 5:e1000265.

Giovannini D, Späth S, Lacroix C, Perazzi A, Bargieri D, Lagal V, Lebugle C, Combe A, Thiberge S, Baldacci P, et al. 2011. Independent roles of apical membrane antigen 1

and rhoptry neck proteins during host cell invasion by Apicomplexa. Cell Host Microbe 10:591–602.

Gomes A, Bushell E, Schwach F, Girling G, Anar B, Quail M, Herd C, Pfander C, Modrzynska K, Rayner J. 2015. A genome-scale vector resource enables high-throughput reverse genetic screening in a malaria parasite. Cell Host Microbe 17:404–413.

Gooders J, Boyer T. 1986. Ducks of North America and the northern hemisphere. Facts on file.

Grassé P-P. 1959. La reconstruction du nid et les coordinations interindividuelles chez Bellicositermes natalensis etcubitermes sp. la théorie de la stigmergie: Essai d'interprétation du comportement des termites constructeurs. Insectes Soc. 6:41–80.

Harupa A, Sack BK, Lakshmanan V, Arang N, Douglass AN, Oliver BG, Stuart AB, Sather DN, Lindner SE, Hybiske K. 2014. SSP3 is a novel Plasmodium yoelii sporozoite surface protein with a role in gliding motility. Infect. Immun. 82:4643–4653.

Hegge S, Kudryashev M, Smith A, Frischknecht F. 2009. Automated classification of Plasmodium sporozoite movement patterns reveals a shift towards productive motility during salivary gland infection. 4:903–913.

Hegge S, Münter S, Steinbüchel M, Heiss K, Engel U, Matuschewski K, Frischknecht F. 2010. Multistep adhesion of Plasmodium sporozoites. FASEB J. 24:2222–34.

Hegge S, Uhrig K, Streichfuss M, Kynast-Wolf G, Matuschewski K, Spatz JP, Frischknecht F. 2012. Direct manipulation of malaria parasites with optical tweezers reveals distinct functions of Plasmodium surface proteins. ACS Nano 6:4648–62.

Heintzelman MB. 2015. Gliding motility in Apicomplexan parasites. Semin. Cell Dev. Biol. 46:135–142.

Heintzelman MB, Schwartzman JD. 1997. A novel class of unconventional myosins from Toxoplasma gondii. J. Mol. Biol. 271:139–146.

Heintzelman MB, Schwartzman JD. 1999. Characterization of myosin-A and myosin-C: two class XIV unconventional myosins from Toxoplasma gondii. Cell Motil. Cytoskeleton 44:58–67.

Heiss K, Nie H, Kumar S, Daly TM, Bergman LW, Matuschewski K. 2008. Functional characterization of a redundant Plasmodium TRAP family invasin, TRAP-like protein, by aldolase binding and a genetic complementation test. Eukaryot. Cell 7:1062–70.

Hellmann JK, Münter S, Kudryashev M, Schulz S, Heiss K, Müller AK, Matuschewski K, Spatz JP, Schwarz US, Frischknecht F. 2011. Environmental constraints guide migration of malaria parasites during transmission. PLoS Pathog. 7:e1002080.

Herm-Götz A, Weiss S, Stratmann R, Fujita-Becker S, Ruff C, Meyhöfer E, Soldati T, Manstein DJ, Geeves MA, Soldati D. 2002. Toxoplasma gondii myosin A and its light chain: a fast, single-headed, plus-end-directed motor. EMBO J. 21:2149–58.

Hopp CS, Chiou K, Ragheb DR, Salman AM, Khan SM, Liu AJ, Sinnis P. 2015. Longitudinal analysis of *Plasmodium* sporozoite motility in the dermis reveals component of blood vessel recognition. Elife 4:4.

Ingham CJ, Ben Jacob E, Jacob E Ben. 2008. Swarming and complex pattern formation in Paenibacillus vortex studied by imaging and tracking cells. BMC Microbiol. 8:36.

Janzen HG, Wright KA. 1971. The salivary glands of Aedes aegypti (L.): an electron

microscope study. Can. J. Zool. 49:1343–6.

Josling G, Llinás M. 2015. Sexual development in Plasmodium parasites: knowing when it's time to commit. Nat. Rev. Microbiol. 13:573–87.

Kaiser K, Matuschewski K, Camargo N, Ross J, Kappe SHI. 2004. Differential transcriptome profiling identifies Plasmodium genes encoding pre-erythrocytic stage-specific proteins. Mol. Microbiol. 51:1221–1232.

Kappe S, Bruderer T, Gantt S, Fujioka H, Nussenzweig V, Ménard R. 1999. Apicomplexan Parasites. 147:937–943.

Kappe SHI, Buscaglia CA, Nussenzweig V. 2004. Plasmodium sporozoite molecular cell biology. Annu. Rev. Cell Dev. Biol. 20:29–59.

Kappe SHI, Kaiser K, Matuschewski K. 2003. The Plasmodium sporozoite journey: a rite of passage. Trends Parasitol. 19:135–143.

Kariu T, Yuda M, Yano K, Chinzei Y. 2002. MAEBL is essential for malarial sporozoite infection of the mosquito salivary gland. J. Exp. Med. 195:1317–23.

Keeley A, Soldati D. 2004. The glideosome: a molecular machine powering motility and host-cell invasion by Apicomplexa. Trends Cell Biol. 14:528–532.

Kehrer J, Singer M, Lemgruber L, Silva PAGC, Frischknecht F, Mair GR. 2016. A putative small solute transporter is responsible for the secretion of G377 and TRAP-containing secretory vesicles during Plasmodium gamete egress and sporozoite motility. PLOS Pathog. 12:e1005734.

Klug D, Frischknecht F. 2017. Motility precedes egress of malaria parasites from oocysts. Elife 6:1–32.

Kudrolli A, Lumay G, Volfson D, Tsimring LS. 2008. Swarming and swirling in self-propelled polar granular rods. Phys. Rev. Lett. 100:58001.

Kudryashev M, Münter S, Lemgruber L, Montagna G, Stahlberg H, Matuschewski K, Meissner M, Cyrklaff M, Frischknecht F. 2012. Structural basis for chirality and directional motility of Plasmodium sporozoites. Cell. Microbiol. 14:1757–1768.

Labaied M, Harupa A, Dumpit RF, Coppens I, Mikolajczak SA, Kappe SHI. 2007. Plasmodium yoelii sporozoites with simultaneous deletion of P52 and P36 are completely attenuated and confer sterile immunity against infection. Infect. Immun. 75:3758–3768.

Lacroix C, Menard R. 2008. TRAP-like protein of Plasmodium sporozoites: linking gliding motility to host-cell traversal. Trends Parasitol. 24:428–31.

Lima SL. 1995. Back to the basics of anti-predatory vigilance: the group-size effect. Anim. Behav. 49:11–20.

Lindner SE, Swearingen KE, Harupa A, Vaughan AM, Sinnis P, Moritz RL, Kappe SHI. 2013. Total and putative surface proteomics of malaria parasite salivary gland sporozoites. Mol. Cell. Proteomics 12:1127–43.

Lushi E, Wioland H, Goldstein RE, Swinney HL. 2014. Fluid flows created by swimming bacteria drive self-organization in confined suspensions. Proc. Natl Acad. Sci. U.S.A. 111:9733–9738.

Matuschewski K. 2006. Getting infectious: Formation and maturation of Plasmodium sporozoites in the Anopheles vector. Cell. Microbiol. 8:1547–1556.

Matuschewski K, Nunes AC, Nussenzweig V, Ménard R, Me R. 2002. Plasmodium sporozoite invasion into insect and mammalian cells is directed by the same dual binding system. EMBO J. 21:1597–1606.

Matuschewski K, Ross J, Brown SM, Kaiser K, Nussenzweig V, Kappe SHI. 2002. Infectivity-associated changes in the transcriptional repertoire of the malaria parasite sporozoite stage. J. Biol. Chem. 277:41948–41953.

Meissner M, Schlüter D, Soldati D. 2002. Role of Toxoplasma gondii Myosin A in powering parasite gliding and host cell invasion. Science. 298:837–840.

Ménard R, Sultan AA, Cortes C, Altszuler R, van Dijk MR, Janse CJ, Waters AP, Nussenzweig RS, Nussenzweig V. 1997. Circumsporozoite protein is required for development of malaria sporozoites in mosquitoes. Nature 385:336–40.

Menard R, Tavares J, Cockburn IA, Markus M, Zavala F, Amino R. 2013. Looking under the skin: the first steps in malarial infection and immunity. Nat. Rev. Microbiol. 11:701–712.

Miller MJ, Wei SH, Cahalan MD, Parker I. 2003. Autonomous T cell trafficking examined in vivo with intravital two-photon microscopy. Proc. Natl. Acad. Sci. U.S.A. 100:2604–9.

Montagna GN, Matuschewski K, Buscaglia C. 2012. Plasmodium sporozoite motility: an update. Front. in Biosci. 21:726–744.

Montagna GN, Matuschewski K, Buscaglia C. 2012. Small heat shock proteins in cellular adhesion and migration: Evidence from Plasmodium genetics. Cell Adh. Migr. 6:78–84.

Morahan BJ, Wang L, Coppel RL. 2009. No TRAP, no invasion. Trends Parasitol. 25:77–84.

Moreira CK, Templeton TJ, Lavazec C, Hayward RE, Hobbs C V, Kroeze H, Janse CJ, Waters AP, Sinnis P, Coppi A. 2008. The Plasmodium TRAP/MIC2 family member, TRAP-Like Protein (TLP), is involved in tissue traversal by sporozoites. Cell. Microbiol. 10:1505–16.

Mota MM, Hafalla JCR, Rodriguez A. 2002. Migration through host cells activates Plasmodium sporozoites for infection. Nat. Med. 8:963–970.

Münter S, Sabass B, Selhuber-unkel C, Kudryashev M, Hegge S, Engel U, Spatz JP, Matuschewski K, Schwarz US, Frischknecht F. 2009. Plasmodium sporozoite motility is modulated by the turnover of discrete adhesion sites. Cell Host Microbe. 6:551–562.

Myung JM, Marshall P, Sinnis P. 2004. The Plasmodium circumsporozoite protein is involved in mosquito salivary gland invasion by sporozoites. Mol. Biochem. Parasitol. 133:53–9.

Nagasawa H, Aikawa M, Procell PM, Campbell GH, Collins WE, Campbell CC. 1988. Plasmodium malariae: distribution of circumsporozoite protein in midgut oocysts and salivary gland sporozoites. Exp. Parasitol. 66:27–34.

Natarajan R, Thathy V, Mota MM, Hafalla JCR, Ménard R, Vernick KD. 2001. Fluorescent Plasmodium berghei sporozoites and pre-erythrocytic stages: A new tool to study mosquito and mammalian host interactions with malaria parasites. Cell. Microbiol. 3:371–379.

Opitz C, Soldati D. 2002. “The glideosome”: a dynamic complex powering gliding motion and host cell invasion by Toxoplasma gondii. Mol. Microbiol. 45:597–604.

Orr RY, Philip N, Waters AP. 2012. Improved negative selection protocol for Plasmodium berghei in the rodent malarial model. Malar. J. 11:103.

Parr AE. 1927. A contribution to the theoretical analysis of the schooling behavior of fishes. Occasional Papers of the Bingham Oceanographic Collection 1:1–32.

Pimenta PF, Touray M, Miller L. The journey of malaria sporozoites in the mosquito salivary gland. J. Eukaryot. Microbiol. 41:608–24.

Posthuma G, Meis JF, Verhave JP, Hollingdale MR, Ponnudurai T, Meuwissen JH, Geuze HJ. 1988. Immunogold localization of circumsporozoite protein of the malaria parasite Plasmodium falciparum during sporogony in Anopheles stephensi midguts. Eur. J. Cell Biol. 46:18–24.

Prudêncio M, Rodriguez A, Mota MM. 2006. The silent path to thousands of merozoites: the Plasmodium liver stage. Nat. Rev. Microbiol. 4:849–56.

Quadt KA, Streichfuss M, Moreau CA, Spatz JP, Frischknecht F. 2016. Coupling of retrograde flow to force production during malaria parasite migration. ACS Nano 10:2091–2102.

Rappel W-J, Nicol A, Sarkissian A, Levine H, Loomis WF. 1999. Self-organized vortex state in two-dimensional Dictyostelium dynamics. Physical Review Letters 83, 1247–1250.

Rénia L, Goh YS. 2016. Malaria parasites: the great escape. Front. Immunol. 7:1–14.

Rieucau G, Martin JGA. 2008. Many eyes or many ewes: vigilance tactics in female bighorn sheep Ovis canadensis vary according to reproductive status. Oikos 117:501–506.

Santos JM, Egarter S, Zuzarte-Luís V, Kumar H, Moreau CA, Kehrer J, Pinto A, Costa M da, Franke-Fayard B, Janse CJ. 2017. Malaria parasite LIMP protein regulates sporozoite gliding motility and infectivity in mosquito and mammalian hosts. Elife 6: e24109.

Sato Y, Montagna GN, Matuschewski K. 2014. Plasmodium berghei sporozoites acquire virulence and immunogenicity during mosquito hemocoel transit. Infect. Immun. 82:1164–72.

Sattler JM, Ganter M, Hliscs M, Matuschewski K, Schüler H. 2011. Actin regulation in the malaria parasite. Eur. J. Cell Biol. 90:966–971.

Schaller V, Weber C, Semmrich C, Frey E, Bausch AR. 2010. Polar patterns of driven filaments. Nature 467:73–77.

Schmitz S, Grainger M, Howell S, Calder LJ, Gaeb M, Pinder JC, Holder AA, Veigel C. 2005. Malaria parasite actin filaments are very short. J. Mol. Biol. 349:113–125.

Schneirla TC. 1944. A unique case of circular milling in ants, considered in relation to trail following and the general problem of orientation. American Museum novitates ; no. 1253.

Schwach F, Bushell E, Gomes AR, Anar B, Girling G, Herd C, Rayner JC, Billker O. 2015. PlasmoGEM, a database supporting a community resource for large-scale experimental genetics in malaria parasites. Nucleic Acids Res. 43:1176–1182.

Shute PG. 1943. Successful transmission of human malaria with sporozoites which have not come into contact with the salivary glands of the insect Host. J. Trop. Med. Hyg. 46:57–8.

Sidjanski SP, Vanderberg JP, Sinnis P. 1997. Anopheles stephensi salivary glands bear receptors for region I of the circumsporozoite protein of Plasmodium falciparum. Mol. Biochem. Parasitol. 90:33–41.

Sinden RE, Butcher GA, Beetsma AL. 2002. Maintenance of the Plasmodium berghei life cycle. Malaria Methods and Protocols. 72:25–40.

Sinden RE, Croll NA. 1975. Cytology and kinetics of microgametogenesis and fertilization in Plasmodium yoelii nigeriensis. Parasitology 70:53–65.

Sinden RE, Strong K. 1978. An ultrastructural study of the sporogonic development of Plasmodium falciparum in Anopheles gambiae. Trans. R. Soc. Trop. Med. Hyg. 72:477–91.

Skillman KM, Diraviyam K, Khan A, Tang K, Sept D, Sibley LD. 2011. Evolutionarily divergent, unstable filamentous actin is essential for gliding motility in Apicomplexan parasites. PLoS Pathog. 7:e1002280.

Smith RC, Barillas-Mury C. 2016. Plasmodium oocysts: overlooked targets of mosquito immunity. Trends Parasitol. 32:979–990.

Steinbuechel M, Matuschewski K. 2009. Role for the Plasmodium sporozoite-specific transmembrane protein S6 in parasite motility and efficient malaria transmission. Cell. Microbiol. 11:279–88.

Sterling CR, Aikawa M, Vanderberg JP. 1973. The passage of Plasmodium berghei sporozoites through the salivary glands of Anopheles stephensi: an electron microscope study. J. Parasitol. 59:593–605.

Sturm A, Amino R, van de Sand C, Regen T, Retzlaff S, Rennenberg A, Krueger A, Pollok J-M, Menard R, Heussler VT. 2006. Manipulation of host hepatocytes by the malaria parasite for delivery into liver sinusoids. Science 313:1287–90.

Sultan AA, Thathy V, Frevert U, Robson KJH, Crisanti A, Nussenzweig V, Nussenzweig RS. 1997. TRAP is necessary for gliding motility and infectivity of Plasmodium sporozoites. Cell 90:511–522.

Sumpter DJT. 2010. Collective animal behavior. Princeton University Press.

Tavares J, Formaglio P, Thiberge S, Mordelet E, Van Rooijen N, Medvinsky A, Ménard R, Amino R. 2013. Role of host cell traversal by the malaria sporozoite during liver infection. J. Exp. Med. 210:905–15.

Terzakis JA, Sprinz H, Ward RA. 1967. The transformation of the Plasmodium gallinaceum oocyst in Aedes aegypti mosquitoes. J. Cell Biol. 34:311-326.

Thathy V, Fujioka H, Gantt S, Nussenzweig R, Nussenzweig V, Ménard R. 2002. Levels of circumsporozoite protein in the Plasmodium oocyst determine sporozoite morphology. EMBO J. 21:1586–1596.

Thompson J, Fernandez-Reyes D, Sharling L, Moore SG, Eling WM, Kyes SA, Newbold CI, Kafatos FC, Janse CJ, Waters AP. 2007. Plasmodium cysteine repeat modular proteins 1-4: complex proteins with roles throughout the malaria parasite life cycle. Cell. Microbiol. 9:1466–1480.

Todd FS. 1979. Waterfowl : ducks, geese and swans of the world. Sea World Press.

Touray MG, Warburg A, Laughinghouse A, Krettli AU, Miller LH. 1992. Developmentally regulated infectivity of malaria sporozoites for mosquito salivary glands and the vertebrate host. J. Exp. Med. 175:1607–12.

Tunstrøm K, Katz Y, Ioannou CC, Huepe C, Lutz MJ, Couzin ID. 2013. Collective states, multistability and transitional behavior in schooling fish. PLoS Comput. Biol. 9:e1002915.

Vanderberg J, Rhodin J. 1967. Differentiation of nuclear and cytoplasmic fine structure during sporogonic development of Plasmodium berghei. J. Cell Biol. 32:C7-10.

Vanderberg JP. 1975. Development of infectivity by the Plasmodium berghei sporozoite. J. Parasitol. 61:43–50.

Vanderberg JP. 1974. Studies on the motility of *Plasmodium* sporozoites. J. Protozool. 21:527–537.

Vanderberg JP, Frevert U. 2004. Intravital microscopy demonstrating antibody-mediated immobilisation of Plasmodium berghei sporozoites injected into skin by mosquitoes. Int. J. Parasitol. 34:991–996.

Vicsek T, Zafeiris A. 2012. Collective motion. Phys. Rep. 517:71–140.

Vincke IH, Lips M. 1948. Un nouveau plasmodium d'un rongeur sauvage du Congo Plasmodium berghei N. Sp. Ann. la Soc. belge Med. Trop. 28:97–104.

Vollmer J, Vegh AG, Lange C, Eckhardt B. 2006. Vortex formation by active agents as a model for *Daphnia* swarming. Phys. Rev. E 73:61924.

Weiss GE, Gilson PR, Taechalertpaisarn T, Tham WH, de Jong NWM, Harvey KL, Fowkes FJI, Barlow PN, Rayner JC, Wright GJ. 2015. Revealing the sequence and resulting cellular morphology of receptor-ligand interactions during Plasmodium falciparum invasion of erythrocytes. PLoS Pathog. 11:1–25.

Wengelnik K, Spaccapelo R, Naitza S, Robson KJH, Janse CJ, Bistoni F, Waters AP, Crisanti A. 1999. The A-domain and the thrombospondin-related motif of Plasmodium falciparum TRAP are implicated in the invasion process of mosquito salivary glands. EMBO J. 18:5195–5204.

Wetzel DM, Håkansson S, Hu K, Roos D, Sibley LD. 2003. Actin filament polymerization regulates gliding motility by apicomplexan parasites. Mol. Biol. Cell 14:396–406.

Wheeler W. 1910. Ants: their structure, development and behavior. New York: Columbia University Press.

White NJ. 2011. Determinants of relapse periodicity in Plasmodium vivax malaria. Malar. J. 10:297.

Wioland H, Woodhouse FG, Dunkel J, Kessler JO, Goldstein RE. 2013. Confinement stabilizes a bacterial suspension into a spiral vortex. Phys. Rev. Lett. 110:268102.

Wood AJ, Ackland GJ. 2007. Evolving the selfish herd: emergence of distinct aggregating strategies in an individual-based model. Proc. R. Soc. B Biol. Sci. 274:1637–1642.